Mineralogical and Petrogenetic Study of Gold Ore from the Boddington Gold Deposit, W.A.

Norton Kalleske

A1148036

Supervisor
Nigel J. Cook

Co-supervisor
Cristiana L. Ciobanu

Centre for Tectonics, Resources and Exploration
Department of Geology and Geophysics
School of Earth and Environmental sciences
University of Adelaide, South Australia
norton.kalleske@alumni.adelaide.edu.au

26 October, 2010

Table of contents

FIGURES

TABLES

APPENDIX

ABSTRACT

The Boddington gold mine, situated in the Saddleback greenstone belt, Yilgarn Craton, W.A., is a geologically complex and highly varied deposit. A variety of genetic models have been invoked in the past to explain the genesis of the deposit and features observed, including porphyry- and orogenic- models, as well as more recently, an intrusion-related gold system. Mineralisation occurs as veins, veinlets, shears, lenses and disseminations with host rocks of diorite, andesite and dacites. Veins and alteration are pervasive and consist of multiple stages of quartz-sericite, quartz-biotite, quartz-albite and actinolite alteration. Detailed ore mineralogical, petrographic and mineral-chemical study of representative ore samples from five of the eight domains within the deposit have given insights into the distribution of precious metals and also provided evidence for the formation of the Boddington deposit and provide evidence for its genetic evolution.

Mineralisation is characterised by a reduced assemblage, with chalcopyrite and pyrrhotite as the dominant sulphides. Pyrite (often replacing pyrrhotite), sphalerite, cubanite, cobaltite, arsenopyrite and pentlandite are minor sulphides. Molybdenite is also relatively abundant and occurs as a major mineral in localised areas throughout the deposit. The study has shown that the deposit also contains an extremely diverse array of trace minerals which can provide supporting evidence for aspects of ore genesis. Native gold and electrum are the main gold minerals; maldonite (Au_2Bi) is a minor component. LA-ICPMS analysis of pyrite and arsenopyrite revealed that these minerals are not significant Au-carriers at Boddington. In addition to maldonite, the deposit contains a suite of Bi-minerals, including native bismuth and a suite of Bi, Bi-Ag, Ag- and Pb-tellurides and selenides. These minerals are identified both in ore samples and in Cu-concentrates.

There is a strong and systematic Bi-Au signature across the deposit, reflected within individual mineral associations and in geochemical data. Aside from maldonite, melt-like droplets of Bi±Au±Te are recognised, suggesting that Au-scavenging by Bi-melts contributed to the observed gold distribution through (repeated) gold upgrading and remobilisation. Microprobe analysis of Bi-chalcogenides of the tetradymite group (Bi_xX_y, where X=Te,Se,S) shows compositions from across the full range of the series, demonstrating the multiphase character of the Boddington mineralisation and, specifically, (often incomplete) overprinting by more oxidising fluids. This dataset also includes several previously unreported and non-stoichiometric compositions of tetradymite group phases; these may represent unnamed phases, but may also be disordered at the lattice-scale. There is also a wide variety of Ni-bearing minerals present, including parkerite, $Ni_3(Bi,Pb)_2S_2$, lending weight to that mafic/ultramafic source rocks were involved in primary ore genesis. Nickel-bearing minerals are prominent components of ore remobilisates.

LA-ICPMS of molybdenite from the Boddington deposit reveal that this mineral is highly enriched in Au and Re, as well as a wide array of other elements (Bi, Te etc). High Re contents (up to 2,449 ppm) are indicative of a porphyry precursor. Re contents within molybdenite also display inhomogeneity at both the deposit and grain scales. Elevated Au (Bi,Te) contents in molybdenite are interpreted as sub-microscopic inclusions of discrete minerals within fractures and cleavage planes in the molybdenite.

Boddington is clearly not the product of a single ore-forming event but is rather a multiphase system recording successive overprinting and replacement of minerals, often very localised, and displaying strong lithological control. Boddington lacks many of the features consistent with a reduced intrusion-related gold system (RIRG), however some features observed can be explained by this model. It is believed, however, that fluids of granitic origin were probably an agent for remobilisation of existing mineralisation.

1. INTRODUCTION

The Boddington copper-gold mine, located within the northern part of the Archaean Saddleback greenstone belt, Southwest Yilgarn Block, W.A. commenced production in July 2009 and is set to be Australia's largest gold mine, with gold reserves in excess of 26 Moz and capacity for an annual production of 35 million tonnes of ore. The deposit is geologically complex and highly varied with respect to host rock, mineral assemblage and ore geochemistry.

The genesis of the Boddington deposit has been attributed to numerous genetic models. These range from a deformed and metamorphosed porphyry deposit formed broadly synchronous with the host rock intrusions (Roth 1992; Roth & Anderson 1993), a post peak metamorphism, shear zone hosted deposit that postdates the intrusive host rocks by at least 25 m.y. (Allibone *et al.* 1998) and a more recently proposed and more widely accepted intrusion-related model in which Boddington is viewed as a structurally controlled deposit with two distinct mineralisation stages (McCuaig *et al.* 2001). Stein *et al*. (2001) also suggest two distinct ages of mineralisation but attributes them to most likely a porphyry system and the second associated with the development of late orogenic gold mineralisation across much of the Yilgarn Craton with similarities suggesting an orogenic system.

This project aimed to characterise ore from 5 of the current 8 orebodies within the deposit focussing on current levels as of March 2010 using a combination of microanalytical methods. Specific main goals were to achieve:
(i) an understanding of the gold distribution in the deposit (identifying the gold minerals present and their compositions, assessment of 'invisible' gold in common sulphides) and an assessment of variation of distribution across distinct ore types and orebodies; and
(ii) provide data on the speciation and association of Bi-minerals that report to the copper concentrate and thus incur penalties.

Both primary goals have direct implications for ore processing and thus company revenue. Thus far unreported Au-minerals may contribute to lower-than-expected Au recoveries, and efforts to lower Bi-concentrations in the concentrates depend on understanding bismuth mineralogy and paragenesis.

Subordinate goals include an evaluation of trace element concentrations of the widespread, but currently not-recovered molybdenite. Mineralogy, mineral chemistry and ore textures are also used to place further constraints on the genetic model for the Boddington deposit and similar deposits elsewhere. In particular, attention is given to the possible role of Au-Bi melts during ore genesis.

The main ore minerals are chalcopyrite, pyrrhotite, pyrite, and arsenopyrite. Molybdenite is abundant in certain locations within the deposit and adjacent monzogranite but is currently not exploited as an ore mineral even though some reports to the Cu-concentrate.

Geologists at Boddington report a strong association between Au and Bi within the deposit. Native bismuth and Bi tellurides are found in trace amounts within the ore and are common and widespread across the Boddington deposit, commonly in close spatial and paragenetic association with gold. The possibility therefore exists that these minerals may have played a role in upgrading gold concentrations within the system. Bismuth tellurides, selenides and sulphosalts are becoming increasingly useful in determining the genesis of a deposit

as their relationships and mineralogy can be used as indicators of the conditions of the ore forming system since they are highly sensitive to temperature, Eh-pH conditions and oxygen/sulphur fugacity (Ciobanu & Cook 2002)

2. GEOLOGICAL SETTING

2.1 Regional Geology

The Yilgarn Craton is composed of volcanic and sedimentary rocks formed between 3000 and 2600 Ma and metamorphosed to upper greenschist/amphibolites facies at 2649 Ma (Nemchin *et al*. 1993). The formation of the Yilgarn Craton marks a major episode of tectonic activity on Earth and is interpreted to have formed from the accretion of a number of crustal terrains including volcanic arcs, back arc basins and microcontinents with ages from 3730 to 2550 Ma (Myers 1993). The period from 2760 to 2620 Ma in the late Archaean marks the formation of the majority of the greenstone belts in the Yilgarn Craton of W.A. (Nelson 1998). Greenstone belts were earlier believed to have formed in ensialic rift environments (Groves *et al.* 1987). However it is now understood that greenstone belts within the South-western portion of the Yilgarn are the result of subduction related processes. The Saddleback greenstone belt has a chemistry suggesting formation in an island arc setting (McCuaig *et al*. 2001). The Boddington deposit lies within the northern part of the Archaean Saddleback greenstone belt, Southwest Yilgarn Block within a steeply-dipping and extensively faulted sequence of greenschist to lower amphibolite metamorphosed sedimentary, felsic, and mafic volcanic and pyroclastic rocks, which have been extensively faulted (Anand 2005) (Figs. 1 and 2). The primary mineralisation is hosted in 2715-2690 Ma intermediate to felsic intrusive and volcanic rocks diorite, andesite and dacite. It is a low sulphide gold deposit with a Au-Cu-Mo-W-Bi association (Symons *et al.* 1990; McCuaig *et al*. 2001). Mineralisation at Boddington occurs as shear zones, brittle ductile faulting, veins and reactivated veins, veinlets, lenses and disseminated ores.

The interpretation of the Boddington deposit as a structurally-controlled, intrusion related Au-Cu deposit formed by two overprinting magmatic hydrothermal systems in which the bulk of the mineralisation is associated with the second event would be the first well documented occurrence of an Archaean Au-Cu deposit associated with post tectonic granitiods (McCuaig *et al*. 2001). Some argue, however, that primary mineralisation displays features consistent with a porphyry copper model and is considered to be an Archaean example of a gold rich porphyry ore system (Symons *et al.* 1990), associated with convergent plate tectonics at 2714-2696 Ma (Barley *et al.* 1992). It is also suggested that the deposit formed some 30-80 m.y. after the emplacement of arc sequences, with mineralisation bracketed by movement on late brittle faulting and the intrusion of pyroxenite dikes less than approximately 2675 Ma and the intrusion of approximately 2611 Ma unmineralised monzogranite plutons (Allibone *et al.* 1998) Results of Re-Os dating of Boddington molybdenite show that gold mineralisation occurred at both times creating complex veining and alteration of the deposit (Stein *et al*. 2001). The bedrock gold mineralisation is characterised by a metallogenetic association of Au-Cu-Mo-Te-Bi in a low-sulphide system within a host rock of Archaean porphyritic andesitic volcanic and dioritic intrusives. Primary gold mineralisation shows a strong structural control of gold distribution. The genetic debate is centred on the role of the Wourahming monzogranite which intrudes just east of the deposit and whether this may have been a source for the metals or just a heat engine that led to remobilisation and concentration of pre-existing ore.

2.2 **Deposit description**

The Boddington deposit is divided up into two open cuts during the present exploitation; North pit and South pit. These have been further broken down into domains based on lithology and grade. The North pit comprises of; Blob, Son of Blob, ABreccia and North Diorite. In the South pit domains are; Blackbutt, Pipeline, Central Diorite and Southern Diorite deep which at the current working level has not yet been intersected. These domains can be seen in Fig. 3.

2.2.1 MINERALISATION AND ALTERATION PATTERNS

The Boddington deposit is hosted within the northern Saddleback greenstone belt. This portion of the belt is composed of a mafic formation known as the Marradong Formation of basalts, gabbro and dolerite and the Wells formation of andesites, dacite volcanic and volcaniclastic rocks. These formations are intruded by diorite bodies dated at ca. 2714-2696 Ma with a trace element geochemistry indicating an island arc setting. Following two periods of deformation a suite of ultramafic dykes intrudes these at ~2675 Ma. A suite of dolerite dykes intrude the deposit and cut all mineralisation; ages for this event are, however, poorly constrained. The area underwent upper greenschist facies metamorphism and accompanied ductile deformation at ~2650-2630 Ma (Allibone *et al*., 1998). A late monzogranite intrudes the greenstone belt just east of the deposit and marks the end of the magmatic history at Boddington. This body has an age of ca. 2612 Ma and a geochemistry consistent with melting of mid-crustal rocks in an intraplate setting (post-tectonic or "A-type" granite) (McCuaig *et al.* 2001).

Allibone *et al*. (1998) suggest an alteration sequence where there is a complex history of mineralisation, deformation and alteration. They have argued for formation stages consisting of: early quartz-plagioclase fluorite veins with traces of chalcopyrite and pyrrhotite with no gold grade prior to initial deformation D1 shear zones and possibly blue quartz veins; a second stage of quartz-albite-clinozoisite-muscovite-biotite-actinolite-chlorite associated with D1 shears and mineralogy dependent on host rock; a sericite-quartz + pyrite alteration associated with a second (D2) deformation event. This was overprinted by quartz-albite-sericite-epidote-pyrite alteration, associated with a third deformation (D3) shear zones which overprint D1 and D2 events. Later silica alteration was also associated with the D3 event. A fourth deformation (D4) was associated with emplacement of pyroxenite dykes which features actinolite alteration with the dykes, and development of a biotite-clinozoisite +/- actinolite halo around the dykes. Mineralisation is associated with the occurrence of dykes with actinolite veining and quartz-sericite selvages associated with intense hydrothermal activity and later actinolite veining. A final stage with later movement on D4 faults coincides with Au, Cu, Mo, and W mineralisation and is expressed by quartz veins with molybdenite, pyrite, gold and clinozoisite-biotite-pyrrhotite-chalcopyrite Au veins.

More recent work by McCuaig *et al.* (2001) however, defined the deformation-alteration history of the deposit as: a widespread silica biotite alteration associated with diorite intrusions; an initial deformation event (D1) associated with molybdenite +/- Au mineralisation; a D1/D2 event associated with ductile deformation of the greenstone belt and silica-sericite-pyrite alteration; and third-generation deformation (D3) shear zones with ductile brittle mylonite zones of silica-albite-epidote-pyrite alteration. Clinozoisite-sulphide-silica-biotite assemblages control the bulk of the low-grade Au-Cu mineralisation and appear to pre-date the final deformation event (D4) which is associated with the main stage of mineralisation and which crosscuts D1-D2 structures. This was a brittle ductile deformation event and resulting assemblages comprise: (1) silica + albite

+ molybdenite +/- muscovite, biotite, fluorite, clinozoisite and chalcopyrite; and (2) actinolite +/- sulphide, silica veins, with silica albite or biotite-clinozoisite selvages. The D4 event reactivated D1-D3 structures.

Rock type has been noted to have a major influence on structures, alteration style and mineralisation due to certain lithologies being more favourable to alteration and also chemically favourable for metal precipitation.

3. APPROACH, SAMPLE SUITE AND EXPERIMENTAL/ANALYTICAL METHODS

3.1 Approach

Grab samples from 5 orebodies from around the mine site were collected in March 2010. These, and a number of additional samples from drillcore, were prepared into one-inch polished blocks for analysis of the ore using microscopic techniques; a total of 41 blocks and 5 thin sections were made. These were examined using reflected light and scanning electron microscopes to establish the main and accessory ore minerals, gangue phases and their mutual relationships. Particular attention was given to gold minerals (identifying compositional trends and size variation among grains of native gold and electrum, as well as observing other potential Au-bearing minerals such as Au-(Ag)-tellurides or maldonite) and to other 'exotic' phases present in the ore (Ni- and Co-sulphides, Bi-tellurides) whose presence and relationships could provide information pertinent to the genetic model. In addition, two copper concentrate samples were studied in order to establish the distribution of Au- and Bi-minerals, as well as an additional sample of molybdenite from the monzogranite.

Selected samples were then analysed by electron probe microanalyser (EPMA) to quantitatively determine mineral compositions, and by laser-ablation inductively-coupled mass-spectroscopy (LA-ICPMS) to determine concentrations of trace elements in sulphides. For the latter, attention was given to pyrite and arsenopyrite (which are less common at Boddington, but nevertheless potential hosts for invisible gold), and also molybdenite, which is currently not recovered following a feasibility study. Molybdenite can host significant amounts of valuable by-product elements such as rhenium.

3.2 Sample suite

Samples from the Boddington deposit were collected from current working levels as of 22/03/2010, samples were collected to try and present a representative suite of the working levels currently mined at Boddington. However as these are grab samples, visibly enriched in sulphides, they generally represent a higher grade ore than what is processed. A table of polished sections prepared can be seen in Table 1. Locations of the collected samples and domains can be seen in Fig. 3. Note that this map uses mine coordinates at the time of collection. A more detailed description of sample suite can be found in Appendix 1a.

3.3 **Analytical methods**

3.3.1 ASSAY

A selection of bulk ore samples and the two concentrates were sent for assay where a suite of elements were assayed (Au, Ag, As, Bi, Co, Cu, Mo, Ni, Pb, Sb, Se, Te and Zn). The objective was to identify typical concentrations in bulk ore from different orebodies, identify if there were any systematic variation on the deposit scale, and to identify possible inter-element correlations.

3.3.2 OPTICAL MICROSCOPY

The prepared blocks were first examined using reflected light microscopy under a Leitz Laborlux-12-Pol polarizing microscope up to 320x magnification using an oil immersion lens to document ore mineralogy. The objective was to identify the main ore and gangue minerals, document their relationships and assess whether the ore mineral assemblage varies with host lithology or position in the deposit. Images were taken using mounted digital camera. Results are discussed below.

3.3.3 SCANNING ELECTRON MICROSCOPY

Following reflected light microscopy, scanning electron microscopy (SEM) was conducted using a Philips XL30 instrument at Adelaide Microscopy Centre, University of Adelaide, Australia, equipped with energy dispersive X-ray spectrometry and back-scattered electron (BSE) imaging. Conditions used were at 20 eV with spot size 4. BSE imaging allowed the association of sulphides and other minerals with the silicates to be understood at the microscale, while identification of minerals in the ore that could not be made by optical methods alone was conducted using the built-in EDAX system.

3.3.4 ELECTRON MICROPROBE ANALYSIS

Microprobe analysis was conducted on selected samples to obtain the stoichiometry and minor element composition of ore minerals present in the samples as well as confirming the mineralogy of minerals identified using EDAX analysis and optical microscopy. A CAMECA SX-51 electron microprobe (EMP) with wavelength dispersion spectrometers at Adelaide Microscopy Centre was used. The measurements were performed at 20 kV with a beam current of 19.5 nA, using the following X-ray lines and standards; Au (Au Mα), Bi_2Se_3 (Bi Mα, Se Lα), PbS (Pb Mα), Ag_2Te (Ag Lα, Te Lα), Sb_2S_3 (Sb Lα), CoAsS (Co Kα, As Lα), Ni (Ni Kα), $CuFeS_2$ (Cu Kα), HgS (Hg Mα) and FeS_2 (Fe Kα, S Kα).

3.3.5 LA-ICPMS

LA-ICPMS analysis of pyrite, arsenopyrite and molybdenite was made using the Agilent HP7700 Quadripole ICPMS instrument at CODES (University of Tasmania, Hobart, Australia). This instrument is equipped with a high-performance New Wave UP-213 Nd:YAG Q-switched laser-ablation system equipped with MeoLaser 213 software. The laser microprobe was equipped with an in-house small volume (2.5 cm^3) ablation cell characterized by <1 s response time and <2 s wash-out time. Ablation was performed in an atmosphere of pure He (0.7 l/min). The He gas carrying the ablated aerosol was mixed with Ar (1.23 l/min) immediately after the ablation cell and the mix is passed through a pulse homogenizing device prior to direct introduction into the

torch. The ICPMS was optimized daily to maximize sensitivity on mid- to high-mass isotopes (in the range 130–240 a.m.u.). Production of molecular oxide species (i.e., $^{232}Th^{16}O/^{232}Th$) and doubly-charges ion species (i.e., $^{140}Ce{+}{+}/^{140}Ce+$) was maintained at <0.2%. Due to the low level of molecular oxide and doubly charged ion production, no correction was introduced to the analyte signal intensities for such potential interfering species.

Each analysis was performed in the time-resolved mode, which involves sequential peak hopping through the mass spectrum. The laser system was operated at constant 5 or 10 Hz pulse rate; laser energy was typically 1.5-2.5 J cm^{-2}. At these conditions each pulse removes ~0.3 µm of the samples, resulting in ablation rates of 1.5 µm/s and 3.0 µm/s for 5 and 10 Hz, respectively. Pre-defined areas of the polished blocks were ablated; spot sizes of the analyses were 5 µm in diameter and 10 µm for standards. The following isotopes were monitored: ^{49}Ti, ^{51}V, ^{53}Cr, ^{55}Mn, ^{57}Fe, ^{59}Co, ^{60}Ni, ^{65}Cu, ^{66}Zn, ^{69}Ga, ^{72}Ge, ^{75}As, ^{77}Se, ^{93}Nb, ^{95}Mo, ^{107}Ag, ^{111}Cd, ^{115}In, ^{118}Sn, ^{121}Sb, ^{125}Te, ^{182}W, ^{185}Re, ^{197}Au, ^{205}Tl, ^{208}Pb, ^{209}Bi and ^{238}U. Results are reported in elemental ppm.

The analysis time for each sample was 90 s, comprising a 30 s measurement of background (laser off) and a 70-s analysis with laser-on. Acquisition time for all masses was set to 0.02 s, with a total sweep time of 0.6 s. Data reduction was undertaken according to standard methods (Longerich *et al.* 1996) using Fe as the internal standard for pyrite and arsenopyrite and Mo for molybdenite. Calibration was performed using an in-house standard (STDGL2b-2), comprising powdered sulphides doped with certified element solutions and fused to a lithium borate glass disk. This standard is suitable for quantitative analyses in different sulphide matrixes (Danyushevsky *et al*. 2003; in press). Element mapping was performed using the New Wave UP-213 Laser, coupled to an Agilent HP 4500 Quadropole ICP-MS at CODES. Trace element maps were generated by ablating sets of parallel lines in a grid across the sample. The lines were ablated at a frequency of 10 Hz, with a beam size of 10 µm, rastering at 10 µm/s. See Large *et al*. (2009) for further details of the methodology.

4. RESULTS

4.1 Bulk sample geochemistry

A summary table of samples that were sent for assay can be found in Appendix 1b which also describes rock type and alteration.

Assay results in Table 2 show a strong association of Au with Bi (see also Fig. 4). This trend is seen in numerous other results done throughout this study. The results show that sample ANK6, an actinolite shear from the Pipeline orebody, has very high Au grade for this deposit which commonly reports a head grade of only 0.85 ppm. This sample also contains less visible sulphides and has a proportionally lower Cu content than many of the other samples. Gold concentrations for the other samples are much lower in Au than the actinolite shear from Pipeline and also have a more pronounced correlation of Cu with Au content. Actinolite shear zones have been noted by geology staff at Boddington to often have higher Au grades. However, there are also barren actinolite shears.

4.2 **Mineralogy and petrography**

The sample suite consists of samples collected from five of the eight domains that currently make up the Boddington deposit (Fig. 3). Where possible, the results and subsequent discussion are presented on the basis of these divisions and have focused on establishing the character of each domain and the significant differences between them. Descriptions of each sample are given in Appendix 2.

Ores in the Boddington deposit were seen to be of disseminations, lenses and veinlets. There is a strong structural control on mineralisation, with ore concentrated within veins, reactivated structures and shear zones. Representative examples of ore bearing structures and features can be seen in Fig. 5.

The North pit has a more felsic character, with dacites more prevalent and stronger porphyritic textures in the diorites, the south pit comprises of a more intermediate suite of andesites and diorites. Samples collected comprise of weak to moderate porphyritic diorites, andesites and dacite. Mineralisation appears to favour diorite host rocks within structures such as shear zones and silica veins with the occurrence of disseminated ore minerals present within most samples.

Similar alteration assemblages were seen across all deposits within the mine, with widespread quartz-albite alteration common, as well as quartz biotite or quartz sericite. The ore minerals display a paragenetic association with chlorite observed overprinting quartz albite alteration in samples from both north and south deposits. Visible sulphides are most commonly associated the presence of clinozoisite or actinolite when overprinting an earlier alteration or as a result of reactivation of structures. Quartz-albite veins were often seen together with quartz-biotite alteration, visible sulphides with clinozoisite, biotite and actinolite alteration containing selvages of quartz-albite. Quartz-albite alteration appears stronger in the North, whereas in the south quartz+sulphide veins are more abundant.

The dominant ore minerals are chalcopyrite and pyrrhotite. Such an assemblage is typical of an ore formed under slightly reducing conditions. Sphalerite, native bismuth, various Bi-Te species and electrum occur as inclusions within the main ore minerals, indicating that Au deposition occurred at the same time as crystallisation of the main sulphides. Cubanite exsolution as lamellae in chalcopyrite occur in most samples from both north and south parts of the deposit. Sporadic pyrite also occurs in samples from most domains and typically replaces pyrrhotite indicating pyrite crystallisation occurred later. Veins containing magnetite and carbonate occur in both the north and south and are coupled with this later pyrite mineralisation. The relationships suggest oxidising conditions during the later, pyritic overprinting. Flame-like exsolution of pentlandite in pyrrhotite is a feature observed only in the north diorite. These features are illustrated in Fig. 6. Exsolution of argentopentlandite in pyrrhotite was observed in sample NK20 from Pipeline (Fig. 7c). The Pipeline orebody has a strong Ni signature with a number of Ni-bearing minerals identified in many of the samples (Fig. 7a, b). Pyrite from this orebody also has a notable Ni contents (see section below and Table 3a). Arsenopyrite and arsenian pyrite were only seen in samples from Blackbutt and ABreccia, respectively.

Although visible gold/electrum occurs within both silicate and sulphide species, it has been observed predominantly as inclusions in sulphides and at grain boundaries between minerals. Grain size is generally less than 20 µm. Gold is most commonly observed enclosed within chalcopyrite, pyrite and pyrrhotite. Molybdenite was also observed to commonly contain inclusions of visible Au aligned along cleavage planes. Figures 8 and 9 show representative images of the gold mineralogy observed in the samples. Gangue

minerals that contain visible gold include actinolite and quartz. Within the gangue, gold is often in direct contact and included with native bismuth and often occurs as composite grains of bismuth+gold (see Fig. 10d) These associations occur at grain boundaries and within gangue predominately, however when observed in sulphides they occur along fractures and porous areas (as seen in Fig. 8f). The Au content of gold/electrum grains has a wide variation (see below) and may often show compositional variation with respect to Ag content within an individual grain (Fig. 9h).

As well as native bismuth, tellurides were also noted as an abundant trace mineral and are present in most samples. They occur mostly within gangue phases, but were also seen as inclusions in sulphides. The tellurides include various species of Bi-tellurides of the tetradymite group (Bi_xX_y, where X=S, Se, Te), but also Ag- and Pb-tellurides; hessite, volynskite, altaite, stützite, as well as varying amounts of selenides including clausthalite and naumannite. The Bi-tellurides and -selenides are rarely greater than 15 µm in size and are often complexly intergrown with one another. The tetradymite group of phases, in particular, are diverse (with many individual species observed) and are widespread throughout the deposit. Figures 11 and 12 illustrate representative images of the telluride mineralogy and associations; names are based on EDAX analysis and where possible were confirmed using microprobe analysis, as summarised in Tables 4 and 5, with the full data set tabulated in Appendix 3.

Molybdenite was seen as disseminations of euhedral laths in Blackbutt and North Diorite within the diorite host rock and quartz veins, commonly 100 µm in size. Molybdenite also occurred within shear zones that consisted of molybdenite with biotite and clinozoisite seen in the north diorite (Fig. 5d). Quartz veins with chalcopyrite, pyrrhotite, +/-pyrite, native gold and molybdenite were also present, the molybdenite within these veins occurs as euhedral laths and as shredded and kinked stringers encasing chalcopyrite grains and as inclusions within (Fig. 5e).

4.3 **Mineral chemistry Microprobe analysis**

4.3.1 MAIN SULPHIDES

Microprobe analysis of pyrite (Table 3a), shows elevated Ni and Co in pyrite from sample NK1, with up to 5.34 wt.% Ni in one analysis (full details are given in Appendix 4). Analysed pyrrhotite ($Fe_{1-x}S$ where ×=0.941 - 0.954) also contained some Ni and Co up to 0.14 wt.% and 0.05 wt.% respectively. While cubanite contained neither element above minimum detection limits (Table 3c). Arsenopyrite was only analysed from sample NK5 from ABreccia body and contains consistent amounts of Se and Co up to 0.37 wt.% and 0.85 wt.% respectively (Table 3b). Arsenopyrite displays no enrichment of Ni.

4.3.2 NICKEL AND COBALT BEARING PHASES

Analysis of cobaltite from samples NK16 and NK5 gave the empirical formulae $(Co_{0.56\text{-}0.78}Ni_{0.11\text{-}0.20}Fe_{0.10\text{-}0.20})_{0.96\text{-}1.00}As_{0.98\text{-}0.99}S_{1.01\text{-}1.05}$ when calculated on the basis of 3 atoms per formulae unit (a.p.f.u) (Table 3b).

Microprobe analysis of costibite from sample NK10 gave the empirical formulae $(Co_{0.63}Fe_{0.02}Ni_{0.30})_{0.95}Sb_{0.99}S_{1.01}$ when calculated on the basis of 3 atoms per formulae unit (a.p.f.u) (Table 3b).

Analysis of Ni-bearing minerals in samples NK20 and NK16 from Pipeline orebody allowed identification of the minerals argentopentlandite, with empirical formula $Ag_{0.90}(Fe_{5.28}Ni_{2.53})_{7.81}S_{8.19}$ (calculated to17 a.p.f.u), the rare Ni-Bi-sulphide parkerite with empirical formula $(Ni_{2.80\text{-}2.90}Co_{0.01\text{-}0.02})_{2.81\text{-}2.92}Bi_{1.94\text{-}1.98}S_{2.00\text{-}2.04}$ (calculated to7 a.p.f.u) and a further unnamed Ni-(Fe)-Bi sulphide mineral with formula $[(Ni_{1.79}Fe_{1.25}Co_{0.12}Cu_{0.54})_{3.70}Bi_{1.32}]_{5.04}S_{2.96}$ if calculated to 8 a.p.f.u. (see Table 6). Edax analysis also allowed identification of the mineral breithauptite (NiSb) in sample NK20. Violarite ($FeNi_2S_4$) was also identified in sample NK16, however poor EPMA totals for this mineral did not allow for its stoichiometry to be documented.

4.3.3 GOLD/ELECTRUM

Microprobe analyses of native gold grains show up to 0.44 wt. % Hg in one grain. Analysed electrum typically gives 40 wt. % Au and 60 wt. % Ag. Such a ratio was also commonly observed in electrum during EDAX analysis. Other Au:Ag ratios were, however, noted, with Ag contents as high as 70 wt.% and as low as 20 wt.%, indicating there is some variation within the deposit. Gold grains occurring within molybdenite (Fig. 8a) and associated with native bismuth typically gave compositions approaching 95 wt.% Au (Table 7).

Bismuth levels were also high in some gold/electrum. Individual analyses gave up to 35.52 wt. % Bi (corresponding to $Au_{2.14}Bi_{0.63}$ when calculated to a.p.f.u of 3), but this is almost certainly a mixed analysis resulting from complex intergrowth of gold and bismuth or gold and maldonite (Au_2Bi) (Fig. 13). The mineral maldonite (Au_2Bi) was observed in the studied concentrate but not in the rock samples.

4.3.4 TELLURIDES/SELENIDES

Electron probe analysis showed that a suite of compositionally different Bi-tellurides and related –sulphides and –selenides of the tetradymite group are present within the sample suite. The tetradymite group is a complex, homologous series of layered compounds with general formula Bi_xX_y where X=Te, Se,S (Cook *et al*. 2007a; Ciobanu *et al*. 2009). The group displays varying stoichiometry from Bi-rich members such as hedleyite (ideally Bi_7Te_3) to Te-rich end-members such as tellurobismuthite (Bi_2Te_3) (Fig. 12a). Lattice-scale disorder is common within the group, leading to non-stoichiometric compositions. In addition, there are various compositions which do not correspond to named minerals, but which are nevertheless homogeneous and may, in the future, become accepted mineral species once their crystal structures have been determined.

In the Boddington samples, a full range of compositions across the series have been confirmed (Tables 4 and 5; Appendix 3). Compositional variations among Bi-tellurides of the tetradymite group are shown on Fig. 14 in terms of Bi-Te-(S+Se).

Hedleyite, Bi_7Te_3 is observed in samples NK2a, -b and –d (Central diorite). The empirical compositional range was $Bi_{6.93\text{-}7.46}Te_{3.07\text{-}2.51}$ (calculated to 10 a.p.f.u), In addition, compositions extending to Bi_8Te_3 (empirical composition $(BiPb)_{8.01}Te_{2.99}$ at 11 a.p.f.u) were observed in NK2d and to Bi_2Te in NK2b and NK3 in the Central diorite (formula range $Bi_{1.97\text{-}1.99}Te_{1.01\text{-}1.04}$ at 3 a.p.f.u) and NK30 in the northern diorite (empirical formula $Bi_{5.90}Te_{3.09}$). In both cases, deviation from ideal composition is best attributed to lattice-scale disordering (Cook *et al*. 2007a; 2007b), although there is also evidence for a homogeneous, unnamed Bi_2Te phase. Additionally, other compositions with a Bi_2X stoichiometry were measured: $Bi_2(Te,S)$ (empirical formula $Bi_{1.93}(Te_{0.59}S_{0.48})_{1.07}$ at a.p.f.u 3), $Bi_2(Te,S,Se)$ (empirical formula $Bi_{1.97}(Te_{0.6}6S_{0.18}Se_{0.17})_{1.01}$ at a.p.f.u 3) and $Bi_9Te_4Se_2$ (empirical formula $Bi_{9.05}Te_{3.69}SeS_{2.26}$ calculated to 15 a.p.f.u). Similar compositions have been described elsewhere

(Cook *et al*. 2007a; 2007b) but do not correspond to named minerals. Unnamed $Bi_9Te_4Se_2$ was observed only in a sample from ABreccia.

Three members of the Bi_4X_3 sub-group (Fig. 14b) have been analysed. These are pilsenite, Bi_4Te_3, with empirical compositional ranges $(Bi,Pb)_{4.10\text{-}4.24}Te_{2.90\text{-}2.89}$ and $Bi_{3.81\text{-}4.14}Te_{3.18\text{-}2.86}$ in the south pit and north pit, respectively (laitakarite, $Bi_4(Se,S)_3$ with empirical compositional range $Bi_{3.87\text{-}4.03}(Te_{0.30\text{-}0.52}Se_{2.21\text{-}2.33}S_{0.23\text{-}0.56})_{3.13\text{-}2.97}$ and ikunolite with empirical compositional range $Bi_{3.92\text{-}4.04}(S,Se)_{3.08\text{-}2.96}$. Laitakarite was confirmed only in the Central diorite, ikunolite only in the Northern Diorite.

Tsumoite, ideally BiTe, was analysed in samples from both Central Diorite and Northern Pit. The empirical compositional ranges were $Bi_{0.95\text{-}1.06}Te_{1.05\text{-}0.94}$ and $Bi_{1.05\text{-}1.08}Te_{0.95\text{-}0.92}$, respectively, calculated to 2 a.p.f.u. A phase with consistent and apparently homogeneous composition $(Bi_{5.42\text{-}5.63}Pb_{0.30\text{-}0.42})_{5.87\text{-}5.98}Te_{5.13\text{-}5.02}$ (7 a.p.f.u) was observed in northern pit drillcore. This corresponds to ideal $(BiPb)_6Te_5$, currently an unnamed phase, and probably a S-free analogue of the named species baksanite, $Bi_6Te_2S_3$. The same sample also contained a second unnamed composition, ideally Bi_5Te_3 (compositional range $Bi_{5.08\text{-}5.20}(Te_{1.68\text{-}2.68}Se_{0.18\text{-}0.75}S_{0.02\text{-}0.51})_{2.92\text{-}2.80}$ calculated to 8 a.p.f.u.). Two further compositions that do not correspond to named minerals were seen in samples from Central Diorite. These are Bi_5Te_4 (empirical formula $Bi_{4.80}Te_{4.20}$ at 9 a.p.f.u) and Bi_4X_5 (empirical formula $Bi_{4.03}X_{4.98}$ at 9 a.p.f.u.). The two probe analyses on each are insufficient to confirm whether these are consistent compositions (and thus discrete phases) or simply a disordered variant of a named mineral such as tsumoite.

Tellurobismuthite, ideally Bi_2Te_3, was analysed only from a single sample from the Central Diorite ore body. The empirical compositional range is $Bi_{1.98\text{-}2.02}Te_{3.02\text{-}2.98}$, calculated to 5 a.p.f.u.

Other Te-bearing species identified and confirmed by EPMA (Table 5) are: hessite, ideally Ag_2Te (empirical formulae $Ag_{1.98\text{-}2.00}Te_{3.02\text{-}1.00}$, $Ag_{1.98}Te_{1.02}$ and $Ag_{2.01}Te_{0.98}$ in samples from Central Diorite, North Diorite and ABreccia, respectively; volynskite, ideally $AgBiTe_2$ (empirical formula $Ag_{1.47}Bi_{0.73}Te_{1.78}$, calculated to 3 a.p.f.u), seen in the Central Diorite only; and altaite (PbTe) with near perfect stoichiometry in both Central Diorite and Pipeline.

Clausthalite (ideally PbSe) was analysed in samples from Central Diorite, Pipeline and ABreccia. Compositions were very close to ideal stoichiometry in all cases, but significant S-components in both the Central Diorite and ABreccia samples**.** The empirical compositional ranges were $Pb_{0.99\text{-}1.02}Se_{0.65\text{-}0.75}S_{0.24\text{-}0.33}$ (Central Diorite), $Pb_{1.02}(Se_{0.94}S_{0.01}Te_{0.03})_{0.98}$ (Pipeline) and $Pb_{0.98\text{-}0.99}(Se_{0.77\text{-}0.79}S_{0.22\text{-}0.24})_{1.01\text{-}1.03}$ (Fig. 15b).

Compositional variation among Bi-tellurides of the tetradymite group are shown on Fig. 14 in terms of both stoichiometry (Bi:X ratio) and also variation between Te, Se and S. The compositions of the Ag-tellurides are shown diagrammatically on Fig. 15.

4.4 **Study of copper concentrates**

Boddington mine currently produces a copper concentrate and gold doré, the Cu concentrate is produced using flotation methods and there are currently stockpiles that compose of a high-Cu, low-Bi product (ConcA A) and a problematic higher-Bi, lower-Cu concentrate (ConcB). Two samples of copper concentrate (ConcA/B) were prepared in a similar way as rock samples for similar analysis, and an area of approximately 1 cm² was analysed by SEM rastering at high magnification. The assay results (Table 2) show that there is indeed a detrimentally high level of Bi in ConcB (734 ppm), as well as higher Au concentrations (132 ppm). Silver, As, Mo, Ni, Sb, Te and Zn are also higher in ConcB. Investigation by SEM revealed the following ore minerals in the concentrates; pyrite, chalcopyrite, scheelite, galena, pyrrhotite, cubanite, arsenopyrite, cobaltite and molybdenite. In ConcA, 14 grains of native gold and electrum were observed; eleven grains were identified in ConcB. The following bismuth minerals were observed; native bismuth (ConcA, 76 grains; ConcB, 80 grains), Bi-Tellurides of the tetradymite group (ConcA, 9 grains; ConcB, 11 grains) and maldonite (7 grains in ConcA, 3 grains in ConcB). These are shown in Fig 10e, f). The size and liberation characteristics of the gold and bismuth minerals are summarised in Appendix 5 and size distributions of the phases are displayed on histograms in Fig. 16.

The results show that the speciation of bismuth is varied in the concentrates, even if native bismuth is by far the most abundant phase. These observations echo the findings in the ore samples. These data are evaluated in the context of the bismuth concentrations in the concentrates (assay data, Table 2) in the 'Discussion' section.

4.5 **LA-ICPMS trace element data**

4.5.1 PYRITE AND ARSENOPYRITE

Primary pyrite and arsenopyrite that occur within Cu-Au mineralisation are accessory phases in the Boddington deposit and although absent in most samples, were noted in samples from the North pit. Primary pyrite with compositional zonation with respect to As was seen in sample NK26. This sample consists of a quartz-albite assemblage carrying pyrite with a mylonitic fabric. Images of examples of these grains can be seen in Fig. 7 d), e).

LA-ICPMS analysis of 21 spots (Table 8) show this pyrite carries very minor amounts of gold. The average Au concentration is 1.0 ppm, with a maximum of 3.0 ppm. The time-resolved LA-ICPMS depth profile (Fig. 17 a) does, however, confirm that this Au is in solid solution within the pyrite, since the Au spectrum is flat and elevated well above background levels. The measured Au concentrations show a positive correlation with As concentrations (Fig. 17 b), but at levels well below the solubility limit of Au in pyrite (Reich *et al.* 2005).

Zoned arsenopyrite in sample NK24 was also analysed by LA-ICPMS (Table 9). The highest recorded value was 59 ppm, but the other points were all <5 ppm, giving a mean of 17 ppm for the five points. As for pyrite, the Au values show a positive correlation with As (Fig. 17 b). These trends are discussed further in the "Discussion" section.

4.5.2 MOLYBDENITE

LA-ICPMS analysis of molybdenite in five samples from different parts of the deposit demonstrates that the mineral carries significant concentrations of a range of trace elements, including Re, Au, Bi, Ag, W, Sn, Ni, Pb, Fe, Cu, Se and Te (Table 10) (Appendix 6). The concentrations of these elements and the trends among the concentrations in the different samples have implications for understanding ore genesis.

Mean Re concentrations vary markedly from 5.3 ppm in the sample from the granite (molybdenite as a disseminated clot within granite some chalcopyrite-pyrrhotite was also present in the granite) to a mean concentration of 669 ppm in NKmoly (molybdenite shear zone in ABreccia body). All ore samples are strongly enriched in the element, typically several hundreds of ppm (Fig. 18), although the disseminated molybdenite from the Blackbutt sample was somewhat lower than those from the veins and shears. The smooth time-resolved depth profiles indicate that Re is in solid solution within molybdenite throughout all samples (Fig. 19a,b). The highest single data spot gave a concentration of 2,449 ppm Re.

Molybdenite from Boddington is also characterised by extremely high concentrations of Au. Similar to Re, the granite sample is by far the lowest (mean 0.19 ppm), but the Blackbutt (mean 6.9 ppm), ABreccia samples (means 32.9 and 70.5 ppm Au), and especially the Central diorite molybdenite (mean 110.2 ppm Au) are very strongly enriched in gold. In the latter sample, the maximum concentration in a single spot was 2,712 ppm. Such concentrations of gold are exceptionally high for molybdenite, or indeed for any sulphide mineral. Even though some of the time-resolved depth profiles in sample NK25 are flat (Fig. 19a), many of the higher concentrations are best attributed to fine-grained gold particles located along molybdenite cleavages and in fractures. Visible gold inclusions are seen as pronounced spikes on some of the profiles (Fig. 19b). Molybdenite is not generally recognised as a significant host for gold, yet the mineral does seem to concentrate gold, with other occurrences known (Cook and Ciobanu, unpublished data).

The Boddington molybdenite also contains appreciable concentrations of Bi, Te, Cu and Fe, again especially in the Central diorite sample (NK21), where high Ag values and elevated Sn contents are also noted. Molybdenite containing large concentrations of trace elements such as Au, Bi, Te, Ag etc. has been referred to as ‘dirty’ molybdenite and probably contains sub-microscopic inclusions of different minerals containing these elements. Trace element inclusions in molybdenite, particularly in the less common 3R polytype, have been discussed by Newberry (1979a). Here, we can speculate that inclusions of minerals such as maldonite and Bi-tellurides (also Ag-tellurides?) may be present, even if the LA-ICPMS profiles are flat for the elements of interest. Evidence for the presence of maldonite, electrum and Bi-tellurides can be seen in the excellent visible positive correlations between Bi and Au (Fig. 20a), Ag and Au (Fig. 20b) and Bi and Te (Fig. 20c). This can indicate that these minerals are both very fine and are more or less homogenously distributed at the scale of the laser spot. Other elements, such as W, Se and Re are also elevated throughout the dataset, but are generally regarded to reside in the molybdenite lattice and not as submicroscopic inclusions (e.g. Newberry 1979a; 1979b).

The LA-ICPMS element map of one large grain of molybdenite (believed to be a single crystal) from sample NK21 (Central diorite) illustrates that all of the elements discussed above are inhomogeneously distributed in the molybdenite. This may be further evidence for sub-microscopic inclusions of other minerals and their possible clustering into distinct zones within the grain or for overprinting of initially homogeneous patterns during a fluid-assisted remobilisation event (Fig. 21). Note in particular the zones of high- and low-Re, the

distribution of Au, Ag and Te (broadly coincident with one another) in small patches within the molybdenite, and the very heterogeneous distribution of Se in the mapped grain.

Although trace element data for molybdenite was only collected on five samples, the results show a striking pattern with respect to concentration of Re, Au, Bi etc. and position relative to the granite. Binary plots of individual element pairs in molybdenite can be instructive to show patterns within the dataset. Although absolute concentrations of neither element are especially high, the plot of Ni vs. Co (Fig. 22) demonstrates an excellent discrimination between each sample (i.e., location) as well as an increase in Re content away from the monzogranite (Figs. 3 and 23). The significance of these data, in particular how this constrains the role of granite in ore genesis, will be discussed further in the 'Discussion' section.

5. DISCUSSION

5.1 Tetradymite-group minerals as indicators of physicochemical conditions of formation

The tetradymite group of minerals is a complex homogeneous series of mixed layer compounds with rhombohedral or trigonal symmetry encompassing compositions from Bi_2X_3 to Bi_8X_3, where X=Te,Se,S. Discrete minerals within the series are composed of layers of five-atom Bi_2Te_3 units and two-atom Bi_2 layers. Phases from the Bi_4X_3 sub-group (or 'isoseries') thus consist of regular alternations of the two layer types. Each stoichiometric increment within the tetradymite group is represented by an isoseries with a defined Bi:X ratio – pilsenite (Bi_4Te_3), ikunolite ($Bi_4(S,Se)_3$), laitakarite ($Bi_4(Se,S)_3$), joseite-B (Bi_4Te_2S), and joseite-A, (Bi_4TeS_2), are thus the five named minerals within the Bi_4X_3 isoseries (Cook *et al.* 2007a; 2007b; Ciobanu *et al*. 2009).

Minerals of the group can be both ordered and disordered, i.e., display lattice-scale inhomogeneity. Any infinitesimal change in composition can theoretically be stabilised by modifications to the stacking sequence, commonly giving rise to non-stoichiometry. Their homotypic character also allows them to adapt readily to changes in physicochemical conditions and to local variations in Bi and Te from an ore-forming fluid. Their speciation thus has potential as an indicator of evolving conditions within a deposit. In many deposits, only a single species, or a narrow range of species is present – phases like tellurobismuthite (Bi_2Te_3) or tetradymite (Bi_2Te_2S) reflect more oxidising conditions, whereas phases in the compositional range between pilsenite (Bi_4Te_3) and hedleyite ($Bi_{6\text{-}8}Te_3$) are restricted to reduced systems. The latter minerals commonly coexist with native bismuth or maldonite while native bismuth should not appear in equilibrium with tellurobismuthite or tetradymite as was observed and illustrated in (Fig. 9d) implying incomplete reactions during an overprinting event. The presence of compositionally distinct members of the series within a single deposit, textural evidence for reaction among Bi-tellurides, or the presence of disordered, non-stoichiometric compositions can be taken as evidence for a multiphase origin (Ciobanu *et al.* 2009; 2010).

The Boddington deposit contains tetradymite-group minerals from across the full compositional range of the series (Figs. 14a and 24a), as well as probable disordered, non-stoichiometric compositions that do not correspond to named minerals. This diversity, coupled with strong variation in the associations of these minerals and reaction between phases in the group, clearly show that the Boddington deposit is not the product of a single ore-forming event, but rather suggests discrete events during the evolution of the deposit, as well as showing the major role that lithology played during ore genesis. Clarke (1997) earlier noted the

presence of tsumoite, $Bi_{0.96}Te_{1.04}$, and altaite, $Pb_{1.05}Te_{0.95}$, at Boddington. He also recognised aleksite ($PbBi_2Te_2S_2$), and made the discovery of a new mineral, saddlebackite ($Pb_2Bi_2Te_2S_3$), as well as an unnamed phase with composition $Pb_{0.98}Bi_{3.64}Te_{4.32}S_{2.86}$. This further emphasises the great diversity in bismuth mineralogy at Boddington. It is evident that the wide variation in species relates to localised closed systems across the deposit where phases have been preserved, remobilised, overprinted or reformed at varied, and probably highly localised, physico-chemical conditions. The character of the fluids which impacted on the assemblages would, in turn, have depended on lithology, fluids pathways, type and source of fluids and distance from source.

The natural variation in mineral assemblage is exemplified by the North pit, which is split into four domains and from which two were sampled together with samples of drill core that form part of the North Diorite ore body. The North Diorite ore body contains telluride assemblages BiTeSeS+galena+Au, Bi_2TeS+Au in actinolite (sample NK18), Bi+Au, Bi+Ikunolite, BiTeSe+galena as possible melt droplets occurring in a melt trail and fracture infill shown in sample NK30 (Fig. 10c, d), Bi+galena, Bi+hessite+galena, Bi+AgSbS in drill core (sample NK8), Bi+ullmannite in sample NK14, Bi+galena as symplectite like intergrowths in drill core sample NK9 (Fig. 12d), pilsenite+galena, tsumoite, and unnamed $(BiPb)_6Te_5$ and Bi_5Te_3 in drill core NK10. The ABreccia ore body has assemblages electrum+cobaltite (Fig. 8b), Bi+hedleyite+electrum in biotite, bismuth+electrum with a reaction zone between the two where the contact of the two has the composition $Au_{60}Ag_{40}$ and away from the contact the ratio is reversed (Fig. 9h), Bi+hessite+clausthalite+$Bi_9Te_4Se_2$ with textures associated with the alteration of Bi and the immiscibility of the telluride species at formation/overprinting conditions in sample NK22 (Fig. 11g). A similarly diverse set of assemblages is seen in the South pit, also made up of four domains, and from which three were sampled. Central diorite is the main orebody (Fig. 3) and samples from this location had the most diverse range of species (Fig. 14 a, b), including intimate associations of Bi+galena+AgS (NK1), Bi+hessite+altaite and Bi+electrum (NK2a), Bi+tellurobismuthite with a reaction boundary explained by the fact that these minerals are not stable together, Bi+hedleyite+hessite, Bi+Bi_5Te_4+Bi_2Te also with reaction boundaries, Bi+hedleyite+tsumoite+hessite with reaction boundaries, hedleyite+clausthalite with Bi exsolution (Fig. 11f), Bi+altaite with symplectite like intergrowth (Fig. 11e), hedleyite+hessite, hessite+Bi+volynskite+tsumoite with reaction textures and Bi+electrum (sample NK2b), Bi+hessite+hedleyite+Bi_8Te_3, hedleyite+galena+Bi+electrum, Bi+tellurobismuthite+Au with reaction boundary (Fig. 9d), clausthalite+hessite+Bi+hedleyite, Bi+hessite+electrum and Bi+electrum (sample NK2d). Sample NK3 contains pilsenite, Bi+hedleyite, while sample NK4 contains Bi+hessite+tetradymite+volynskite, hessite+Laitakarite+Bi+Bi_4X_5.

Without detailed crystal-structural data, it is difficult to say with certainty whether the unnamed phases identified are new, additional members of the tetradymite group, or instead are caused from lattice-scale intergrowths of ordered phases, or even completely disordered. Their presence though, as well as the reaction textures involving replacement of one telluride by another, is however, strongly suggestive of reaction between crystallised minerals and fluids during an overprinting event. In all cases, this reaction appears to be incomplete, with non-equilibrium conditions preserved.

The overwhelming evidence from textures and associations seen in the Bi-tellurides is a change from reducing (hedleyite-stable) to oxidising conditions. The noticeable rarity of otherwise common S-bearing tetradymite-group minerals such as joseite-B is explained by low fS_2 during overprinting; all S presumably locked within pyrrhotite and other sulphides and which did not become mobile. The reactions identified probably took place in the solid state as stability ranges for the phases concerned increase from the Bi-rich

side of the Bi-Te phase diagram (Okamoto & Tanner 1990) towards the Te-rich end (Fig. 24a). This is concordant with the fact that some of the Bi-tellurides observed do not occur as blebs (i.e., implying deposition from melt; see next section) but rather as subhedral grains. The mineral saddlebackite (a mineral first described from Boddington; Clarke 1997) was not seen in this study, but intergrowths of Bi +/- Te and galena could be the result of breakdown of saddlebackite or another member of the aleksite group (a Pb-bearing parallel series; (Cook *et al.* 2007b). Another mineral not seen, but plausibly present, is jonassonite ($AuBi_5S_4$), which should be stable under reduced conditions, but may have decomposed during reaction with oxidising fluids and releasing Bi +/- Au.

The change from reducing to oxidising conditions is also evidenced by the occurrence of abundant pyrrhotite relics as inclusions in pyrite indicating pyrrhotite was the initial iron sulphide.

Associations among other tellurides also help constrain the sequence of crystallisation. Hessite is stable in three structural modifications giving rise to its broad stoichiometry at temperatures up to 960 °C, $Ag_{2-x}Te_3$ is stable at 120 °C to 420 °C and decomposes to hessite and stützite (Afifi *et al.* 1988).

This wide telluride mineralogy, apparent non-stochiometry and evidence of reaction among the trace minerals, possibly at varying pressure and temperature conditions, is concordant with the sequence of initial formation and subsequent overprinting events proposed for Boddington on the basis of fluid inclusion studies. The data of McCuaig *et al*. (2001), for example, reveals a fluid history for Boddington deposit in which mineralisation initially formed by exsolution of a magma-derived volatile-rich fluid at ca. >600 °C and 1.5 kbars, and emplacement during structurally-induced cooling of the magmatic fluid and depressurisation with boiling over a broad P-T range (~300 - 550 °C, 0.6-0.15 kbar). Later fluid inclusions were recognised that are not directly related to the initial deposition of mineralisation, but could have resulted from collapse of the hydrothermal system with the incursion of meteoric water (at 150-300 °C). A later overprinting of the mineralisation by a late carbonate-rich fluid at ca. 300 °C is also recognised.

5.2 **Bismuth-gold assemblages and the role of bismuth as a gold scavenger**

An intimate association of Bi-minerals with Au-minerals is a feature identified in a broad range of mineral deposits ranging from skarn and reduced intrusion-related gold deposits (RIRG) and, less commonly, in some epithermal and orogenic gold deposits, particularly those formed or metamorphic-overprinted at temperatures exceeding 300 °C (Hart 2007). Such an association is a widespread and common feature of almost all samples from Boddington which have been investigated in this study. As has been shown in Figs. 8, 9 and 10, the strong association between the two elements is seen both at the scale of individual mineral associations and paragenesis, but also in the geochemical data (e.g. correlation plots of Au vs Bi; Figs. 4, 10 and 20a).

Relatively recently, this strong relationship between Au and Bi has been explained in terms of the generation of bismuth melts within the ore during metamorphic overprinting (Ciobanu *et al*. 2006a; 2010). Underlying the concept of melt generation is the rather low melting point of bismuth (271 °C) and the observed tendency for Bi-droplets to scavenge gold from fluid. Textures among Au- and Bi-minerals suggestive of deposition in the form of melts have been given in a number of studies (Ciobanu *et al*. 2005; Ciobanu *et al.* 2006a; Tooth *et al*. 2008). Bismuth is thus considered a powerful scavenger for gold if conditions favour melt generation and Bi-melts have been proven experimentally to scavenge gold from fluids undersaturated in Au (Douglas *et al.* 2000). Tellurides may also be a prominent component of such assemblages, indicating that Au-

Bi-Te melts can be considered analogous to simple Au-Bi melts (Ciobanu *et al*. 2005). Gold-Bi-Te melts can incorporate as much as 43 wt. % Au at the eutectic at 447 °C in the Au-Bi-Te system (Prince *et al*. 1990) and will act similarly to native bismuth in natural systems. In fact, additional impurities (e.g., Sb, Ag etc.) may actually reduce the melting temperatures in complex multiphase systems. Bi melts can scavenge gold from a pre-existing source that may not itself be particularly rich if the metamorphic event is at conditions above greenschist facies ~400 °C (Ciobanu *et al*. 2006a; 2006b). Once mineral precipitation commences, bismuth can remain as a mobile melt and will continue to scavenge Au until crystallisation is complete.

There is substantial evidence for the involvement of Bi-based melts at Boddington, which was formed and/or overprinted at temperatures which overlap those associated with melt generation. Of particular note are the multiphase droplet-like inclusions of Au and Bi (+/- Te) minerals, with characteristic curvilinear boundaries between coexisting phases (Figs. 9 e, f and 10d). These strongly suggest precipitation from a melt that has scavenged Au either from circulating fluids or from pre-existing ore, with phase separation occurring at the eutectic point during cooling of the assemblage.

From the phase diagram of the binary system Bi-Au (Fig. 24b), it can be seen that a Au-Bi melt will crystallise as Bi + maldonite at 241 °C. Bi melts can more efficiently incorporate Au under reducing conditions (Tooth *et al*. 2008) and maldonite will be stable under reducing conditions, such as those seen in the chalcopyrite-pyrrhotite assemblages at Boddington. Upon cooling, a Bi- (Bi-Te, Bi-Au-Te) melt will record assemblages according to the binary phase diagrams for the respective phase systems. For example, a melt initially formed at 400 °C will record three eutectics Bi+hedleyite at 266 °C, Bi+maldonite at 241 °C and Bi+hedleyite+maldonite at 235 °C. From the Au-Bi phase diagram a bismuth melt will form Au+maldonite from 113-375 °C at 35 wt. % Bi and maldonite + Bi at the eutectic below 241 °C, with Au+Bi crystallising below 113 °C. Assemblages formed at the eutectic will show symplectite textures if they are rapidly cooled or if obtained via exsolution. When the cooling rate is slow, as may be expected in a system such as Boddington, assemblages will display classic triple joint intersections between the phases formed at eutectic (Ciobanu *et al*. 2006a). Symplectites of native bismuth and gold have also been explained by pseudomorphic replacement of maldonite during disequilibrium reactions with fluids (Ciobanu *et al*. 2010).

The close association of Au and Bi throughout the Boddington ore and the fact that this was also mirrored in the copper concentrate testifies to the likely significance of melts during the evolution of the deposit. The mineralogical inhomogeneity of the deposit, however (for example the identification of maldonite within the concentrate only, the absence of tellurides in some Au-Bi assemblages, or the exceptionally wide variation in Bi-telluride speciation), indicates that both physicochemical conditions and melt compositions were highly localised.

Since the copper concentrate is representative of the mineralogy of the current ore processed, maldonite is undoubtedly present within the Boddington system, but its importance as a Au-carrier mineral cannot be quantified, with additional work necessary. Its presence does, however, provide additional strong evidence for the occurrence of a Au-scavenging Bi-based melt, either during initial ore deposition, during syn-metamorphic or syn-granite emplacement, remobilisation, and may have been a factor present during all stages of overprinting and mineralisation. The observed assemblages are best attributed to a latest-stage remobilisation along the retrograde path. The abundance of the Au-Bi association in actinolite-dominant host rocks, and occurrence of one maldonite grain in the concentrate attached to actinolite, point to the importance of both a reducing environment and enhanced fluid flow regime during retrograde metamorphism. It is also possible that

maldonite was initially more abundant but that reworking led to the destruction and instability of maldonite across much of the deposit, resulting in release of Au and possible further scavenging by bismuth, giving rise to compound grains of native bismuth and gold but without tellurides if fTe_2 was not sufficiently high at that stage in the deposit evolution to reach the stability field of Au- or Bi-telluride species.

5.3 **Role of shearing and actinolite-dominant lithologies**

On the mine scale, actinolite is commonly identified as associated with higher Au grade, even if barren actinolite-dominant assemblages are also identified. The actinolite-dominant zones would have acted as conduits for fluid, especially during the retrograde part of the metamorphic cycle when it is reasonable to expect that substantial remobilisation of the more mobile components (Au, Bi, Te, probably also Ni) took place. These shear zones probably reactivated and exploited earlier zones of weakness. A scenario can be envisaged in which Au was scavenged and remobilised by bismuth within the shear zones, upgrading the mineralisation along these structural corridors. The mineralised actinolite-dominant shear zones commonly also contain scheelite, which would indicate a granitic source, implying that fluids from the granite served to remobilise and upgrade pre-existing metal endowments and may not themselves be a primary metal source.

5.4 **Pyrite and arsenopyrite as gold carriers**

LA-ICPMS analysis of pyrite that exhibited arsenic zonation gave results showing the presence of solid solution gold, but only at concentrations of 0.5 ppm Au to 3 ppm, with a mean concentration 1 ppm Au (Table 8). This is extremely low and taken together with the relative scarcity of primary pyrite in the deposit, infers that invisible gold locked in the lattice of pyrite does not present any issue that would affect processing or low gold recovery. It is generally accepted that although primary pyrite, e.g., in epithermal deposits, may concentrate significant “invisible gold” (Cook & Chryssoulis 1990), this gold is generally expelled during regional metamorphism or during mineral transformation. The latter, as well as chalcopyrite, the other common sulphide seen at Boddington, are regarded as a very poor host for gold (Larocque *et al*. 1995), while this pyrite is not carrying any significant amount of Au it is likely due to the fluids that formed the pyrite were not of mineralising fluids and it is most likely from the formation of discrete mylonites (D2) with silica-albite-pyrite alteration as recognised by (McCuaig *et al*. 2001). The arsenopyrite analysed in this study also gave low gold values (Table 9) and is not a significant Au-carrier in the deposit due to low presence in most samples and low values given in LA-ICPMS results. Au values measured within both pyrite and arsenopyrite while low did conform to the generally accepted “invisible gold” description where Au is incorporated into the crystal lattice of pyrite and arsenopyrite where the solid solution of As for S increases the ability for Au to be incorporated into the crystal lattice, however Au is well below to proposed solubility limit within pyrite with respect to its As values put forth by Reich *et al*. (2005) as shown in (Fig.17b) and the LA-ICPMS profile indicating Au is in solid solution (Fig. 17a).

5.5 **Ni Co species + exsolution**

This study has shown that Ni-Co-minerals are accessory minerals at Boddington and that the main sulphide minerals may also carry relatively high levels of the two elements, with pentlandite lamellae exsolution in pyrrhotite a common feature. These observations strongly suggest the introduction of nickel into the deposit from a fluid that originated from a mafic/ultramafic source and not from a granitic fluid. Nickel is a highly mobile element (Cook 1992) and breakdown of pre-existing nickel minerals (during granite intrusion and/or regional

metamorphism) would have led to redistribution of the element. It is noted that at least two Ni-Bi minerals are present, as well as Ni-Sb compounds. These could be products of remobilisation of Ni and subsequent recrystalisation as 'new' minerals in combination with other more mobile elements such as Bi. Of the Ni-bearing minerals, parkerite is particularly notable (Fig. 7b), as it is a rare mineral, whose occurrence is generally restricted to Cu-Ni-PGE deposits associated with mafic/ultramafic rocks (e.g., Sudbury, Norilsk) and hydrothermal Ni-Co deposits (Anthony *et al*. 1990). There is only one previous confirmed occurrence of the mineral in Australia; the Otway Ni-deposit, Pilbara Region, W.A. (Marsden 1984). The unnamed phase reported $(Fe_{1.25}Co_{0.12}Ni_{1.79}Cu_{0.54}(BiPb_{1.32}))_{5.04}S_{2.96}$ is potentially a new mineral, since no known mineral has such a composition. However probe results on a single grain are not means for interpretation of such a thing and detailed crystallography would need to be conducted, this would most likely not be possible as the grain is only around 4 µm in diameter.

5.6 **Molybdenite geochemistry and constraints on ore genesis**

As noted by Allibone *et al*. (1998) the features of the Boddington deposit are distinct from others in the Yilgarn Craton and are also often conflicting. As a result, is has proven difficult to satisfy all necessary criteria for classification of the deposit within a single model. The genesis of the Boddington deposit has traditionally been considered as an Archaean porphyry system with the intrusion of host rocks in an early arc sequence (Roth *et al*. 1990; Roth 1992). The first model for Boddington as an epigenetic, structurally-controlled deposit formed later than host rocks has been based on cross cutting relationships and was outlined by Symons *et al*. (1988). Allibone *et al*. (1998) also suggest that cross-cutting relationships imply Au-Cu mineralisation occurred later than the host rocks and do not support a porphyry system, but rather that mineralisation is associated with intrusion of pyroxene dykes and the late monzogranite. The main mineralisation at Boddington appears to have formed after the host volcanic and volcaniclastic rocks (Allibone *et al* 1998; McCuaig *et al*. 2001) but does not rule out the possibility of precursor porphyry system. McCuaig *et al*. (2001) suggest the later mineralisation is conformant with the intrusion of a late post tectonic monzogranite and puts Boddingtons genesis as a structurally-controlled intrusion related gold deposit, with Boddingtons mineralogy this would then be considered an Archaean example of a reduced intrusion-related gold system (Hart 2007; Duuring *et al*. 2007).

Re/Os molybdenite ages for Boddington were published by Stein *et al*. (2001), the authors suggested two temporally distinct, and therefore geologically and tectonically seperate periods for Au mineralisation at Boddington with initial mineralisation at 2707 +/- 17 Ma and main stage of Au mineralisation at 2625-2615 Ma. The first of these (2707 +/- 17 Ma) is concordant with the intrusion of the host rocks at (~2714-2696 Ma) rocks in an island arc setting this suggest an initial porphyry style deposit associated with convergent plate boundary (Roth 1992). At around 2675 Ma, a volcanic-intrusive event occurred following two periods of deformation and is considered analogous to the orogenic gold-forming event seen widely throughout the Yilgarn. Following these events, the deposit suffered subsequent deformation and formation of the greenstone belt 2640 Ma of shearing with later brittle faulting and was intruded by late non-mineralised Wourahming monzogranite at ~2611 Ma (McCuaig *et al.* 2001).

The pronounced Re enrichment in molybdenite is in agreement with a porphyry-type mineralisation. This conceptual model currently stands as the optimal way in which to explain observed features (see Fig. 18, Table 10 and Appendix 5).

McCuaig *et al*. (2001) model for Boddington as a Reduced Intrusion-Related Gold Deposit (RIRG) is an alternative to the porphyry deposit. Deposits of this type are exceptionally rare in Archaean or Proterozoic rocks. This, together with the fact that Boddington lacks many of the key features of RIRG deposits, led Hart *(2007*) to question whether Boddington really is a RIRG deposit in his review of this mineral deposit type. McCuiag *et al*'s (2001) model involved two overprinting magmatic-hydrothermal systems with the later associated with the bulk of the mineralisation.

The genesis of the Boddington mineralisation is unequivocally multi-phase with a broad range of fluids and overprinting but it remains untested whether the ~2611 Ma monzogranite contributed metals to the ore system, or merely supplied fluids which may have assisted in a further remobilisation of parts of a pre-existing orebody. This study reports a systematic increase in Re content away from the granite (see Figs. 3 and 23). With the molybdenite sample from a disseminated clot within the monzogranite itself having the lowest Re content. If the monzogranite had supplied Mo (and other metals), it might be expected that the highest metal concentrations would be in the most proximal samples (i.e., within the granite itself) this is shown to not be the case. Given the very high Re contents are indicative of porphyry-style rather than granite-related mineralisation; the observed spatial patterns are better explained by fluid-assisted remobilisation, and possible recrystalisation of a pre-existing molybdenite, which was presumably initially deposited during the porphyry leading to increased Re away from monzogranite, experimental alteration of molybdenite with various fluids has proven that Re/Os concentrations in molybdenite can be influenced by fluids and this can result in dating of the samples giving misleading ages (Suzuki *et al*. 2000) . This could also explain the marked enrichment of Au in molybdenite, especially in some samples and is probably related to grain-size remobilisation and high fluid/rocks ratios, with gold (along with other mobilised elements) deposited along fractures and cleavage planes in the molybdenite. Further work is required to establish the relationship between molybdenite crystal structure and the enrichment in Au, Bi etc., and to understand why molybdenite acts as such an efficient trap for remobilised elements. The Sn enrichment in molybdenite in sample NK21 (Table 10) is, however, more compatible with a granitic source, leaving open the possibility that the granite may have supplied some metal. Other trace element data suggesting zonation patterns in the molybdenite samples such as the Co-Ni trend (Fig. 22) demand explanation, and are probably related to the relative timing and partitioning of the two elements from a fluid into the mineral (Loftus-Hills & Solomon 1967).

Molybdenite occurs as two plolytypes; Hexagonal (2H) and rhombohedral (3R), the later is capable of carrying up to thousands of ppm Re, U, Nb, Bi, Te, Au, W, Sn, Pb and others and is characteristically the "Dirty" polytype. The (3R) polytype may recrystallise at temperatures above 500 ºC (Newberry 1979a; 1979b) and could explain the low Re in sample NK27 and the deposit/grain scale zonation caused by the influence of fluids from the monzogranite and degree of recrystalisation.

There is good evidence to support the incorporation of Re, W and other element into the crystal lattice of molybdenite (Barkov *et al*. 2000; Takahashi *et al*. 2007) (see Fig. 18a) however there is little evidence to support Au, Bi, Te and others into the lattice and these elements are most likely inclusions of various minerals despite the relatively flat Au time resolved profile for sample NK25 (Fig. 18a). This is more likely explained by the homogenous distribution of nanoparticles of gold within cleavages in the molybdenite, gold as inclusions in molybdenite are common and are also represented well with the time-resolved depth profiles (Fig. 18b)

Any genetic model is dependent upon a constrainable geochronological framework and, as such, age dating plays a vital role in establishing the sequence of geological events. The grain-scale compositional

inhomogeneity in molybdenite from Boddington documented in this study (Fig. 21) associated with the possibility of remobilisation of elements including Re cause great implications for dating of the mineralisation events using the Re/Os isotope method. Due care would need to be given to avoid obtaining misleading dates which are then used to back up any genetic model for Boddington.

5.7 Granite as a metal source

While metal abundances in molybdenite from the monzogranite are low (Table 10) and the monzogranite is relatively unmineralised it does contain similar alteration assemblages and minor chalcopyrite/pyrrhotite mineralisation + molybdenite. Such evidence does not rule out the granite as a potential metal source but could be explained by late stage crystal fractionation and metal incompatibility. Metal enrichment from fractionation of a granite has been suggested by Mustard *et al.* (2006) to explain mineralisation associated with intrusion-related systems. Bi levels in the molybdenite sample are relatively elevated and could have also assisted with the removal of Au from the granite as a result of Au scavenging from a fluid undersaturated in Au.

The Boddington deposit lacks many features typical of a reduced intrusion related deposit (RIRG) notebly the fact that these systems are low-Cu, low-grade, high-tonnage with mineralizing fluids of low salinity unlike porphyry deposits (Hart 2007), and unlike the high-salinity fluids measured at Boddington (Roth & Anderson 1993; McCuaig *et al*. 2001). RIRG deposits have only been recognised as a distinct type since 1999 and are therefore poorly understood, poorly constrained and ill-defined. Within the Boddington deposit there are, nevertheless, a number of features that are well explained by a RIRG type model. RIRG deposits have a strong Au-Bi-W signature, often develop high permeability stockworks and contain structurally-controlled mineralisation with development of small metal bearing veins with mineralisation strongly controlled by fluid teperatures and wall rock interaction, often resulting in stages of defined variation of metal assemblages controlled by distance from source intrusion. Variation in metal assemblages often show early high-temperature mineralisation expressed as scheelite bearing veins with chalcopyrite and pyrrhotite and lower temperature biotite/actinolite hosted arsenopyrite mineralisation with Bi-Te-Sb-Pb-Au minerals (Hart 2007). The strong Bi+Te+Au relationship is a common feature at Boddington and is entirely consistent with features observed in RIRG systems. LA-ICPMS analysis of the molybdenite sample from the monzogranite differs from most of the other analysed molybdenite from the deposit and is low in most trace elements that are enriched in other samples. However, levels are still elevated above background for elements associated with mineralisation in the deposit such as Bi (up to 388 ppm), Pb (up to 8208 ppm), Cu (up to 4.45 ppm), Te (up to 156.8 ppm), Ag (up to 11.57 ppm) and Au (up to 0.45 ppm) (see Table 10). Candela & Piccoli (2005) state that plutons associated with mineralisation lack the size needed to produce metals and volatiles necessary and therefore suggest that larger volumes of primary magmatic fluids and metals are required as would likely be the case at Boddington. This would be consistent with high Ni content and “dirty” high-Re molybdenite implying, in part, a deep mafic fluid source, probably associated with intrusion of the host rocks.

5.8 Processing implications

Observations on the copper concentrates revealed that their bismuth mineralogy is complex, with several species present. The large amount of native bismuth observed, coupled with the high overall Bi/Te ratio in the concentrates (9.6 and 11.6 in concentrates A and B, respectively with Ag-tellurides also observed), suggest that the Bi-tellurides are subordinate to native bismuth and that native bismuth contributes the largest part to

the overall gold balance. Bi-tellurides of the tetradymite group and maldonite probably contribute less than 15% to the total bismuth balance, although this would need to be quantified by further study. No Bi-Pb-sulphosalts were observed in the concentrates; the other Bi-bearing minerals seen at Boddington (parkerite, unnamed Ni-Fe-Bi-sulphide) were not seen in the concentrates and are probably very minor isolated phases on the scale of the deposit.

The observation of several grains of maldonite in the concentrates, although unfortunately none in the ores, is of considerable significance. Maldonite is relatively uncommon, but can be a significant Au-carrier in some Au-deposits, especially those with a reduced, granite-related character, such as the type locality, Maldon, Vic. (Ciobanu *et al*. 2010). The contribution of maldonite to the overall gold balance cannot be quantified unless it is established how abundant it is across the deposit, but it may nevertheless contribute a few %. It is clearly recovered to the Cu-concentrate, yet at the cost of increasing the Bi-content.

Results from LA-ICPMS of molybdenite samples suggest that Re values are at levels high enough to warrant production of a molybdenite concentrate. Molybdenum concentrations in the copper concentrate suggest that this would possibly be a viable product with high Mo levels already produced from processed ore. The elevated Au content also recognised in the molybdenite most likely occurring as fine to nanoparticle inclusions on crystal faces and cleavages could be considered refractory gold and along with the often very fine nature of gold grains within the ore could account for average Au recovery for Boddington ore of 85%. The high Au content in the molybdenite has implications for recovering Re from a molybdenite concentrate, since the Au in the molybdenite would be effectively lost as a result of needing to reprocess (at extra cost) any molybdenite concentrate to recover that Au potentially at costs exceeding Au value. It would therefore be necessary to assess whether the value of contained Re is higher than that of the Au value contained in the molybdenite. LA-ICPMS of pyrite and arsenopyrite suggest that this is not an important Au-carrying phase and poses little processing concerns.

6. CONCLUSIONS

The Boddington deposit is a unique deposit within the Yilgarn Craton and possesses many characteristics that complicate attempts to develop a genetic model that satisfies all observations. The High Re content within molybdenite across much of the deposit, together with the Ni-rich mineralogy observed suggests a mafic component to the system most likely related to an original porphyry system and intrusion of mafic host rocks. The diverse and varied telluride mineralogy suggests a complex history of fluids responsible for mineralisation/remobilisation with overprinting occurring over a diverse pressure/temperature range with varying fS,fO and fTe$_2$. This resulted in the transformation of assemblages, with incomplete reactions resulting in incompatible minerals occurring together.

Native gold and electrum are the main gold minerals; maldonite (Au_2Bi) is a minor component. LA-ICPMS analysis of pyrite and arsenopyrite revealed that these minerals are not significant Au-carriers at Boddington. In addition to maldonite, the deposit contains a suite of Bi-minerals, including native bismuth and a suite of Bi, Bi-Ag, Ag- and Pb-tellurides and selenides. These minerals are identified both in ore samples and in the Cu-concentrates. The presence of maldonite, and the relationship and morphology of bismuth and gold grains suggests the presence of Au-scavenging bismuth melts, possibly at multiple times during the history of the deposit. Assemblages commonly record the final crystallisation temperature, occurring below the stability of

maldonite. This results in further difficulty in understanding and pinpointing the source of Au mineralisation and solving the issue of whether metals have been introduced at different times or were just remobilised.

Despite the fact that Boddington lacks features consistent with reduced intrusion related gold deposits, many features of the deposit do fit such a model, although there remains a possibility that metals were sourced from pre-existing ore. RIRG deposits are a relatively sub-type of deposit, with poor constraints on their typology. There remains the possibility that Boddington could be an Archean example of a structurally-controlled reduced intrusion-related gold system, but possibly superposed on an existing porphyry-style or orogenic deposit. Granitic fluids have undoubtedly played a role in ore development at Boddington, but the question of whether they were a metal source or only responsible for remobilisation of existing ore remains open. The inhomogeneous distribution of Re within the deposit at both the grain- and deposit-scale has implications for understanding the age of mineralisation based on Re/Os molybdenite geochronology and the subsequent use of such ages in developing an evolutionary model.

The bismuth mineralogy of the Cu-concentrates is complex, with several species present; native bismuth is, however, the dominant phase. Other species (Bi-tellurides of the tetradymite group and maldonite) are minor. The high-Ag content of some of the electrum grains observed might also be of potential concern in ore processing.

7. RECOMMENDATIONS

As well as suggestions already mentioned above, further study of trace element distribution in molybdenite and how this relates to spatial position would be useful to help explain the sequence of mineralizing events. This could also be supported by a study of the sulphur isotope systematics of those molybdenites to identify potential multiple fluid sources, and a more detailed Re/Os dating study to assess sample to sample variation within the deposit. Other geochronological methods, such as Ar/Ar dating of suitable minerals (e.g., in the shear zones), would back up the results obtained by Re/Os methods and enable a critical check on inconsistencies caused by potential Re remobilisation.

A correlation of trace ore mineralogy with alteration type (expressed in terms of bulk geochemistry) would help to determine if alteration type has influenced mineralogy in any way.

Further study on granite mineralogy, particularly where Au values are elevated and research into fractionation and metal abundance in fluid inclusions to determine if the granite had been a metal source. This has implications for exploration for further mineralisation associated with this intrusion and others of similar age in the region.

ACKNOWLEDGEMENTS

Thanks go to Newmont for their financial and logistic support with particular acknowledgement to Graeme Reynolds, Dhammika Perera and all the geology team at Boddington.

I would like to gratefully acknowledge my Supervisors Nigel Cook and Cristiana Ciobanu of Adelaide University and South Australian Museum for their continued support throughout the year.

Thanks also go to Adelaide Microscopy with reference to Angus Netting and Ben Wade and to the LA-ICPMS team at CODES in Tasmania for their analytical help with; SEM, microprobe and LA-ICPMS. Codes staff will be co-authors in eventual publication of the LA-ICPMS data and element maps

The South Australian Museum (SAM) is acknowledged for access to microscope facilities.

REFERENCES

AFIFI A. M., KELLY W. C. & ESSENE E. J. 1988. Phase relations among tellurides, sulphides, and oxides: I. Thermochemical data and calculated equilibria. *Economic Geology* **83**, 377-394

ALLIBONE A. H., WINDH J., ETHERIDGE M. A., BURTON D., ANDERSON G., EDWARDS P. W., MILLER A., GRAVES C., FANNING C. M. & WYSOCZANSKI R. 1998. Timing relationships and structural controls on the location of Au-Cu mineralization at the Boddington gold mine, Western Australia. *Economic Geology* **93**, 245-270.

ANAND R. R. 2005. Boddington gold deposit, Western Australia. CRC LEME, *CSIRO Exploration and Mining*

ANTHONY J. W., BIDEAUX R. A., BLADH K. W. & NICHOLS, M. C. 1990. Handbook of Mineralogy Volume I – Elements, Sulphides, Sulphosalts. *Mineral Data Publishing*, Tuscon, Arizona, 588 p

BARKOV A. Y., MARTIN R. F., POIRIER G. & MEN'SHIKOV Y. P. 2000. Zoned tungstenoan molybdenite from a fenitized megaxenolith in the Khibina alkaline complex, Kola Peninsula, Russia. *The Canadian Mineralogist* **38**, 1377-1385

BARLEY M. E., GROVES D. I. & BLAKE T. S. 1992. Archean metal deposits related to tectonics: evidence from Western Australia, Perth, Western Australia. Publication 22, 307-324.

CANDELA P. A. & PICCOLI P. M. 2005. Magmatic provinces in the development of porphyry-type ore systems. *Economic Geology 100th Anniversary Volume*, 25-38

CIOBANU C. L. & COOK N. J. 2002. Tellurides, selenides (and Bi-Sulphosalts) in gold deposits. 11th IAGOD Symposium – Geocongress, CD vol, *Geological Survey Namibia*

CIOBANU C. L., BIRCH W. D., COOK N. J., PRING A. & GRUNDLER P. V. 2010. Petrogenetic significance of Au-Bi-Te-S associations: The example of Maldon, central Victorian gold province, Australia. *Lithos* **116**, 1-17

CIOBANU C. L., COOK N. J., DAMIAN F. & DAMIAN G. 2006a. Gold scavenged by bismuth melts: An example from Alpine shear-remobilizates in the Highis Massif, Romania. *Mineralogy and Petrology* **87**, 351-384

CIOBANU C. L., COOK N. J. & PRING A. 2005. Bismuth tellurides as gold scavengers. *Mineral Deposit Research: Meeting the Global Challenge* **1 and 2**, 1383-1386

CIOBANU C. L., COOK N. J. & SPRY P. G. 2006b. Preface – Special Issue: Telluride and selenide minerals in gold deposits – how and why. *Mineralogy and Petrology* **87**, 163-169

CIOBANU C. L., PRING A. COOK N. J., SELF P., JEFFERSON D., DIMA G. I. & MELNIKOV V. 2009. Chemical-structural modularity in the tetradymite group: A HRTEM study. *American Mineralogist* **94**, 517-534

CLARKE R. M. 1997. Saddlebackite, $Pb_2Bi_2Te_2S_3$, a new mineral species from the Boddington gold deposit, Western Australia. *Australian Journal of Mineralogy* **3**(2), 119-124

COOK N. J. 1992. Antimony-rich mineral parageneses and their association with Au minerals within massive sulphide deposits at Sulitjelma, Norway. Neues Jahrbuch für Mineralogie Monatshefte, **1992**, 97-106.

COOK N. J. & CHRYSSOULIS S. L. 1990. Concentrations of "invisible gold" in the common sulphides. *The Canadian Mineralogist 1990*. **28**, 1-16

COOK N. J., CIOBANU C. L., STANLEY C. J., PAAR W. H. & SUNDBLAD K. 2007a. Compositional data for Bi-Pb tellurosulfides. *The Canadian Mineralogist* **45**, 417-435

COOK N. J., CIOBANU C. L., WAGNER T. & STANLEY C. J. 2007b. Minerals of the system Bi-Te-Se-S related to the tetradymite archetype: Review of classification and compositional variation. *The Canadian Mineralogist* **45**, 665-708

DANYUSHEVSKY L., ROBINSON P., MCGOLDRICK P., LARGE R. & GILBERT S. 2003. LA-ICPMS of sulphides: Evaluation of an XRF glass disc standard for analysis of different sulphide matrixes. *Geochimica et Cosmochimica Acta* **67**(18), A73

DANYUSHEVSKY L. V., ROBINSON P., GILBERT S., NORMAN M., LARGE R., MCGOLDRICK P. & SHELLEY J. M. G. in press. A technique for routine quantitative multi-element analysis of sulphide minerals by laser ablation ICP-MS. Geochemistry: Exploration, Environment, Analysis (in press)

DOUGLAS N., MAVROGENES J., HACK A. & ENGLAND R. 2000. The liquid bismuth collector model: An alternative gold deposition mechanism. *AGC Abstracts* **59**, 135

DUURING P., CASSIDY K. F & HAGEMANN S. G. 2007. Granitoid-associated orogenic, intrusion-related, and porphyry style metal deposits in the Archaean Yilgarn Craton, Western Australia. *Ore Geology Reviews* **32**, 157-186

GROVES D. I. 1993. The crustal continuum model for late Archaean lode-gold deposits of the Yilgarn Block, Western Australia. *Mineralium Deposita* **28**, 366-374

GROVES D. I., PHILLIPS G. N., HO S.E., HOUSTOUN S.M. & STANDING C. A. 1987. Craton scale distribution of Archaean greenstone gold deposits: Predictive capacity of the metamorphic model. *Economic Geology* **82**, 2045-2058

HART C. J. R. 2007. Reduced intrusion-related gold systems. *In* Goodfellow, W.D. (ed) Mineralogical Deposits of Canada: A Synthesis of Major Deposit Types, Distric Metallogeny, the Evolution of Geological Provinces, and Exploration Methods. *Geological Association of Canada, Mineral Deposits Division*, Special Publication No 5, 95-112

LARGE R. R., DANYUSHEVSKY L., HOLLIT C., MASLENNIKOV V., MEFFRE S., GILBERT S., BULL S., SCOTT R., EMSBO P., THOMAS H., SINGH B. & FOSTER J. 2009. Gold and Trace Element Zonation in Pyrite Using a Laser Imaging Technique: Implications for the Timing of Gold in Orogenic and Carlin-Style Sediment-Hosted Deposits. *Economic Geology* **104**, 635-668.

LAROCQUE A. C. L., HODGSON C. J., CABRI L. J. & JACKMAN J. A. 1995. Ion-microprobe analysis of pyrite, chalcopyrite and pyrrhotite from the mobrun VMS deposit in north-western Quebec: Evidence for metamorphic remobilization of gold. *The Canadian Mineralogist* **33**, 373-388

LOFTUS-HILLS G. & SOLOMON M. 1967. Cobalt, nickel and selenium in sulphides as indicators of ore genesis. *Mineralium Deposita* **2**, 228-242

LONGERICH H. P., JACKSON S. E. & GUNTHER D. 1996. Laser ablation inductively coupled plasma mass spectrometric transient signal data acquisition and analyte concentration calculation. *Journal of Analytical Atomic Spectrometry* **11**, 899-904

MARSDEN R. J. 1984. Nickel mineralizationWestern Australia. (Geological Survey of Western Australia: Perth) 272

MCCUAIG T. C., BEHN M., STEIN H. J., HAGEMANN S. G., MCNAUGHTON N. J., CASSIDY K. F., CHAMPION D. & WYBORN L. 2001. The Boddington Gold Mine: A new style of Archaean Au-Cu deposit. *AGSO Geoscience Australia* **37**, 453-455

MUSTARD R., ULRICH T., KAMENETSKY V. S. & MERNAGH T. 2006. Gold and metal enrichment in natural granitic melts during fractional crystallization. *Geology* **34**(2), 85-88

MYERS J. S. 1993. Precambrian history of the west Australian craton and adjacent orogens. *Annual Review of Earth Planetary Sciences*, **21**, 453-485

NELSON D. R. 1998. Granite-greenstone crust formation on the Archaean Earth: A consequence of two superimposed processes. *Earth and Planetary Science Letters* **158**, 109-119

NEMCHIN A. A., PIDGEON R. T. & WILDE S.A. 1993. Timing of the late Archaean granulite facies metamorphism and the evolution of the southwestern Yilgarn Craton of Western Australia: Evidence from U-Pb changes of zircons from mafic granulites. *Precambrian Research* **68**(3-4), 307-321

NEWBERRY R. J. J. 1979a. Polytypism in molybdenite (I): a non-equilibrium impurity induced phenomenon. *American Mineralogy* **64**758-767

NEWBERRY R. J. J. 1979b. Polytypism in molybdenite (II): relationships between polytypism, ore deposition/alteration stages and rhenium contents. *American Mineralogy* **64**, 768-775

OKOMOTO K. & TANNER L. E. 1990. Bi-Te (bismuth-tellurium). *In* Massalski, T.B., Ohamoto, K. (eds) *Binary Alloy Phase Diagrams*, ASM International, Materials Park, Ohio, 800-801

PRINCE A., RAYNOR G. V. & EVANS D. S. 1990. Phase diagrams of ternary gold alloys. Institute of Metals, London, 505

REICH M., KESLER S. E., UTSUNOMIYA S., PALENIK C. S., CHRYSSOULIS S. L. & EWING R. C. 2005. Solubility of gold in arsenian pyrite. *Geochimica et Cosmochim. Acta* **69**(11), 2781-2796

ROTH E., BENNETT J. M. & SYMONS P. M. 1990. Boddington and Black Flag: Anomalous Archean gold deposits: Perth, Western Australia. Geology Department and University Extension, University of Western Australia Publication **20,** 189-194

ROTH E. 1992. The nature and genesis of Archaean porphyry-style Cu-Au-Mo mineralization at the Boddington Gold Mine, Western Australia, Unpublished PhD thesis, University of Western Australia

ROTH E. & ANDERSON G. 1993. Evidence for reduced high salinity ore fluids in the Archaean porphyry-style Cu-Au-Mo deposit at Boddington, Western Australia. Applied to Ore Deposits, Proceedings of the Second Biennial SGA Meeting, Granada, Spain, 233-236

STEIN H. J., MARKEY R. J., MORGAN J. W., SELBY D., CREASER R. A., MCCUAIG T.C. & BEHN M. 2001. Re-Os dating of Boddington molybdenite, SW Yilgarn: Two mineralization events. *AGSO – Geoscience Australia* **37**, 469-471

SUZUKI K., KAGI H., NARA M., TAKANO B. & NOZAKI Y. 2000. Experimental alteration of molybdenite: Evaluation of the Re-Os system, infrared spectroscopic profile and polytype. *Geochimica et Cosmochimica* **64**(2), 222-232

SYMONS P. M., ANDERSON G., BEARD T. J., HAMILTON L. M., REYNOLDS D. G., ROBINSON J. M., STAYLEY R. W. & THOMPSON C. M. 1988. The Boddington gold deposit. Geological society of Australia Abstracts, **22**, 55-61

SYMONS P. M., ANDERSON G., HAMILTON L. M., BEARD T., STAYLEY R., ROTH E., & HO S. E. 1990. The structural and host rock settings of primary mineralization at the Boddington gold mine [abs]. *Australian Geological Convention*, 10th, Hobart, 1990, Abstract, **25**, 145-146

TAKAHASHI Y., URUGA T., SUZUKI K., TANIDA H., TERADA Y. & HATTORI K. H. 2007. An atomic level study of rhenium and radiogenic osmium in molybdenite. *Geochimica et Cosmochimica* **71**, 5180-5190

TOOTH B., BRUGGER J., CIOBANU C. L. & LIU W. 2008. Modeling of gold scavenging by bismuth melts coexisting with hydrothermal fluids. *Geology* **36**(10), 815-818

Fig. 1

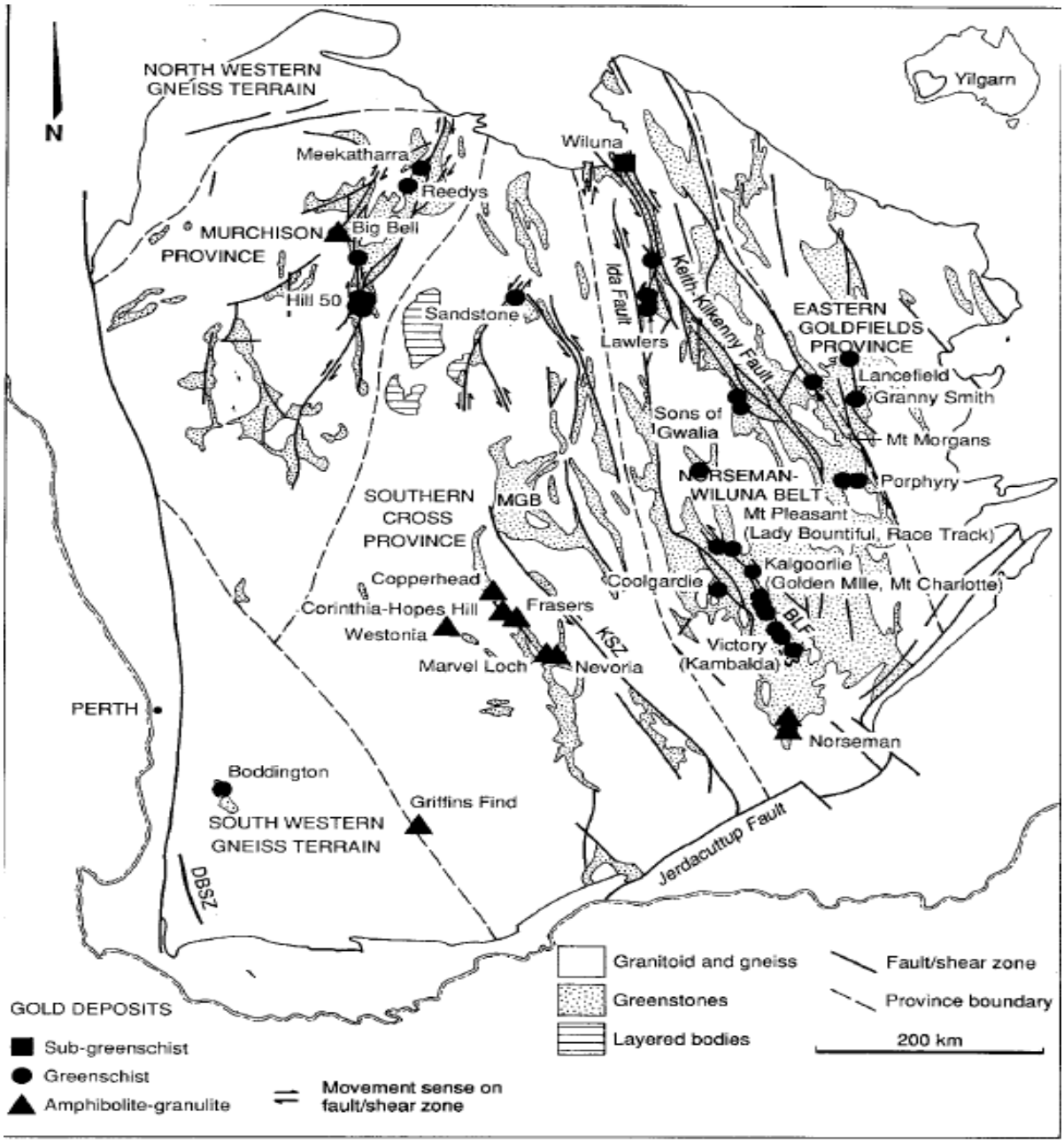

Figure 1. Schematic location map of the Boddington deposit and greenstone belts within the Yilgarn craton W.A. (after Groves, 1993)

Fig. 2

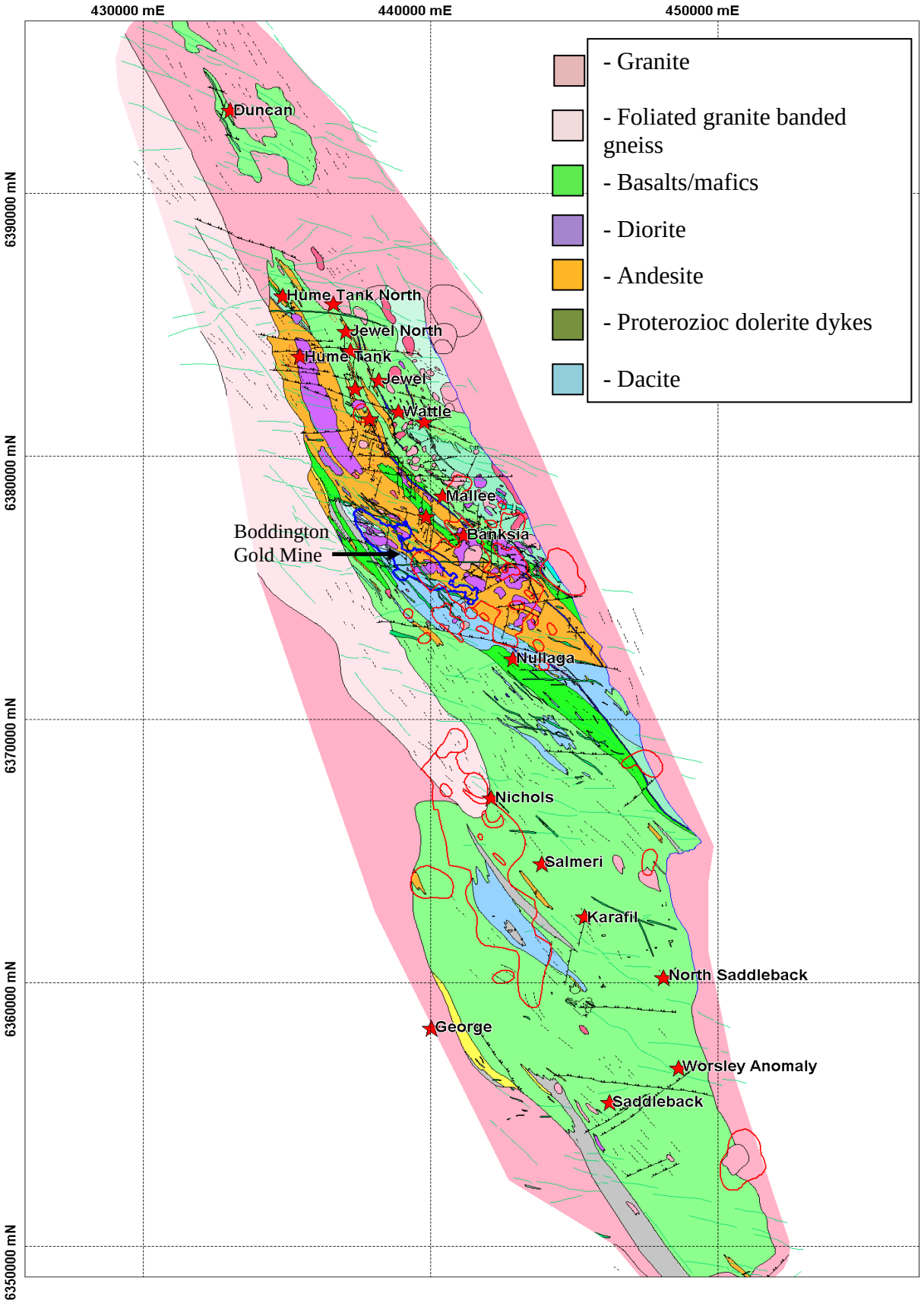

Figure 2. Geological map of the Saddleback greenstone belt using Newmont Boddington gold mine grid coordinate system. (BGM Newmont)

Fig. 3

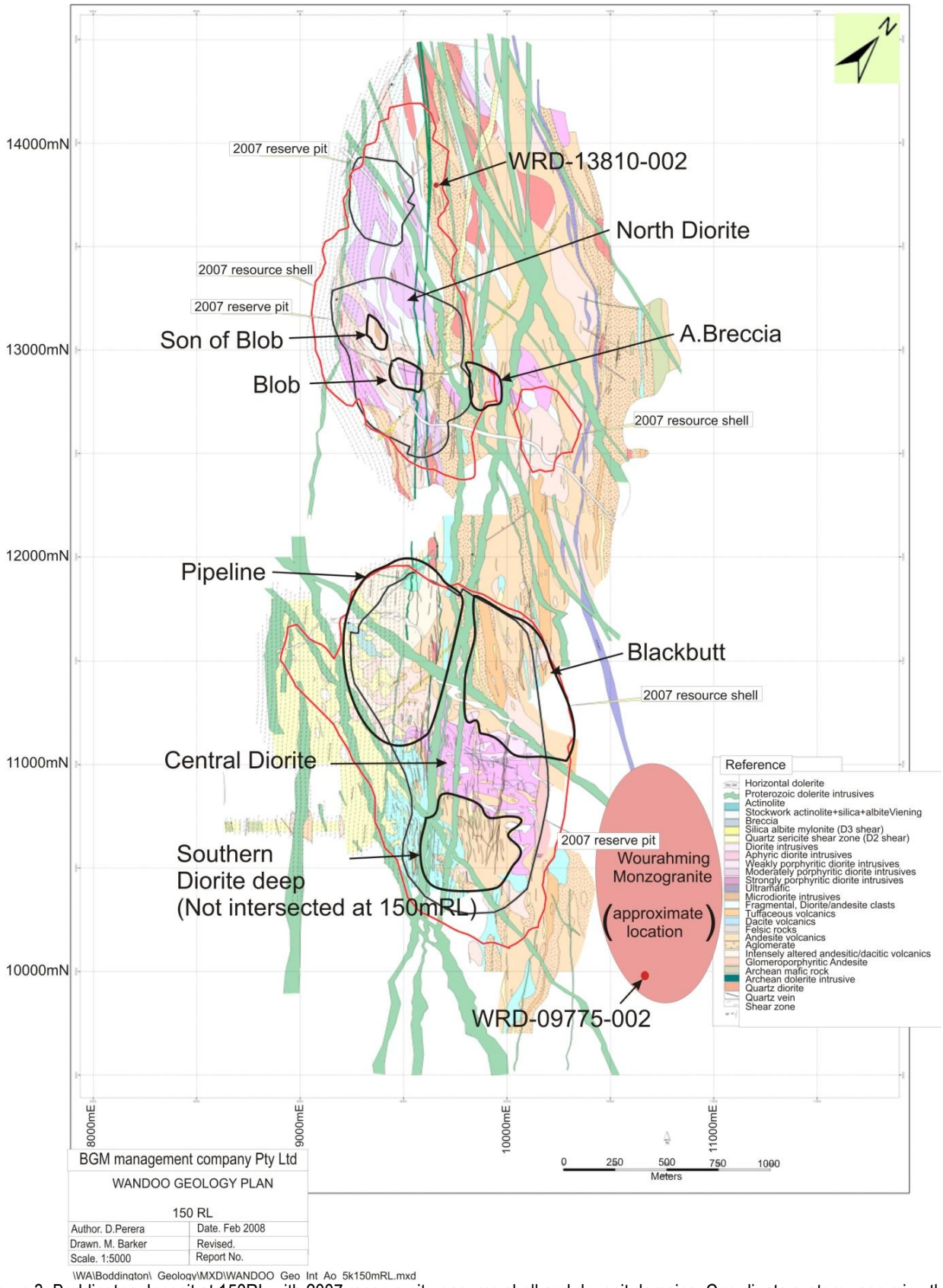

Figure 3. Boddington deposit at 150RL with 2007 reserve pit, resource shell and deposit domains. Coordinate system uses mine the grid system developed by Boddington gold mine. (BGM Newmont)

Fig. 4

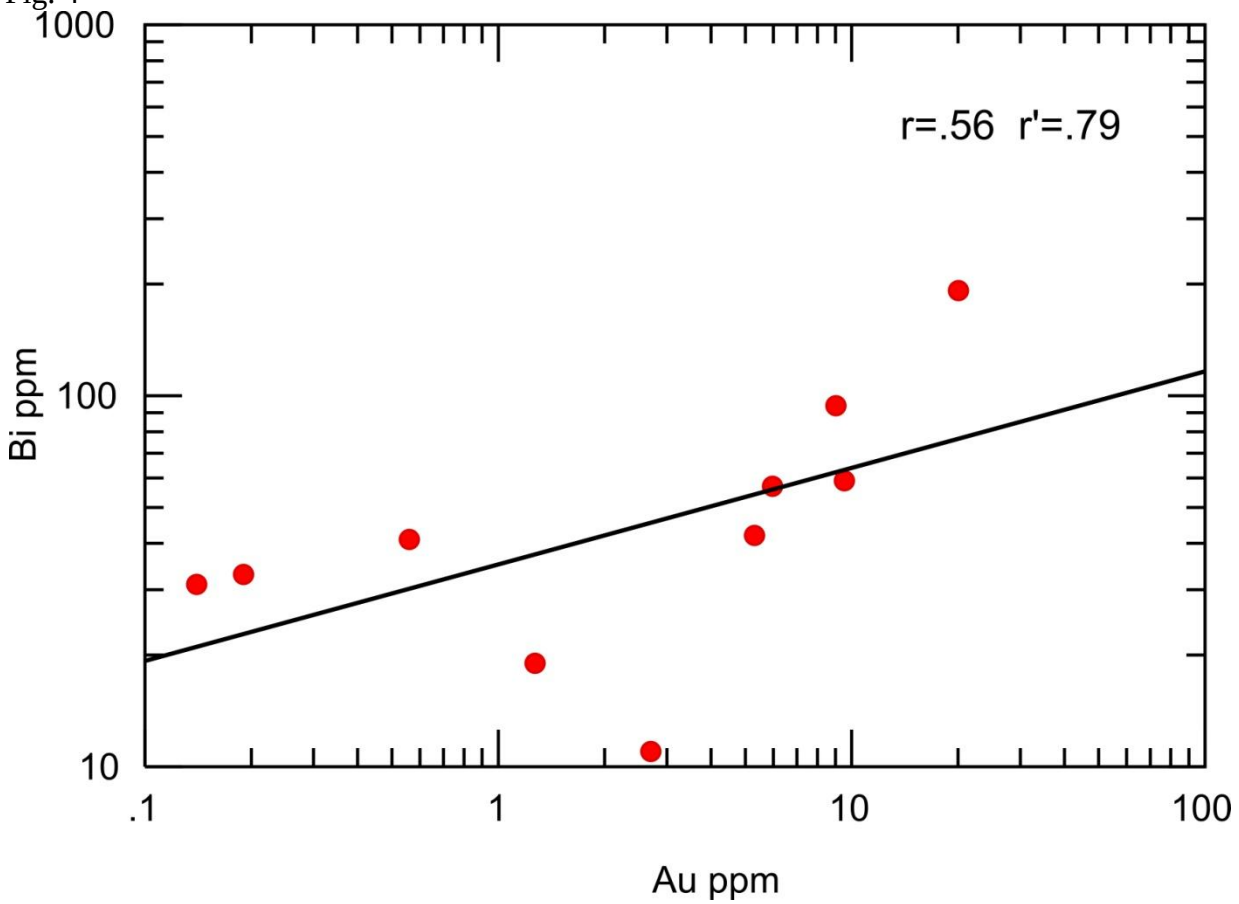

Figure 4. Binary plot of assay results for Au and Bi in ppm using log scale. The data presents an ~1:10 Au/Bi correlation in bulk ore.

Fig. 5

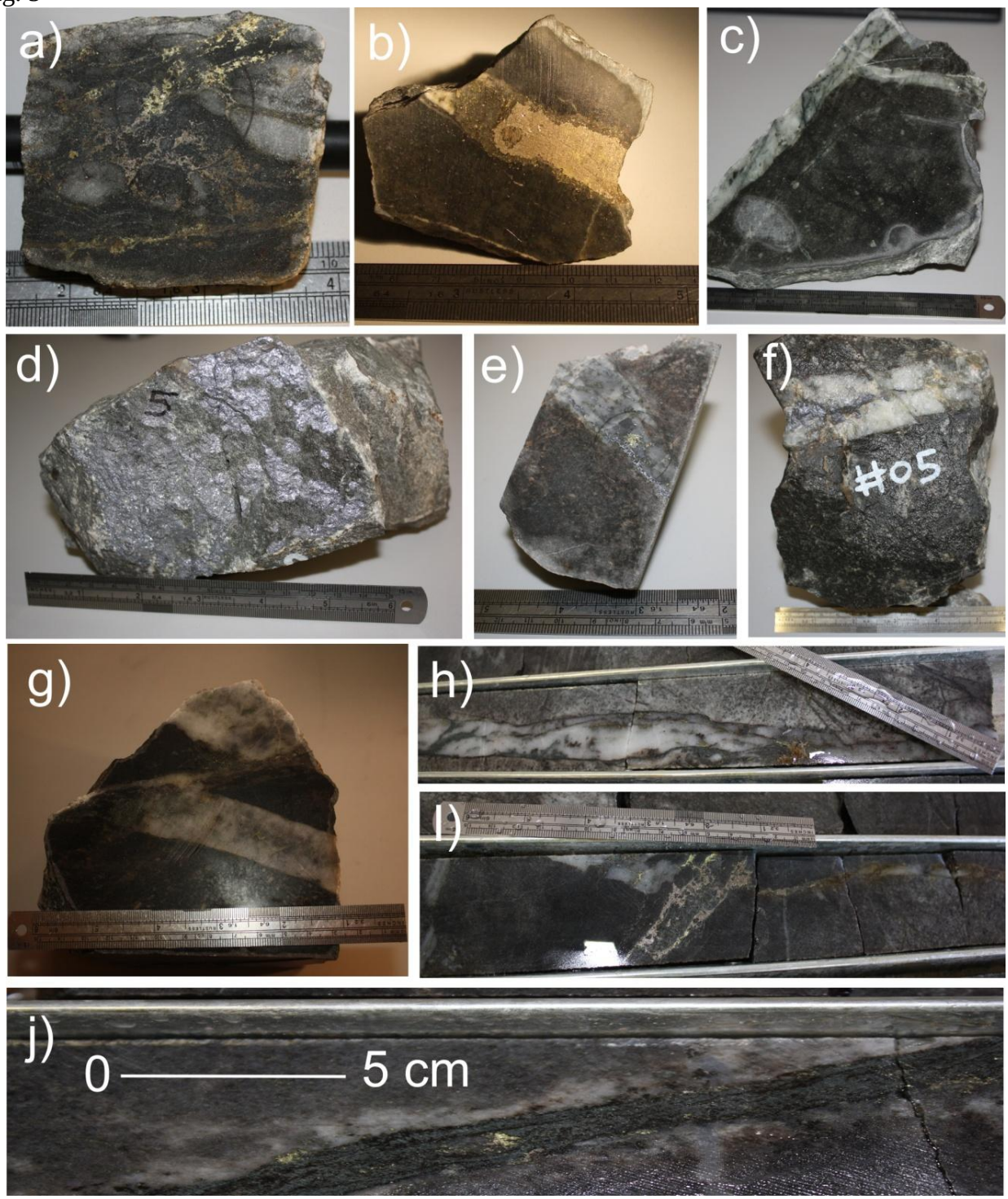

Figure 5. Images of representative samples collected from around the deposit. Scale uses a 6 inch/15 cm ruler, a) clinozoisite/biotite shear zone with sulphides overprinting earlier quartz vein, sample NK22. b) Diorite host rock from pipeline orebody with silica-sulphide vein. c) Diorite host rock from North Diorite with quartz veins reactivated by actinolite. Quartz vein is seen to host visible gold up to 1 mm in diameter. d) Example of molybdenite mineralisation, molybdenite as shear zone in diorite from ABreccia where molybdenite is the sole sulphide and is associated with clinozoisite. e) Molybdenite mineralisation from Central Diorite, molybdenite is associated with chalcopyrite mineralisation within quartz vein. f) Molybdenite within quartz vein associated with chalcopyrite mineralisation from the North pit, has similar appearance to sample e). g) North Diorite sample with quartz vein offset by later clinozoisite shear zone carrying sulphides. h) Images of mineralization commonly seen in drill core, reactivated quartz vein with actinolite controlling mineralisation. I) Sulphide “feeder” cutting mineralised quartz vein with chalcopyrite and pyrrhotite. j) Reactivated vein with actinolite and sulphides demonstrating silica-albite selvage.

Fig. 6

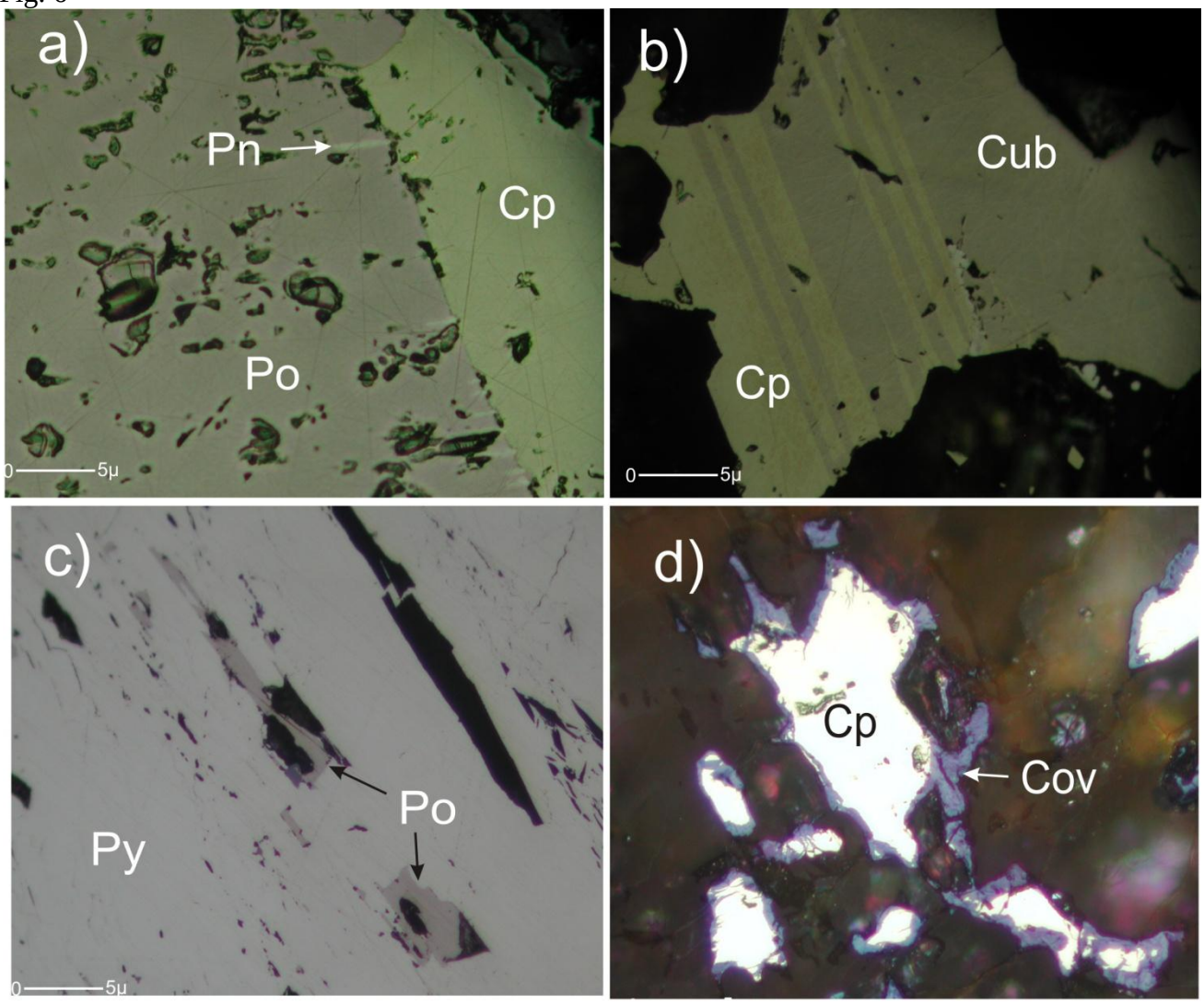

Figure 6. Reflected light microscope images of secondary minerals and exsolution minerals. a) Typical ore association of chalcopyrite (Cp) and pyrrhotite (Po) with exsolution of pentlandite (Pn) from pyrrhotite as flame like textures (sample NK31). b) Lamellae exsolution of cubanite (Cub) from chalcopyrite (sample NK16). c) Example of secondary pyrite (Py) replacing pyrrhotite; pyrrhotite is present as relict inclusions within the pyrite (sample NK2d). d) Chalcopyrite with rim of covellite (Cov) most likely due to supergene enrichment (sample NK 28).

Fig. 7

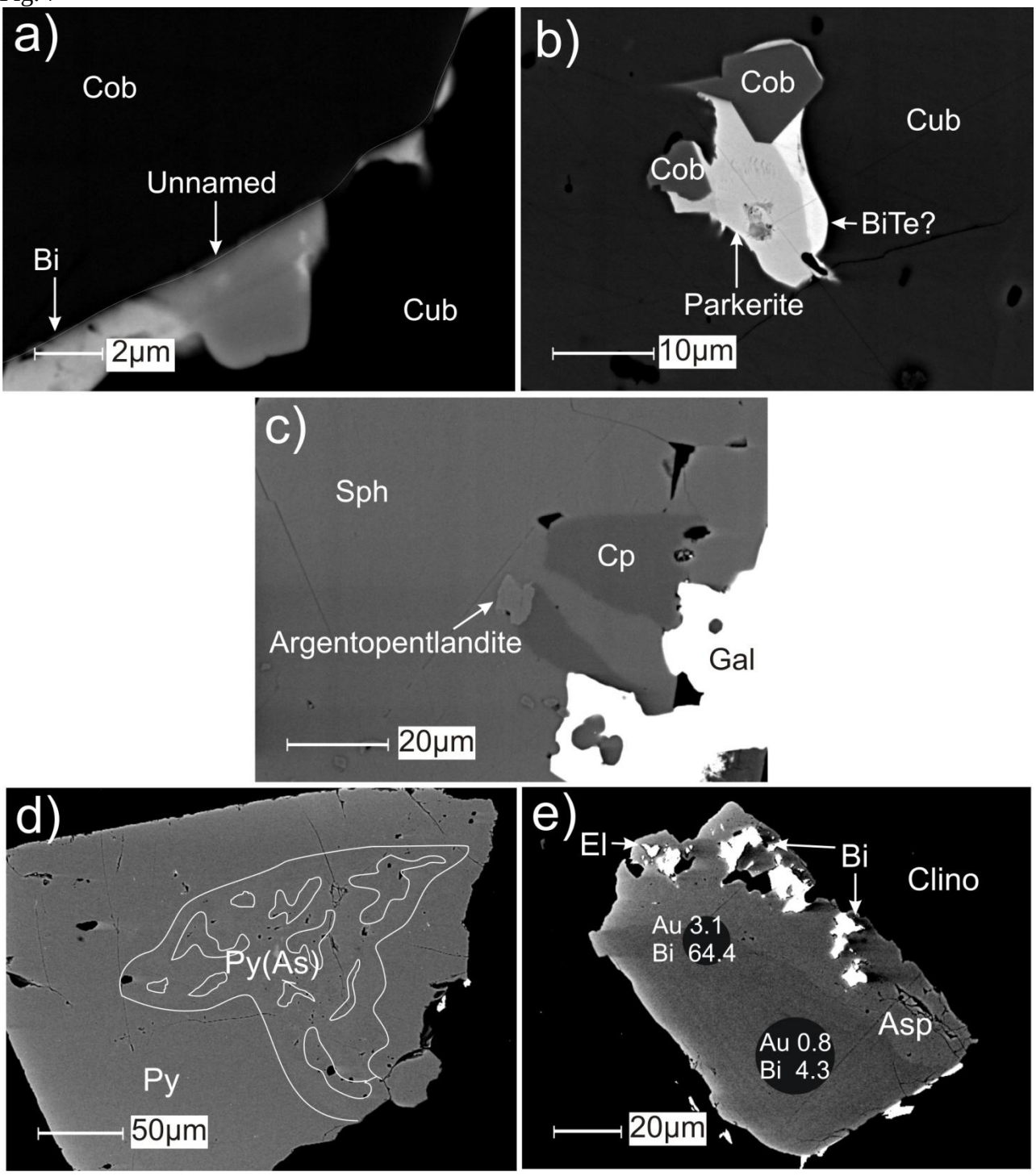

Figure 7. Back-scattered-electron (BSE) images showing rare Ni minerals and potential gold-bearing iron-sulphides identified in the samples. Sample NK16 a) and b) had a high mafic component mineralogy with cubanite (Cub) dominant and almost fully replaced chalcopyrite, inclusions of granular cobaltite (Cob) were common and a unnamed mineral was identified (Ni-(Fe)-Bi sulphide) with native bismuth (Bi). b) Shows the mineral parkerite in the cubanite associated with a Bi-telluride on cobaltite. c) Argentopentlandite in Sphalerite (Sph) with chalcopyrite and galena (Gal) in sample NK20. d) Pyrite (Py) with As bearing zonation from NK26 this sample was analysed with LA-ICPMS to check if it is a gold carrier. e) Arsenopyrite (Asp) zoned with respect to As content with alteration of zonation and inclusions of Bi and electrum (El) associated with this alteration and destruction of the zonation. Grains is within clinozoisite (Clino). This grain was analysed with the LA-ICPMS (note the round holes) to check if it was gold bearing Bi and Au values are given in ppm on the image within their respective spot (sample NK24).

Fig. 8

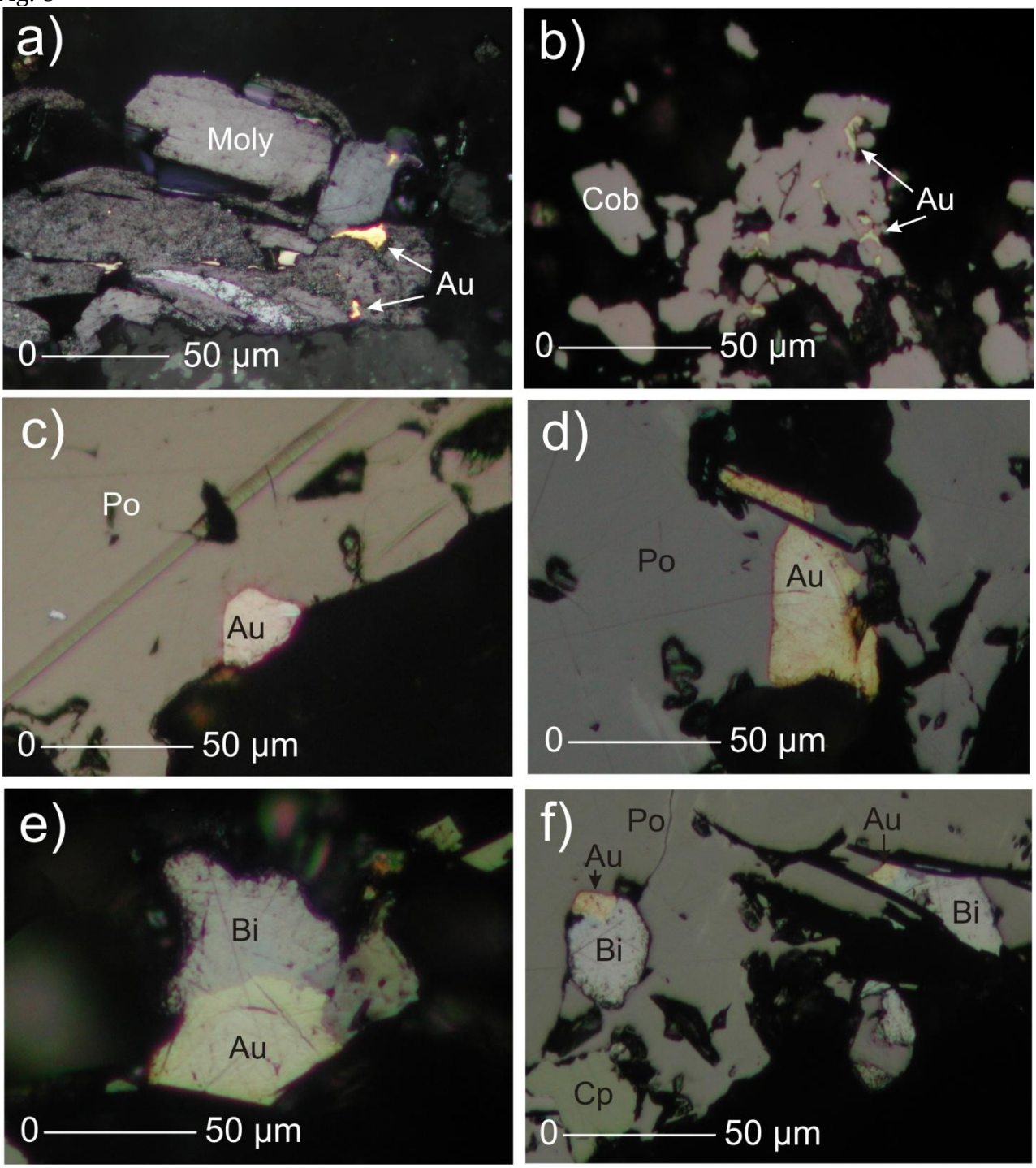

Figure 8. Reflected light photomicrographs showing aspects of gold mineralogy. a) Gold inclusions (Au) (light yellow) in molybdenite (Moly) (silver-grey) from sample NK27 (note bright strong colour of gold this indicates high Au content). b) Gold infilling fractures and grain boundaries of cobaltite (Cob) (dull grey) from sample NK5. c) Gold inclusion in pyrrhotite (Po) (brown-grey) (note pale colour of gold grain this indicates composition more likely electrum)(NK22). d) Gold grain in pyrrhotite and gangue of actinolite and quartz (note varying intensity of gold colour this indicates Ag depletion associated with the gangue minerals) sample NK22. e) Native bismuth (Bi) (silvery white) and gold grain within gangue of quartz from sample NK22. f) Bismuth+gold grains within fractures of pyrrhotite and chalcopyrite (Cp) (yellow-brown) in sample NK22, this gold+bismuth association is a commonly observed feature in the ore.

Fig. 9

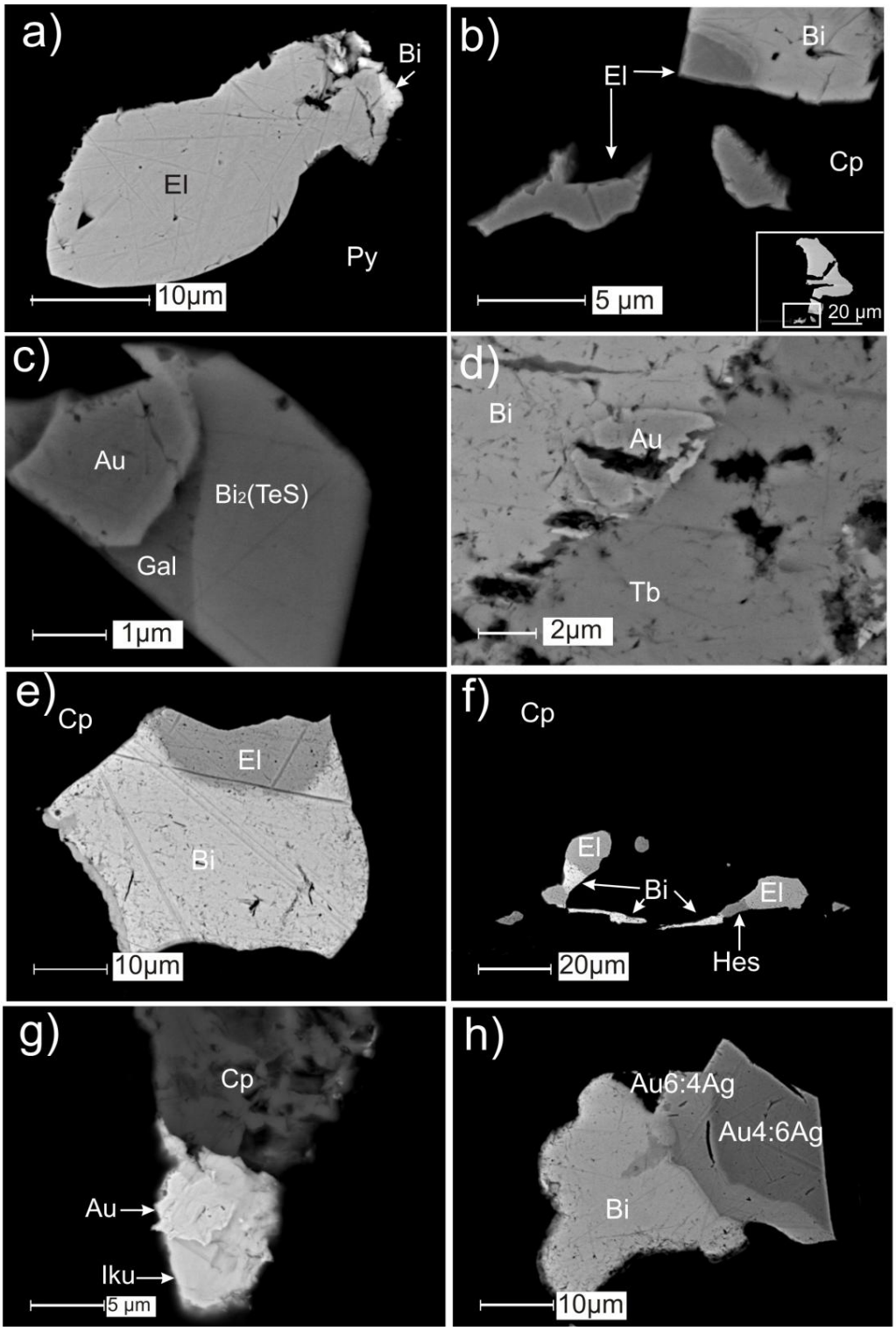

Figure 9. Back-scattered-electron images of Au+Bi associations showing the textural and paragenetic association of Bi+/- Te with gold. a) Grain of typical grain of electrum (El) seen with composition commonly between 30-70% Au, note small amount of native bismuth (Bi) on the edge of the grain, this grain is an inclusion within secondary pyrite (Py) and was most likely originally an inclusion in pyrrhotite (sample NK2b). b) Grain of native bismuth with minor electrum within chalcopyrite (Cp); note contact of electrum and bismuth displays a contact aureole NK2b. c) $Bi_2(TeS)$ with inclusions of gold (Au), galena (Gal) is buffering the contact between gold and $Bi_2(TeS)$ (sample NK18). d) Grain of native bismuth and tellurobismuthite (Tb), note inclusion of gold at the contact between the two minerals and the apparent reaction boundary. e) Native bismuth with smooth rounded contact of electrum, indication of eutectic crystallization likely from a melt (sample NK2d). f) Melt bleb-like inclusions of native bismuth, hedleyite (Hed) and electrum in chalcopyrite, inclusions occur within porous texture and along fractures within the chalcopyrite (sample NK2d). g) Inclusion of gold within ikunolite (Iku) attached to chalcopyrite and within gangue (sample NK3). h) Native bismuth with zoned electrum, contact between electrum and electrum increases in Au with respect to Ag nearer to bismuth contact (NK22).

Fig. 10

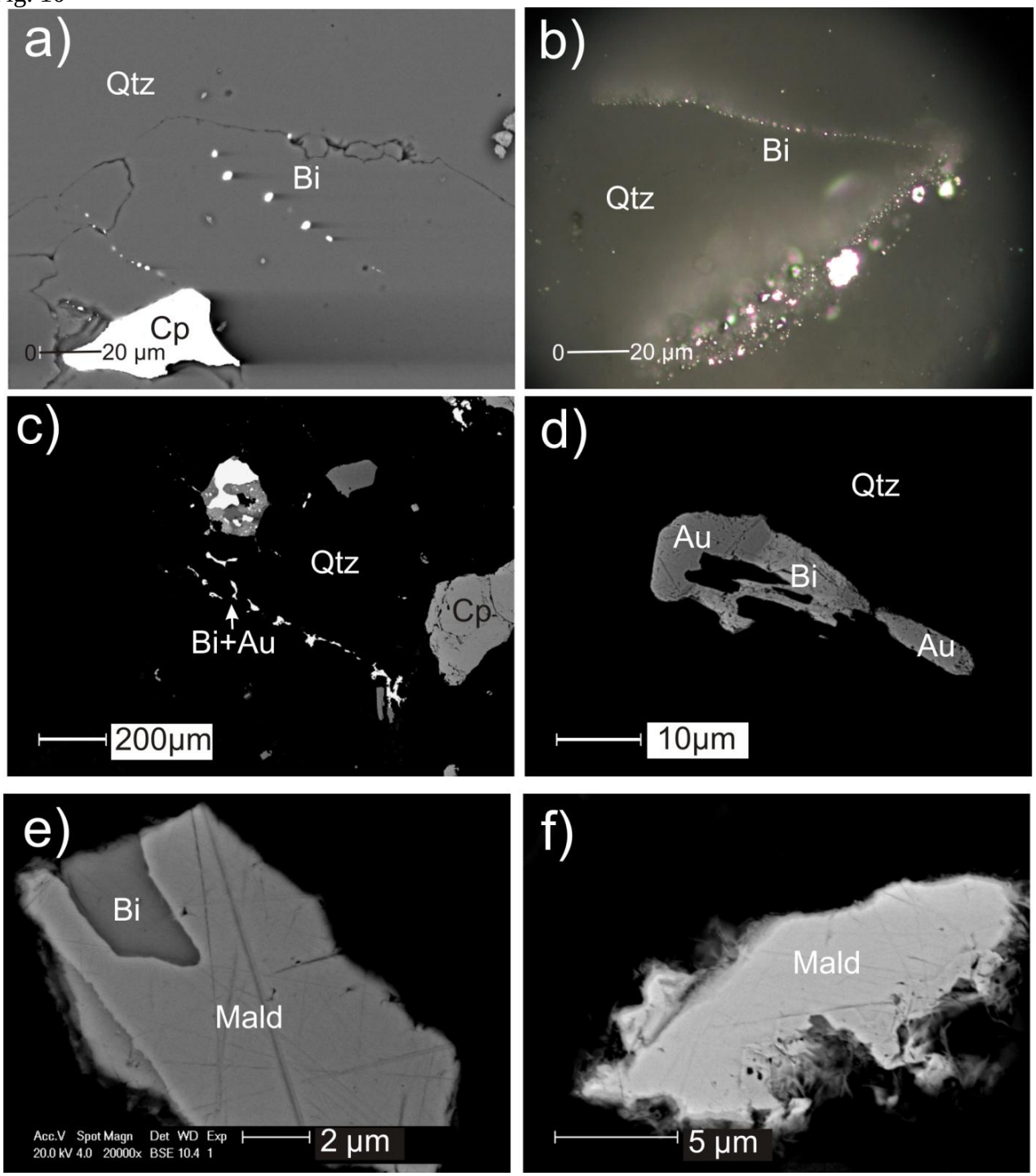

Figure 10. Back-scattered-electron (BSE) images showing evidence for bismuth melts. a) Round, droplet-shaped trails of native bismuth (Bi) in quartz (Qtz) from sample NK24. b) Reflected light microscope image of droplet shaped inclusions of native bismuth in quartz in sample NK9. c) Melt droplet inclusion trail of native bismuth and gold (Au), inclusions occur along fractures and at grain boundaries within quartz (sample NK 30). d) Magnified image of image c) showing a grain of Bi+Au along inclusion trail. e), f) Examples of maldonite (Mald) seen only in concentrate samples from both ConcA and ConcB.

Fig. 11

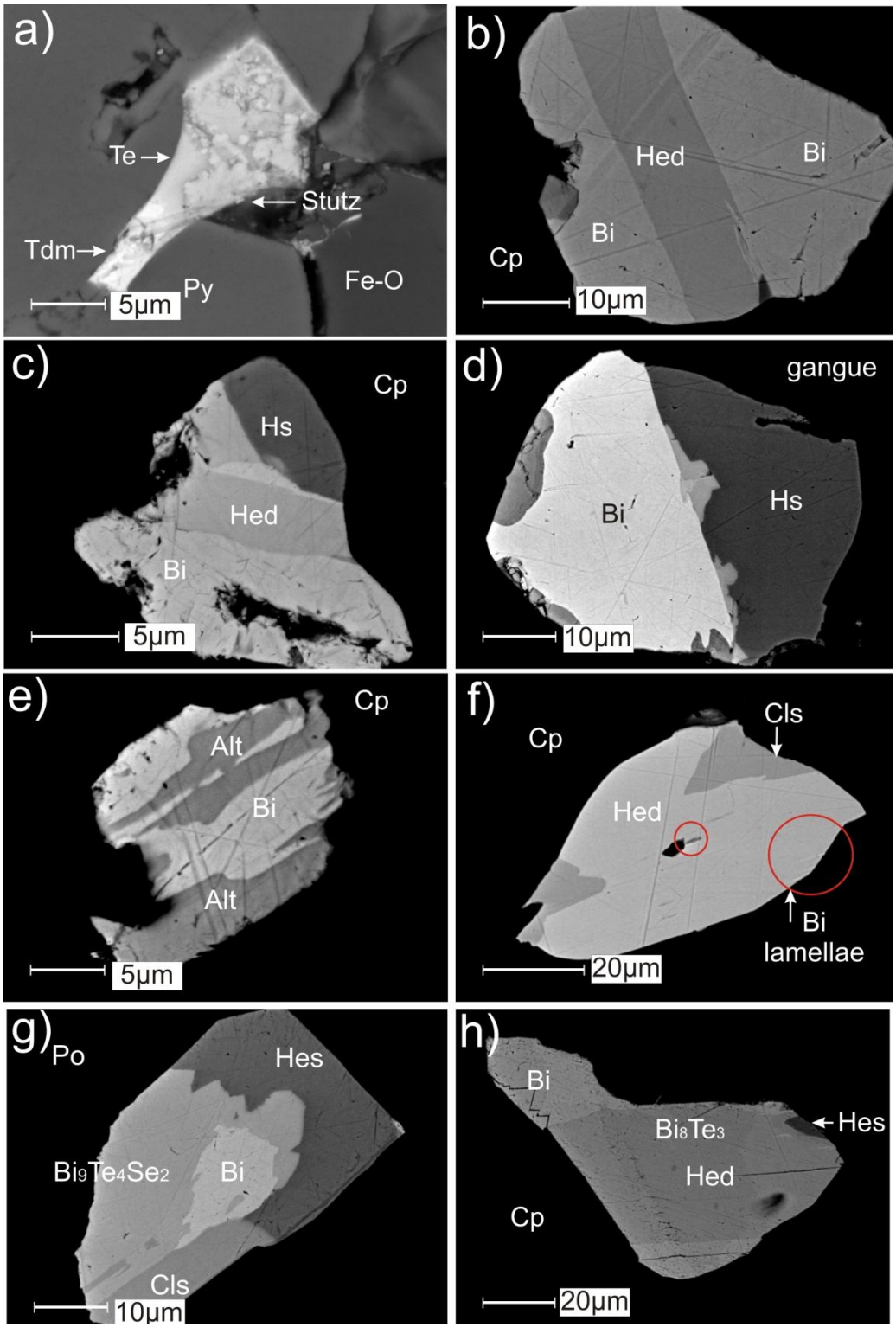

Figure 11. Back-scattered-electron (BSE) images showing examples of telluride mineralogy observed in samples a). Tetradymite (Tet) with stützite (Stutz) and native Tellurium (Te) in pyrite (Py) from sample NK2a. b). Native bismuth (Bi) with lamellae of hedleyite (Hed) in chalcopyrite (Cp) from sample Nk2b. c). Native bismuth with hedleyite and hessite (Hes) in chalcopyrite (sample NK2b). d). Bismuth and hessite with reaction boundary of hedleyite and tsumoite from sample NK2b. e). Complex symplectite-like intergrowth of altaite (Alt) and bismuth (sample NK2b). f). Hedleyite with clausthalite (Cls) and native bismuth exsolution lamellae (sample NK2b). g). Complex of hessite, clausthalite, unnamed $Bi_9Te_4Se_2$ with native bismuth in pyrrhotite (Po) from sample NK 22. h). Bismuth with hedleyite showing non-stoichiometry within grain from hedleyite to Bi_8Te_3 in sample NK2d.

Fig. 12

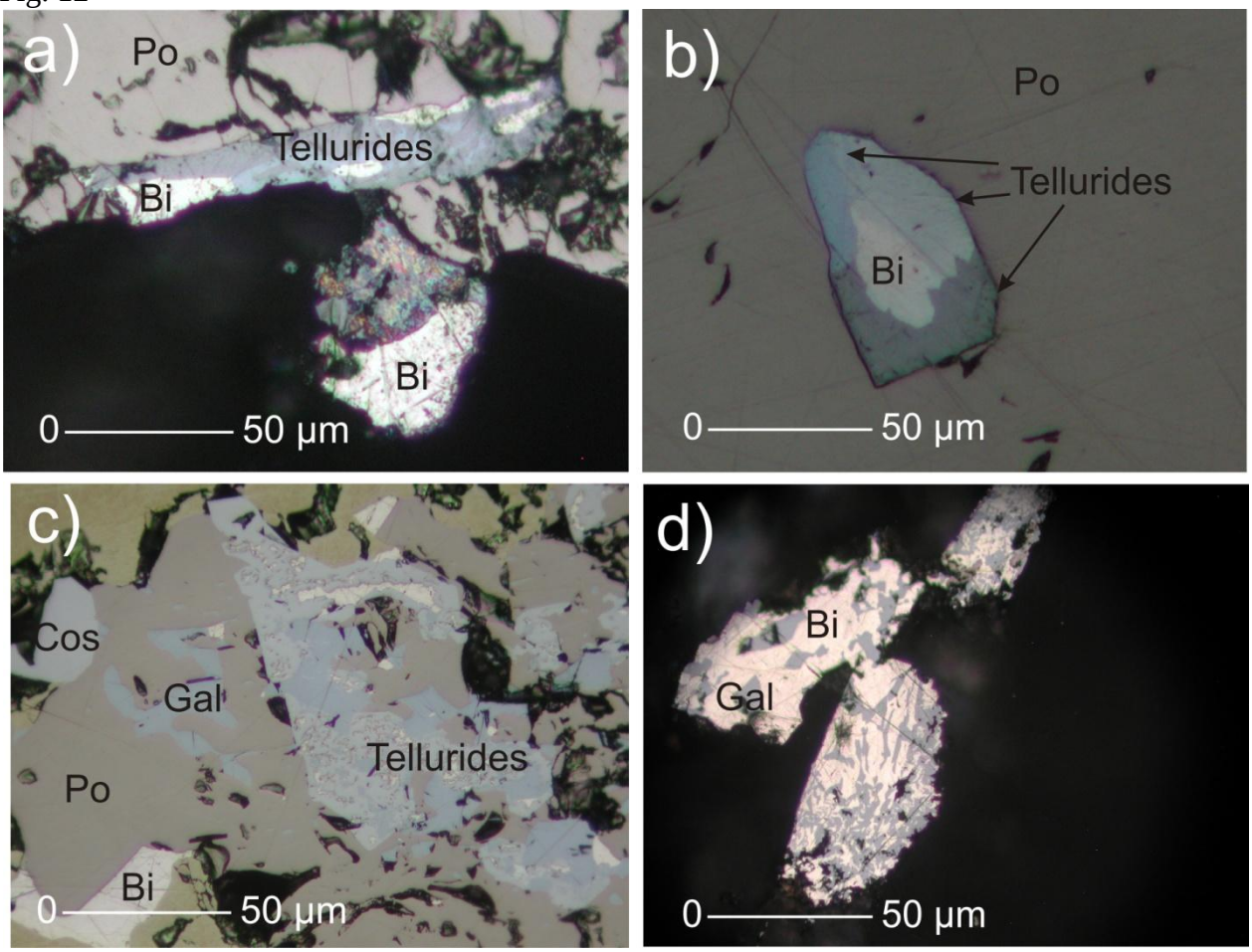

Figure 12. Reflected light microscope images of tellurides. a) Symplectite-like intergrowth of native bismuth (Bi) (silver white) and two other species that could not be identified using optical methods (blue and blue grey) on boundary of gangue (black) and pyrrhotite (Po) (grey) in sample NK8. b) Grain of intergrowth of tellurides showing possible replacement of bismuth within pyrrhotite in sample NK22. c) Symplectite intergrowth of native bismuth, telluride species, galena (Gal) and costibite (Cos) within pyrrhotite and chalcopyrite in sample NK10. d) Symplectite-like intergrowth of native bismuth and galena in quartz from sample NK 9

Fig. 13

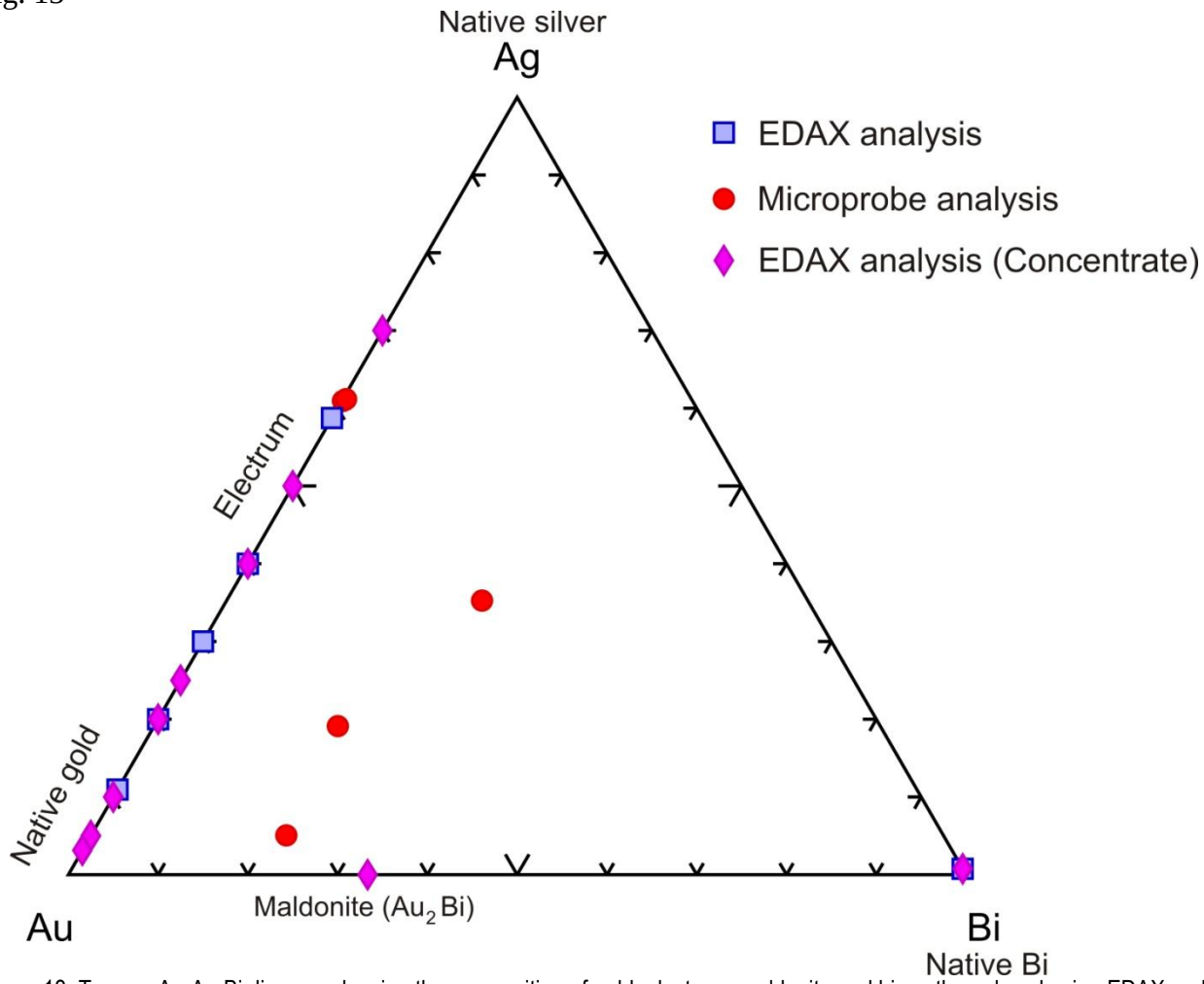

Figure 13. Ternary Au-Ag-Bi diagram showing the composition of gold, electrum, maldonite and bismuth analysed using EDAX and microprobe.

.

Fig. 14

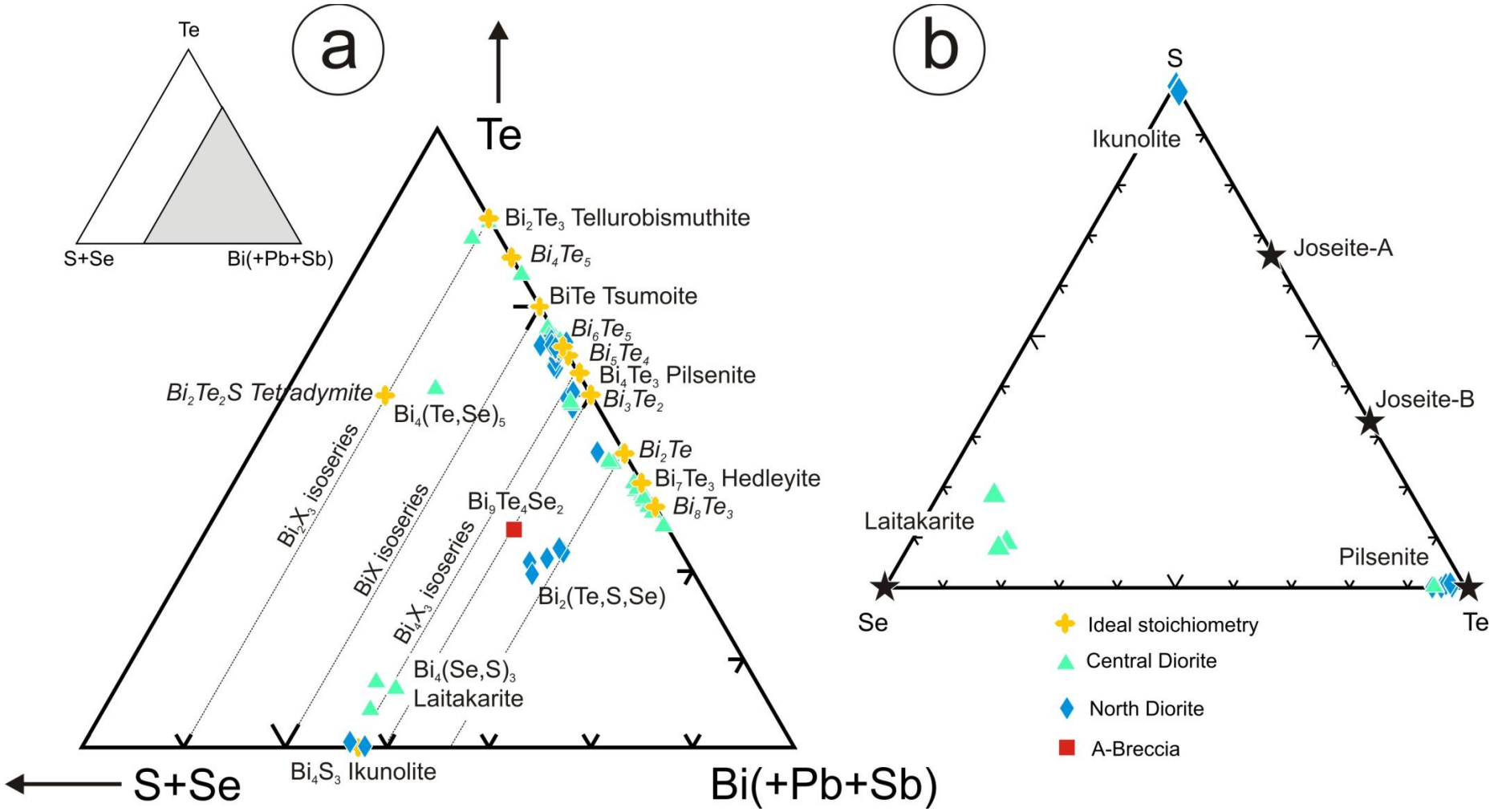

Figure 14. (a) Ternary Bi(+Sb+Pb)-Te-S+Se plot for members of the tetradymite group, showing range of stoichiometries in the analytical data. Note broad variation along the Bi-Te join. (b) Analytical data for minerals within the Bi_4Te_3-Bi_4Se_3-Bi_4S_3 isoseries, indicating projected compositions of analysed pilsenite, ikunolite and laitakarite.

Fig. 15

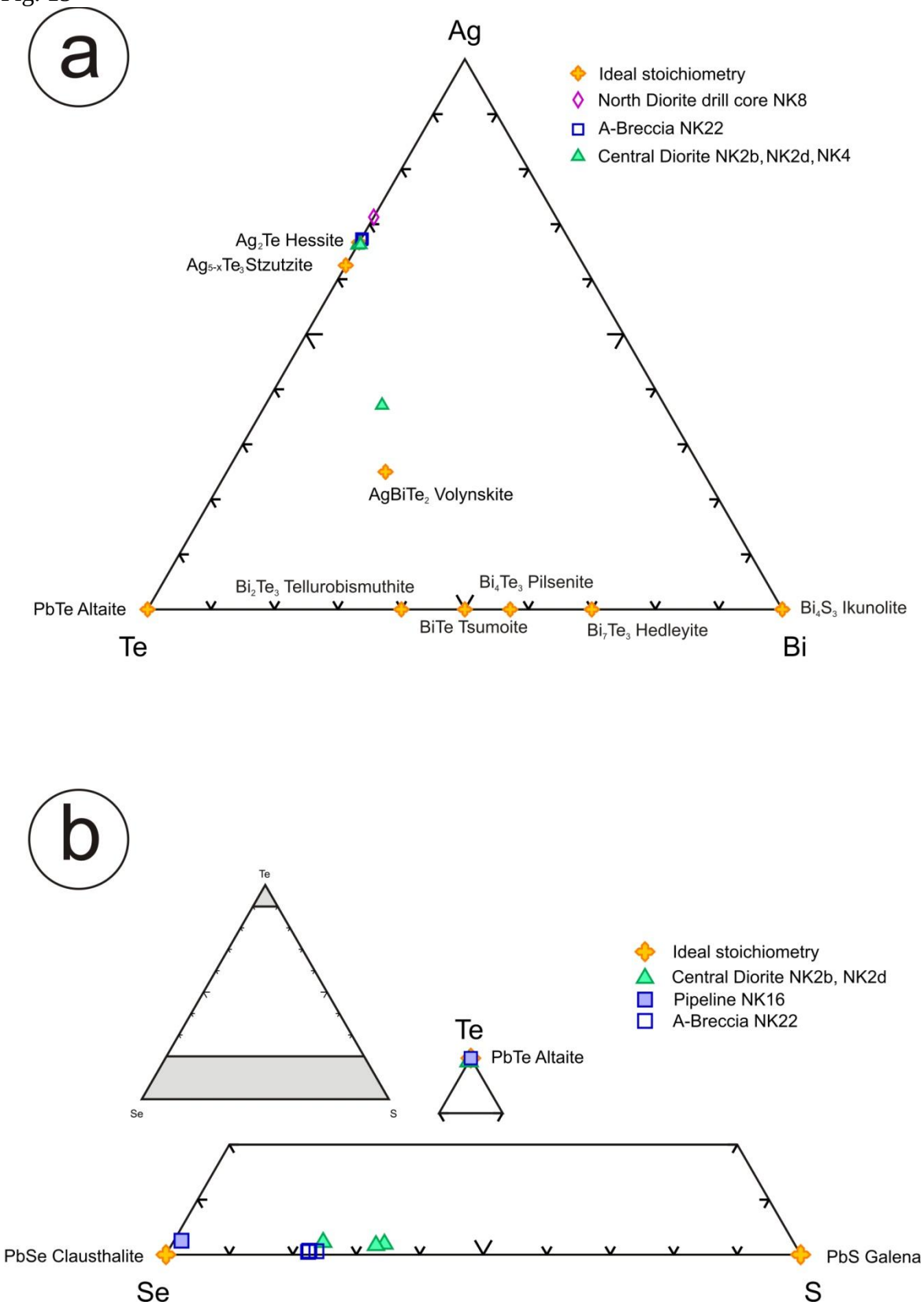

Figure 15. (a) Projected ternary Bi-Ag-Te plot for silver tellurides, showing minerals identified using microprobe and ideal telluride formulae. (b) Analytical data for minerals within the Pb Se-S series, indicating projected compositions of analysed clausthalite and altaite showing solid solution series for clausthalite and galena.

Fig. 16

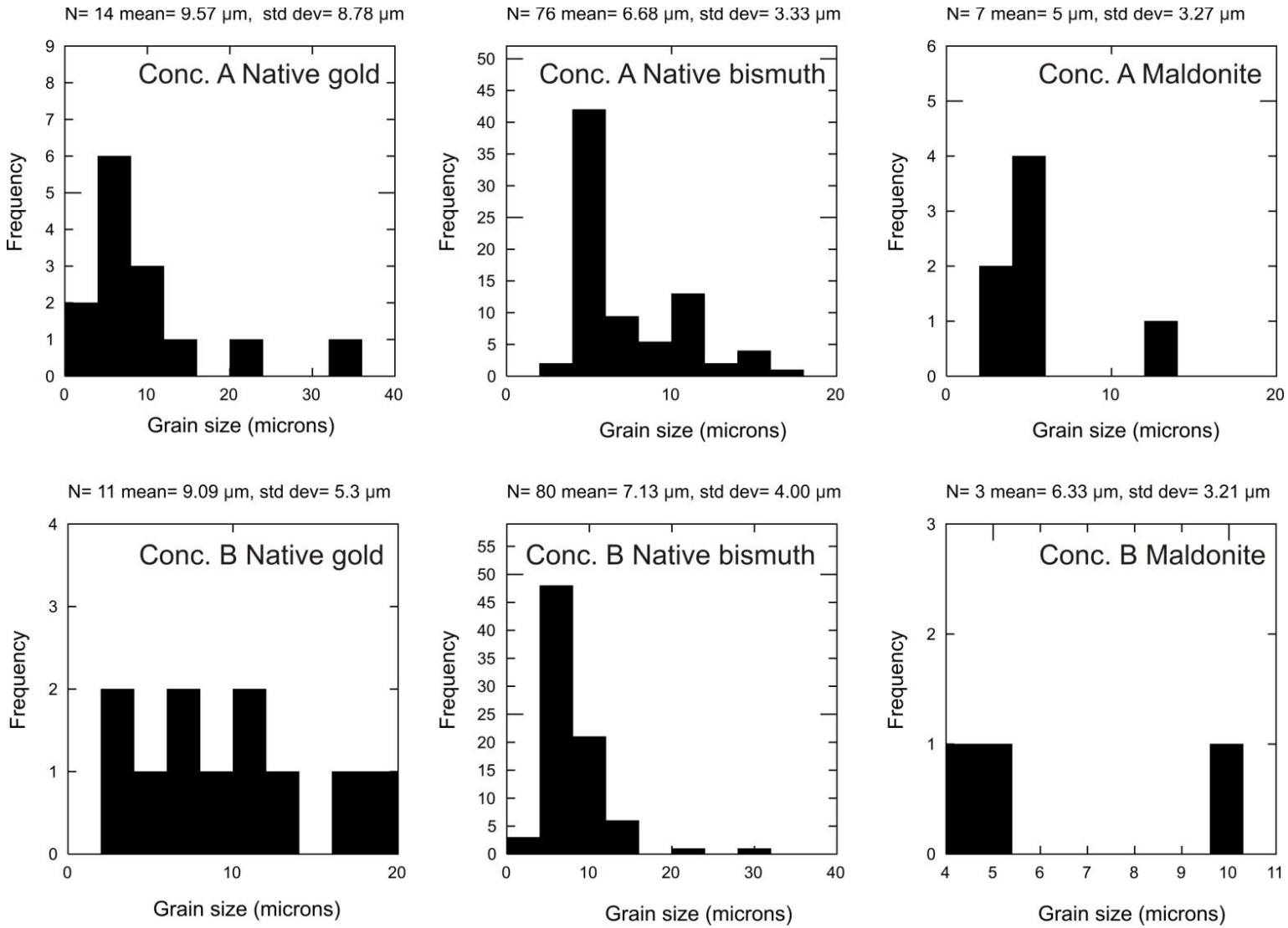

Figure 16. Mean diameters and abundance of native gold/electrum, native bismuth and maldonite grains observed within an ~1 cm^2 area by rastering analysis at high magnification using (SEM) of the two concentrate types from Boddington gold mine

Fig. 17

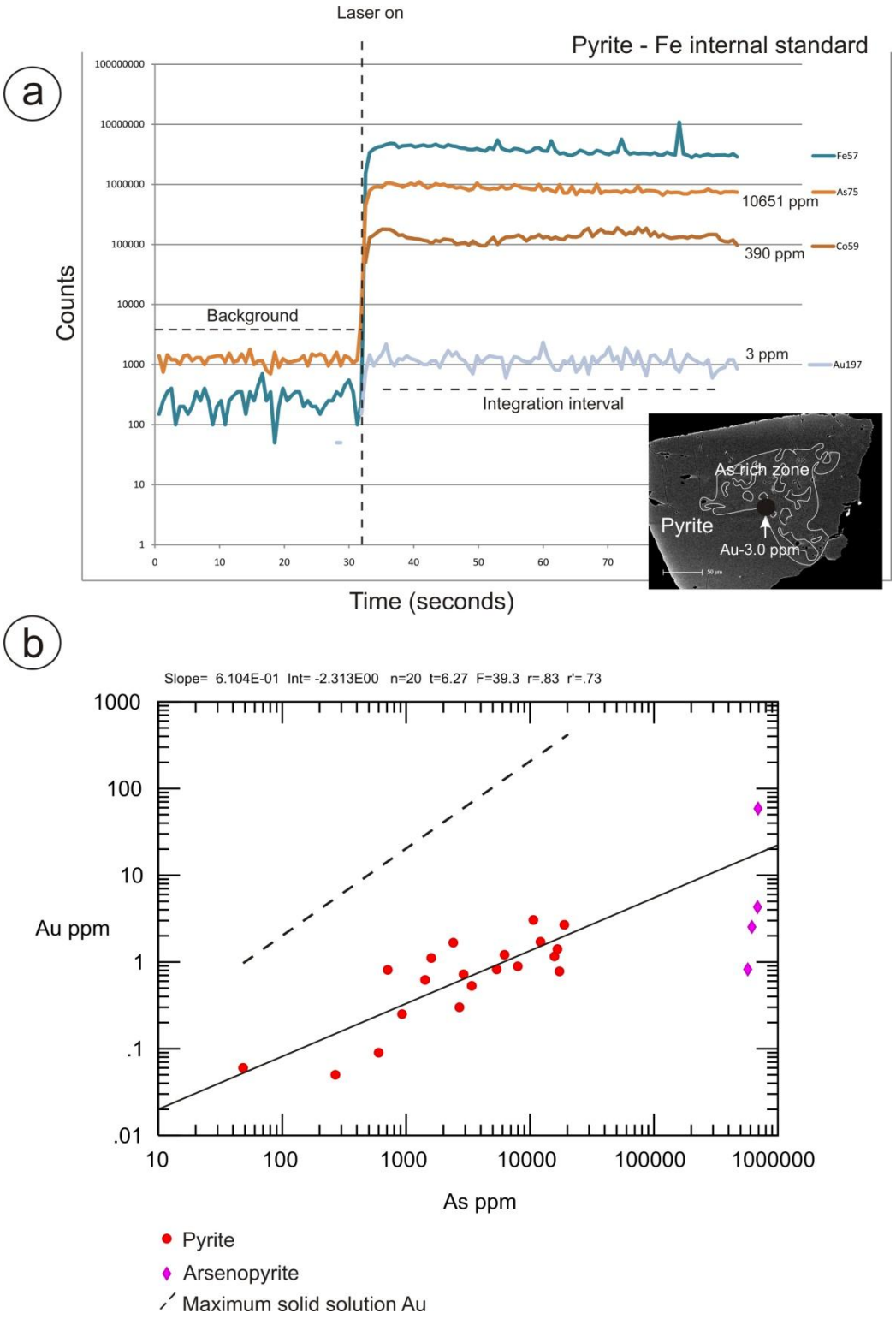

Figure 17. (a) Time-resolved LA-ICPMS depth profile for pyrite (sample NK26) showing solid solution Au(flat spectrum). Arsenic, Co, and Au concentrations are given in ppm. Inset (BSE) image of analysed pyrite grain showing arsenic zonation. (b) LA-ICPMS results for pyrite and arsenopyrite showing arsenic vs Au correlation, maximum solid solution Au line represent the inferred solubility limit for Au with respect to analysed As concentrations approximated by $C_{Au}=0.02 * C_{As} + 4*10^{-5}$ where C_{Au} and C_{As} represent the concentrations of Au and As in mole percent, above this line Au is expected to contain nanoparticles of Au (Reich *et al*. 2005); note equation is used for arsenian pyrite but not arsenopyrite.

Fig. 18

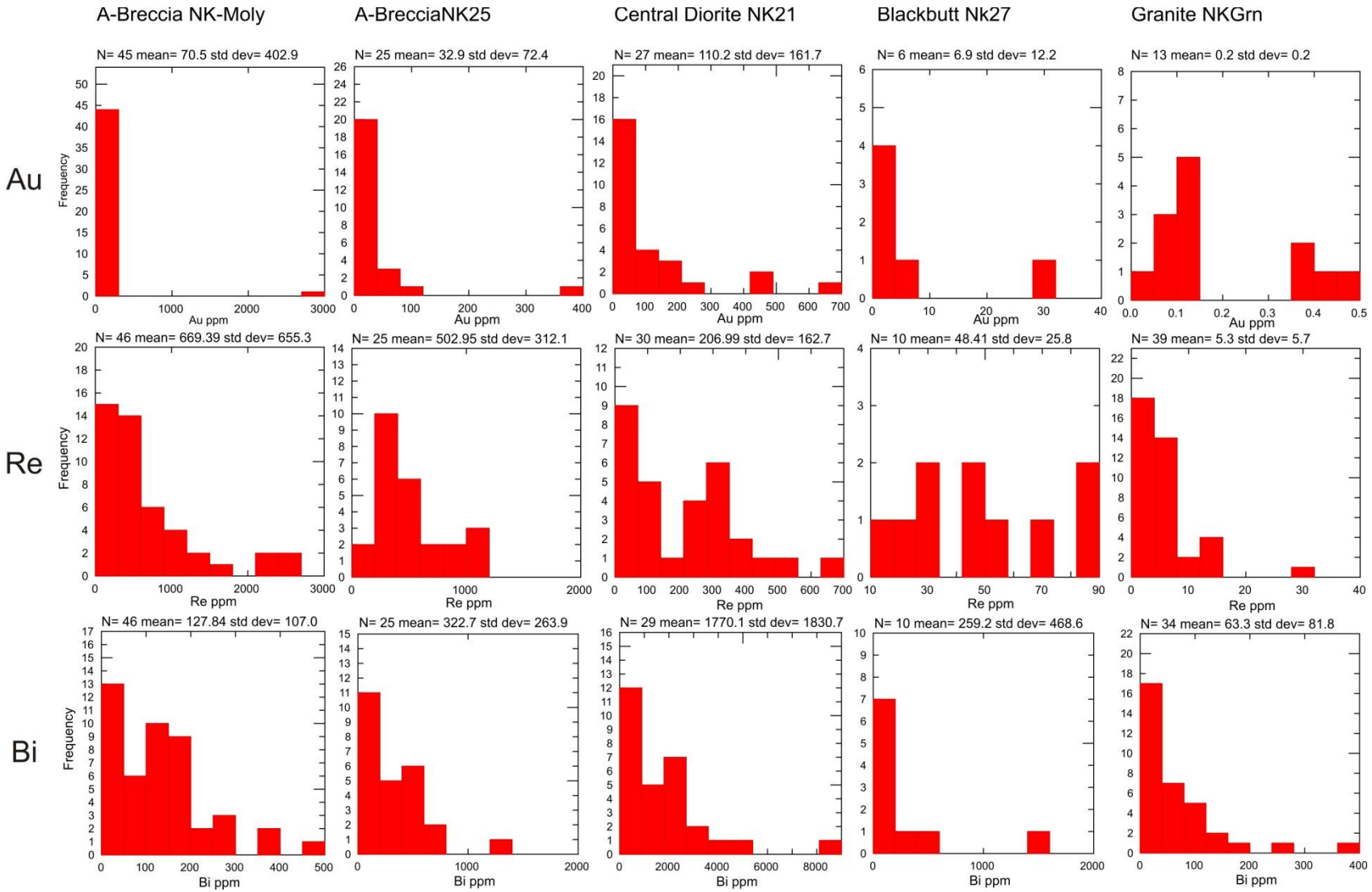

Figure 18. Histograms showing relative LA-ICPMS analysis concentrations of Au, Re and Bi in ppm analysed in molybdenite from five samples collected from the Boddington deposit and from the monzogranite body.

Fig. 19

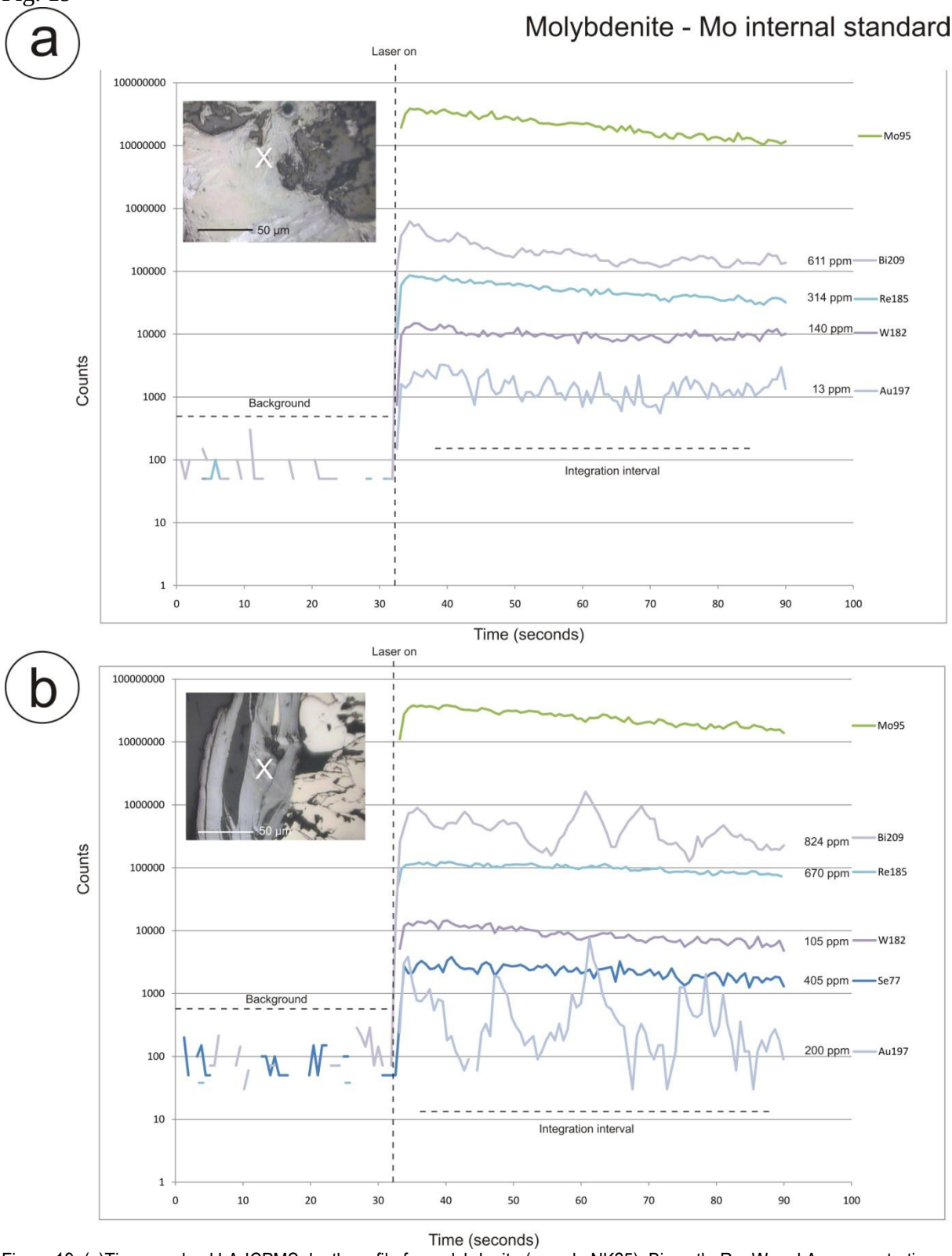

Figure 19. (a)Time-resolved LA-ICPMS depth profile for molybdenite (sample NK25). Bismuth, Re, W and Au concentrations given in ppm, smooth nature of Au indicates homogeneously distributed nanoparticulate inclusions of Au. Inset image of sample with spot site in centre. (b) Time-resolved LA-ICPMS depth profile for molybdenite (sample NK21). Note much more spiky nature for Au indicating gold inclusions/maldonite/electrum. Inset image of spot location.

Fig. 20

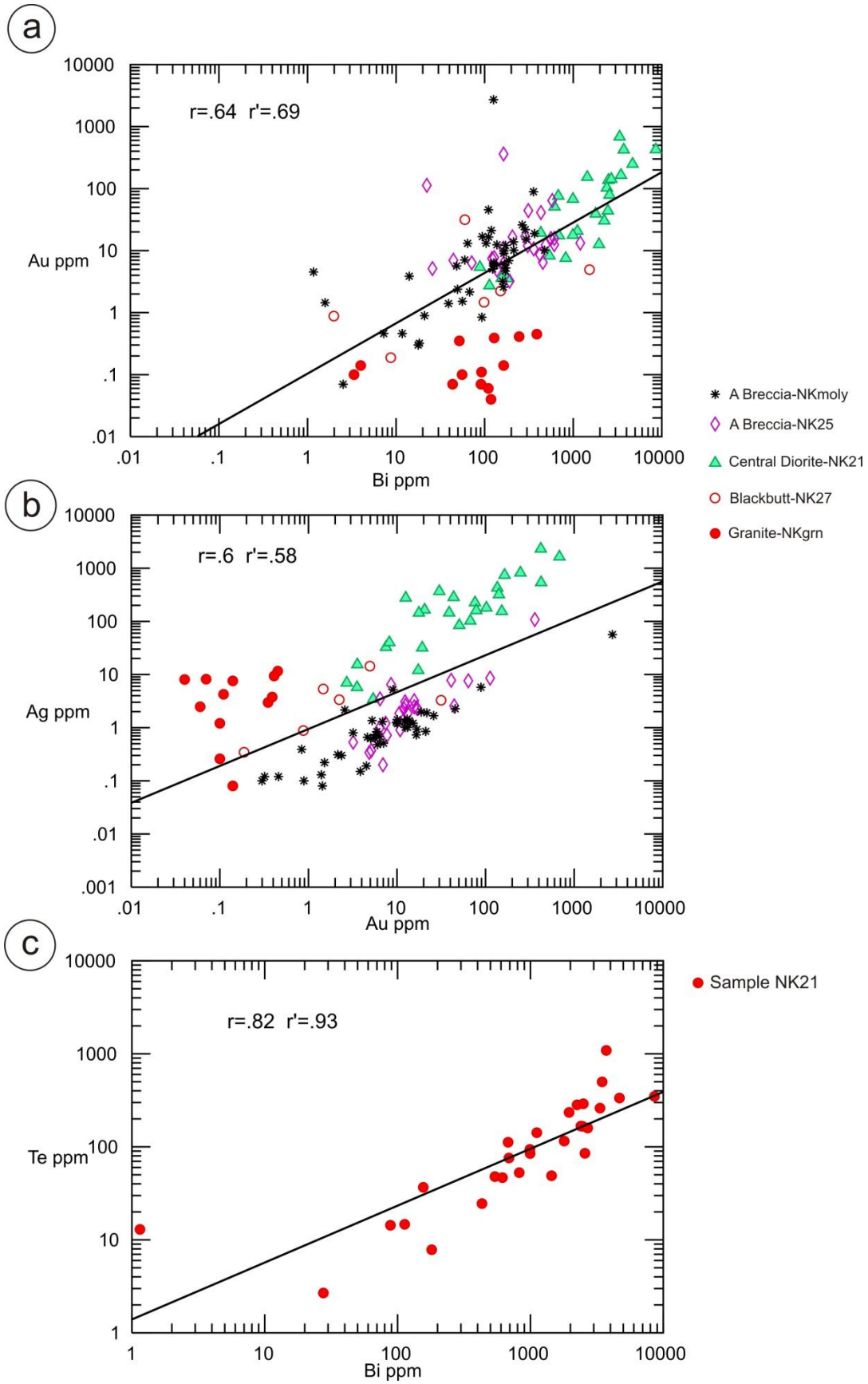

Figure 20. Binary plots for LA-ICPMS results from molybdenite samples (a) binary plot of all analyses for Au vs Bi presenting the correlation of these two elements within molybdenite samples. (b) Correlation of Au vs Ag for all molybdenite samples. (c) Binary plot for Te vs Bi from sample NK21.

Fig. 21

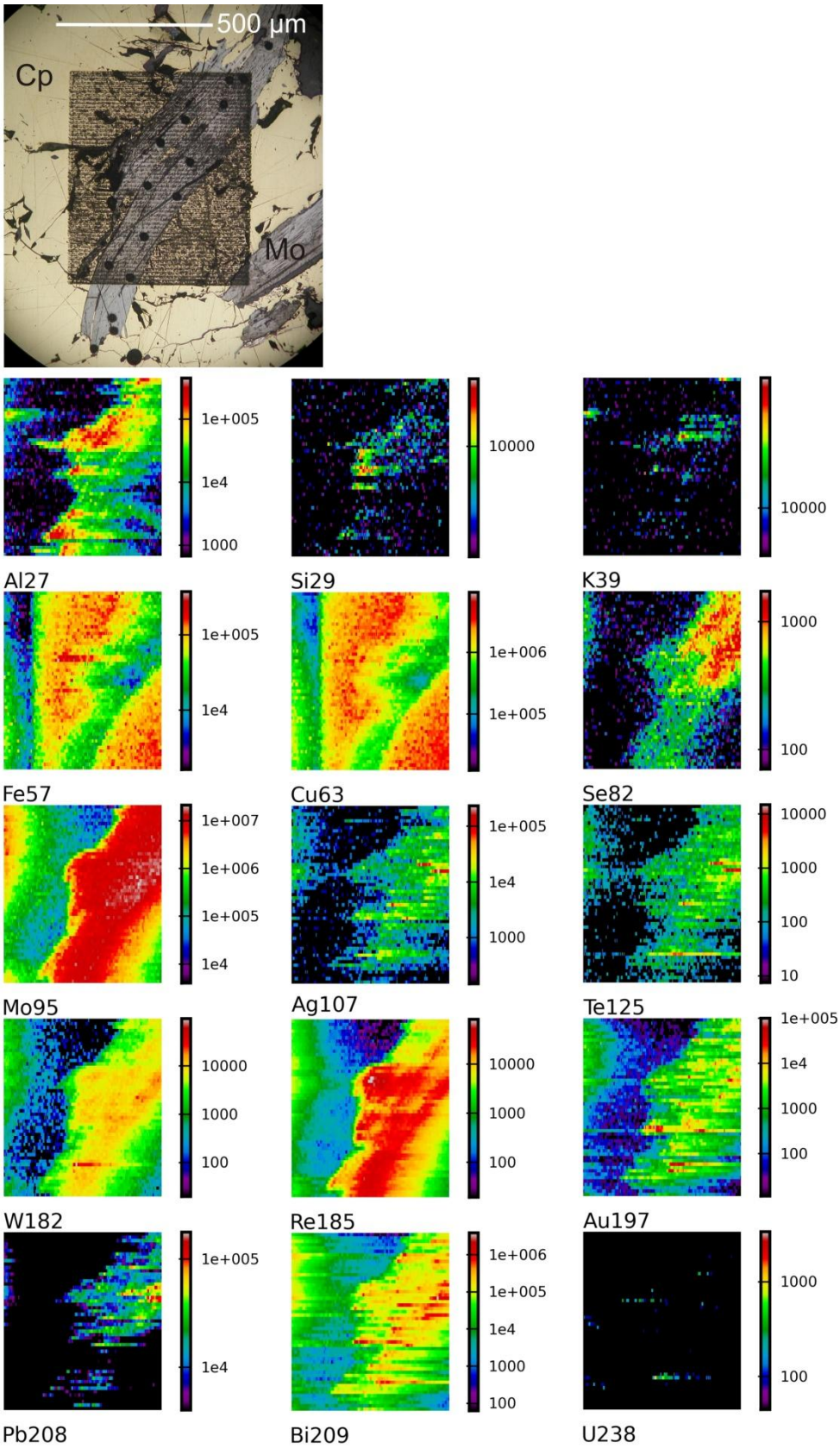

Figure 21. LA-ICPMS element map conducted on molybdenite grain (Mo) within chalcopyrite (Cp)(sample NK21). The reflected light image is at 50 x magnification and shows the position of map.

Fig. 22

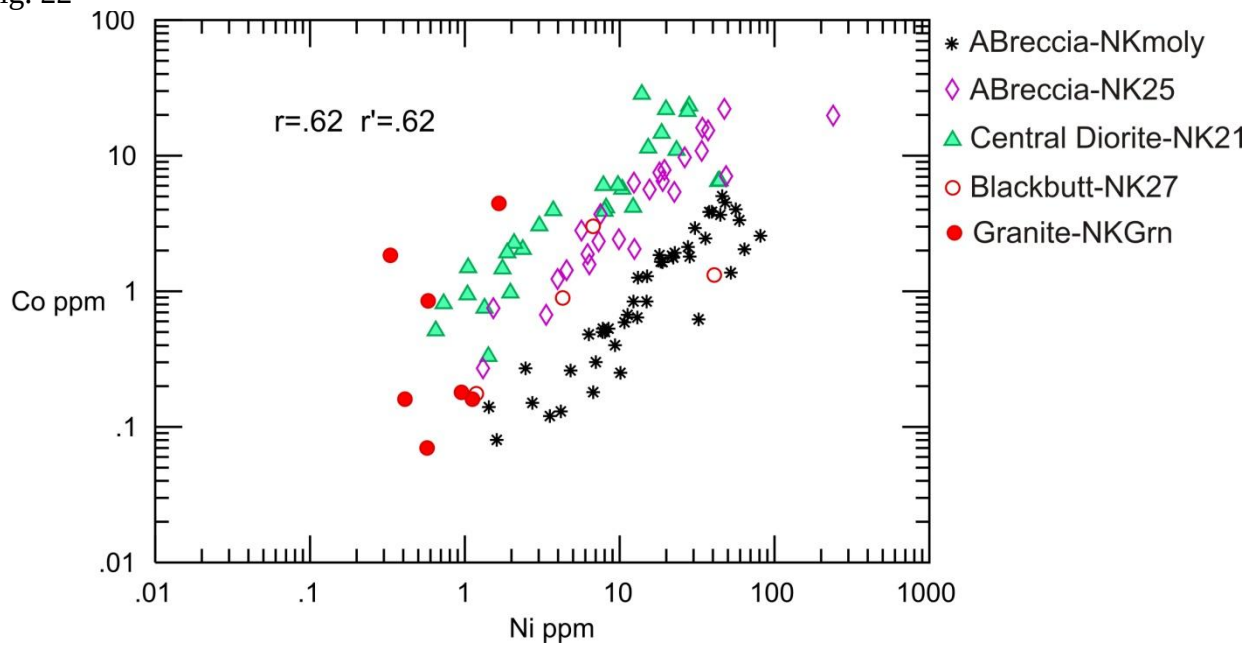

Figure 22. Binary plot of Co vs Ni for LA-ICPMS results obtained from molybdenite samples

Fig. 23

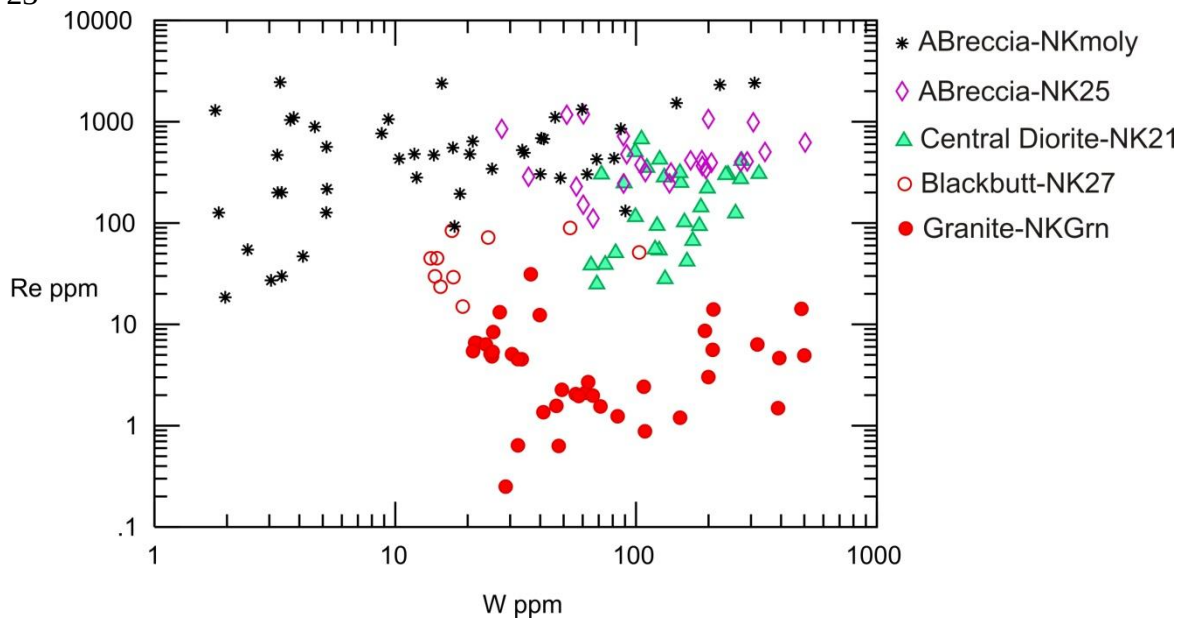

Figure 23. W vs Re binary plot of LA-ICPMS results conducted on molybdenite samples, sample legend is arranged in order of their distal relationship to the monzogranite (furthest at top with monzogranite sample at the bottom) and demonstrates the increase in Re content away from the monzogranite.

Fig. 24

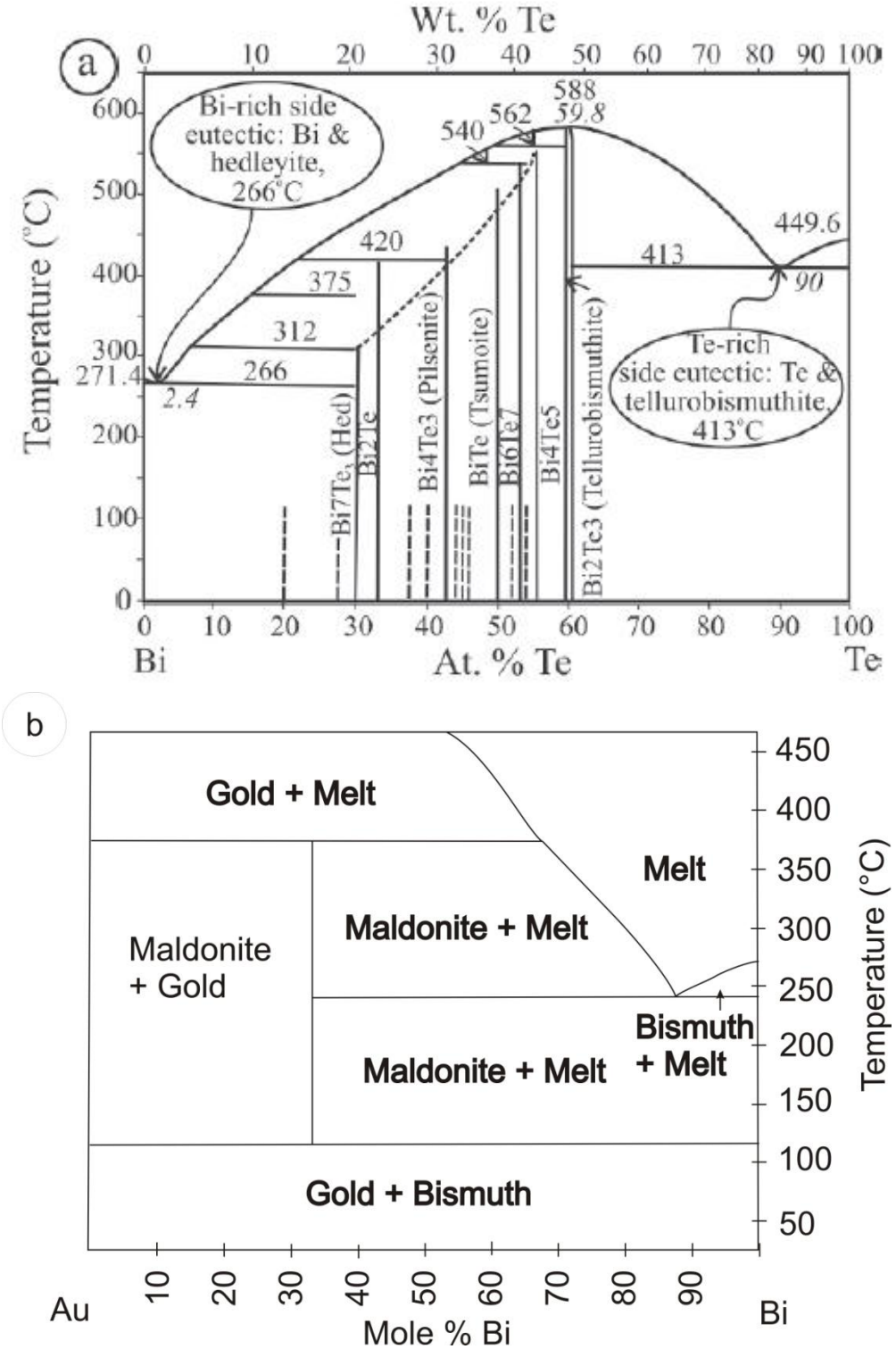

Figure 24. (a) Bi-Te phase diagram (Ciobanu *et al*. 2005) after (Okamoto and Tanner 1990). (b) Phase diagram for Au-Bi system at 1 bar (Tooth *et al*. 2008)

Table 1. Sample suite locations and sample numbers.

Location code	Domain/Date	Rom Level/core ID	Mine grid coordinates	Samples
South pit				
#1	Pipeline	RL-162 shot 013	9600.72mE, 11830.21mN	NK15, NK20
#2	Central Diorite	RL - 168 shot 030	9814.95mE, 10918.14mN	NK1, NK2a, NK2b, NK2c, NK2d, NK3, NK4, NK6, NK34, NK35, NK36
#4	Pipeline	RL - 156 shot 001	-	NK19, NK37, NK38, NK40, NK41
#6	Pipeline	-	-	NK16
#7	Blackbutt	-	Stockpile	NK27, NK28
#8	Central Diorite	-	-	NK17, NK17b, NK21
North pit				
#3	North Diorite	RL – 240 shot ?	9716.4mE, 12721.67mN	NK18, NK29, NK30, NK31, NK32
#5	ABreccia	RL - 252 shot 28	-	NK5, NK22, NK23, NK24, NK25, NK26, NK33, NK39,NKMo/moly
Drill core depth	North Diorite	WRD-13810-002	9650mE, 13810mN	
223.4m				NK12
224.0m				NK11
246.3m				NK8
248.5m				NK10
261.5m				NK14
363.7m				NK9
667.3m				NK13
705.7m				NK7
Others				
ConcA	24/03/2010	High Cu, low Bi	Concentrate sample	ConcA
ConcB	24/03/2010	High Bi	Concentrate sample	ConcB
Granite 472.6m	Monzogranite	WRD-09775-002	~10600mE, 09775mN	NKgranite/grn

Table 2. Assay results for selected ore samples and concentrates (ppm), the number in sample number corresponds to domain; 2,8- central diorite, 4,6 Pipeline, 7 Blackbutt, 5 ABreccia and 3 from North Diorite.

Domain	Sample no.	Au	Ag	As	Bi	Co	Cu	Mo	Ni	Pb	Sb	Se	Te	Zn
Central Diorite	ANK2a	9.54, 9.51	27, 27	<mdl, 10	59, 62	62, 61	32173, 30257	<mdl	120, 119	<mdl	0.63	24	6	679
	ANK2b	5.97	7.7	<mdl	57	16	2170	3	28	14	0.3	5	7.4	154
	ANK2c	5.05	3.4	<mdl	<mdl	19	7065	11	43	8	0.22	7	1.6	137
North Diorite	ANK3a	9.03	3.5	<mdl	94	37	3621	<mdl	89	11	2.12	4	0.9	102
	ANK3b	3.27	2.6	<mdl	<mdl	19	4078	4	53	8	1.48	3	0.5	104
	ANK3c	0.47, 0.51	0.4	<mdl	<mdl	5	316	<mdl	30	9	1.33	<mdl	<mdl	40
	ANK3d	5.31, 5.06	4.1	<mdl	42	43	6415	5	79	7	1.73	5	0.4	103
Pipeline	ANK4a	0.19	6.4	<mdl	33	24	5929	3	48	24	4.57	3	0.2	223
	ANK4b	0.14	0.4	<mdl	31	17	251	<mdl	67	10	1.77	2	<mdl	118
	ANK4c	0.56	0.6	14	41	16	341	7	28	13	0.63	<mdl	3	105
ABreccia	ANK5a	0.33	0.7	221	<mdl	68	1849	5	160	10	1	8	1.2	106
	ANK5b	0.48	0.4	62	<mdl	8	374	4216	34	<mdl	1.05	5	0.5	34
	ANK5c	0.33	0.9	48	<mdl	24	763	13	102	8	2.19	4	0.2	54
	ANK5d	0.15	0.7	52	<mdl	3	17	16	3	11	0.3	<mdl	0.1	5
	ANK5e	<mdl	0.4	<mdl	<mdl	52	163	3	86	7	0.87	2	<mdl	86
Pipeline	ANK6	20.05, 19.35	4.8	<mdl	192	35	6759	25	149	9	3.77	10	7.1	286
Blackbutt	ANK7a	1.73	1	12	<mdl	7	1182	86	73	10	1.37	<mdl	0.5	34
	ANK7b	2.7	2	33	11	21	1179	144	60	8	2.83	<mdl	0.7	38
Central Diorite	ANK8	1.27	2.7	<mdl	19	12	3884	1353	17	<mdl	0.23	3	0.7	178
	NKCONC A	95.06	79	285	429	238	158998	2370	625	52	35.42	143	44.8	3214
	NKCONC B	132.44, 129.74	84, 85	454, 463	734, 725	224, 230	158449, 157171	2855, 2779	735, 744	85, 84	171.75	147	63.5	3871
	Detection limit	0.01	0.2	10	10	1	1	2	1	5	0.05	2	0.1	1
	Method	FA/AAS	AMS	AOES	AOES	AOES	AOES	AOES	AOES	AOES	AMS	AMS	AMS	AOES

Note: Complete duplicate analyses were made for samples ANK02a and NKCONC B; additional duplicate Au analyses were made on ANK03c, ANK03d and ANK06.

Methods: FA/AAS – 25g Lead collection fire assay, Flame Atomic Absorption Spectrometry; AMS – ICP-MS analysis of multi-acid digest (HF, HNO3, HClO3, HCl); AOES ICP (Optical) Atomic Emission Spectrometry of multi-acid digest. Genalysis Laboratory Services, Adelaide.

Table 3a. Summary of electron probe microanalyses of pyrite

Pyrite										
	South pit								North pit	
	Central Diorite						Pipeline		North Diorite	
(wt. %)	NK2b (n=4)		NK2a (5)	NK4 (8)	NK1 (n=5)		NK16 (n=2)		NK18 (n=3)	
	mean	SD			mean	SD	mean	SD	mean	SD
Cu	0.29	0.33	0.00	<mdl	0.75	0.92	0.00	<mdl	0.02	0.02
Mn	<mdl	0.01	0.00	<mdl	0.02	0.01	0.00	<mdl	0.01	0.01
Fe	46.49	0.64	46.72	45.78	43.01	2.86	45.38	0.50	45.93	0.21
Co	0.02	0.02	0.00	0.01	1.57	1.69	0.07	0.10	0.16	0.03
Ni	0.08	0.03	0.10	0.85	2.19	2.34	0.32	0.27	0.24	0.01
As	0.03	0.02	0.02	0.05	0.01	0.01	0.10	0.03	0.04	0.01
Sb	0.02	0.01	0.02	0.06	0.02	0.02	0.00	<mdl	0.02	0.03
Se	0.04	0.03	0.08	0.01	0.03	0.03	0.02	0.00	0.02	0.03
S	**54.04**	**0.37**	53.11	54.27	51.60	1.49	53.44	0.14	53.05	0.21
Total	**101.01**	**0.59**	**100.05**	**101.02**	**99.20**	**0.39**	**99.33**	**1.03**	**99.49**	**0.15**
Calculated formulae (a.p.f.u 3)										
Cu	0.01	0.01	-	-	0.01	0.02	-	-	0.00	0.00
Mn	-	-	-	-	0.00	0.00	-	-	-	-
Fe	0.99	0.01	1.01	0.97	0.94	0.05	0.98	0.00	0.99	0.00
Co	0.00	0.00	-	-	0.03	0.04	0.00	0.00	0.00	0.00
Ni	0.00	0.00	0.00	0.01	0.04	0.04	0.01	0.00	0.00	0.00
As	0.00	0.00	-	0.00	-	-	0.00	0.00	0.00	0.00
Sb	-	-	-	0.00	0.00	0.00	-	-	0.00	0.00
Total M	**1.00**	**0.01**	**1.01**	**0.99**	**1.03**	**0.04**	**0.99**	**0.01**	**1.00**	**0.00**
Se	0.00	0.00	0.00	-	0.00	0.00	-	-	0.00	0.00
S	2.00	0.01	1.99	2.01	1.97	0.04	2.01	0.01	2.00	0.00
Total (S+Se)	**2.00**	**0.01**	**1.99**	**2.01**	**1.97**	**0.04**	**2.01**	**0.01**	**2.00**	**0.00**

Table 3b. Electron probe microanalyses of arsenopyrite, cobaltite and costibite

	Arsenopyrite (FeAsS)						Cobaltite (CoAsS)					Costibite (CoSbS)
(wt. %)												
Sample	NK5	NK5	NK5	NK5	NK5		NK16	NK16	NK16	NK16	NK5	NK10
Spot	(3)	(4)	(5)	(6)	(7)		(10)	(11)	(12)	(20)	(1)	(20)
Cu	<mdl	<mdl	0.03	<mdl	0.04		<mdl	<mdl	0.06	0.66	<mdl	0.14
Mn	<mdl	<mdl	0.03	0.01	<mdl		0.01	<mdl	0.02	<mdl	<mdl	0.02
Fe	33.74	33.70	34.10	33.97	34.67		3.49	5.57	3.82	7.07	6.19	0.40
Co	0.56	0.61	0.76	0.85	0.12		28.12	22.69	27.35	19.95	22.29	17.19
Ni	0.02	<mdl	<mdl	0.03	0.26		4.61	7.96	4.93	8.39	6.76	9.45
As	43.17	43.10	42.99	41.89	42.66		44.94	45.14	44.91	44.79	44.31	2.04
Sb	0.08	<mdl	0.02	<mdl	0.05		<mdl	<mdl	0.09	0.01	<mdl	56.25
Se	0.29	0.37	0.35	0.33	0.29		0.39	0.42	0.38	0.37	0.34	0.04
S	21.52	21.22	21.68	22.72	21.80		19.88	19.64	19.42	19.65	20.33	15.06
Total	**99.39**	**99.01**	**99.96**	**99.81**	**99.89**		**101.44**	**101.43**	**100.97**	**100.90**	**100.22**	**100.59**
Calculated formulae												
apfu	3	3	3	3	3		3	3	3	3	3	3
Cu	-	-	-	-	-		-	-	-	0.017	-	0.005
Mn	-	-	-	-	-		-	-	-	-	-	0.001
Fe	0.971	0.976	0.975	0.963	0.990		0.102	0.164	0.113	0.210	0.183	0.015
Co	0.015	0.017	0.021	0.023	-		0.781	0.634	0.767	0.560	0.624	0.625
Ni	-	-	-	-	0.006		0.110	0.191	0.119	0.202	0.162	0.295
As	0.927	0.930	0.916	0.885	0.908		0.983	0.993	0.990	0.989	0.976	0.059
Sb	-	-	-	-	-		-	-	-	-	-	0.991
Total M	**1.915**	**1.922**	**1.914**	**1.872**	**1.910**		**1.976**	**1.982**	**1.992**	**1.978**	**1.946**	**1.991**
Se	0.006	0.008	0.007	0.007	0.006		0.008	0.009	0.008	0.008	0.007	0.001
S	1.079	1.070	1.079	1.122	1.085		1.016	1.009	1.000	1.014	1.047	1.008
Total (S+Se)	**1.085**	**1.078**	**1.086**	**1.128**	**1.090**		**1.024**	**1.018**	**1.008**	**1.022**	**1.054**	**1.009**

Table 3c. Electron probe microanalyses of pyrrhotite and cubanite

	Cubanite ($CuFe_2S_3$)					**Pyrrhotite ($Fe_{1-x}S$)**					
(wt. %)											
Spot	NK2b (40)	NK2b (41)	NK16 (15)	NK16 (25)		NK2b (42)	NK10 (12)	NK10 (35)	NK5 (2)	NK15 (2)	NK14 (3)
Cu	23.55	23.80	23.63	23.61		<mdl	0.04	0.03	0.06	0.06	0.08
Mn	<mdl	0.01	0.01	0.01		0.02	0.01	<mdl	<mdl	0.04	0.03
Fe	40.30	41.72	40.54	40.23		60.73	59.21	60.88	60.58	60.70	60.61
Co	<mdl	<mdl	<mdl	<mdl		0.05	0.05	0.05	<mdl	0.04	0.03
Ni	<mdl	<mdl	<mdl	<mdl		0.03	<mdl	0.07	0.08	0.14	0.14
As	0.08	0.13	0.04	0.01		0.03	0.13	0.03	0.03	0.01	0.13
Sb	<mdl	<mdl	0.04	0.03		<mdl	<mdl	0.01	0.04	0.05	<mdl
Se	0.01	0.07	0.03	0.06		0.03	0.02	<mdl	0.02	<mdl	<mdl
S	35.82	35.64	35.61	35.61		39.33	39.36	38.87	39.16	38.37	38.77
Total	**99.76**	**101.38**	**99.89**	**99.56**		**100.21**	**98.82**	**99.94**	**99.97**	**99.41**	**99.79**
Calculated formulae											
apfu	6	6	6	6		2	2	2	2	2	2
Cu	1.006	1.005	1.010	1.012		-	0.001	-	0.001	0.001	0.001
Mn	-	-	-	-		-	-	-	-	0.001	-
Fe	1.959	2.005	1.971	1.961		0.939	0.925	0.473	0.940	0.950	0.944
Co	-	-	-	-		0.001	0.001	0.000	-	0.001	0.000
Ni	-	-	-	-		-	-	-	0.001	0.002	0.002
As	0.003	0.005	0.001	-		-	0.002	-	-	-	0.002
Sb	-	-	0.001	0.001		-	-	-	-	-	-
Total M	**2.967**	**3.015**	**2.983**	**2.974**		**0.941**	**0.928**	**0.474**	**0.942**	**0.954**	**0.949**
Se	-	0.002	0.001	0.002		-	-	-	-	-	-
S	3.032	2.982	3.016	3.023		1.059	1.071	0.526	1.058	1.046	1.051
Total (S+Se)	**3.033**	**2.985**	**3.017**	**3.026**		**1.059**	**1.072**	**0.526**	**1.058**	**1.046**	**1.051**

Table 4. Summary of electron probe microanalyses of Bi-telluride phases (Tetradymite Group)

Named minerals	Hedleyite Bi_7Te_3						Pilsenite Bi_4Te_3				laitakarite $Bi_4(Se,S)_3$		Ikunolite Bi4S3		Tsumoite BiTe				Tellurobismutite Bi2Te3	
(wt. %)	nk2a (n=2)		nk2b (n=13)		nk2d (n=2)		nk3 (n=2)		nk10 (n=8)		nk4 (n=3)		nk30 (n=2)		nk2b (n=2)		nk10 (n=7)		nk2b (n=3)	
	mean	**SD**	**mean**	**SD**	**mean**	**SD**	**mean**	**SD**	**mean**	**SD**	**mean**	**SD**	**mean**	**SD**	**mean**	**SD**	**mean**	**SD**	**mean**	**SD**
Ag	0.01	0.02	0.02	0.03	0.02	0.01	0.01	0.01	0.01	0.02	0.07	0.07	<mdl	0.00	1.34	0.26	0.01	0.03	0.22	0.08
Pb	3.23	0.52	2.59	0.75	2.24	0.04	5.19	0.27	1.98	1.19	0.00	0.00	<mdl	0.00	0.98	0.53	3.42	0.18	0.03	0.06
Bi	77.37	1.95	77.68	1.38	76.51	0.52	64.37	0.18	65.13	2.68	76.93	1.13	87.98	0.62	59.22	4.24	61.38	0.63	51.87	0.99
Sb	0.22	0.07	0.10	0.06	0.13	0.01	0.14	0.19	0.28	0.09	<mdl	0.00	0.02	0.03	0.13	0.03	0.23	0.04	0.32	0.03
Te	19.73	1.11	19.40	0.99	19.22	0.06	28.39	0.06	30.99	2.03	5.07	1.34	0.36	0.32	37.67	3.57	34.33	0.48	47.46	1.41
Se	0.29	0.03	0.25	0.06	0.23	0.00	1.03	0.06	0.76	0.24	16.74	0.45	0.01	0.01	0.10	0.14	0.36	0.06	0.65	0.83
S	0.01	0.01	0.01	0.02	0.02	0.00	0.01	0.01	0.03	0.02	1.08	0.55	10.14	0.35	<mdl	0.00	0.01	0.01	0.04	0.02
Total	**100.86**	**0.21**	**100.05**	**0.81**	**98.38**	**0.61**	**99.15**	**0.23**	**99.20**	**0.93**	**99.88**	**0.26**	**98.51**	**0.08**	**99.43**	**1.12**	**99.75**	**0.48**	**100.37**	**1.70**
Formulae (a.p.f.u)	10		10		10		7		7		7		7		2		2		5	
Ag	0.00	0.00	0.00	0.01	0.00	0.00	0.00	0.00	0.00	0.00	0.01	0.01	-	0.00	0.04	0.01	0.00	0.00	0.016	0.01
Pb	0.29	0.04	0.23	0.07	0.20	0.00	0.38	0.11	0.12	0.07	0.00	0.00	-	0.00	0.02	0.01	0.06	0.00	0.001	0.00
Bi	6.78	0.20	6.87	0.17	6.88	0.01	3.78	0.00	3.78	0.20	3.94	0.08	3.98	0.09	0.95	0.08	1.00	0.01	1.966	0.02
Sb	0.03	0.01	0.02	0.01	0.02	0.00	0.01	0.02	0.03	0.01	-	-	0.00	0.00	0.00	0.00	0.01	0.00	0.021	0.00
Total M	**7.10**	**0.15**	**7.12**	**0.13**	**7.10**	**0.01**	**4.17**	**0.10**	**3.93**	**0.13**	**3.95**	**0.08**	**3.98**	**0.08**	**1.01**	**0.08**	**1.07**	**0.01**	**2.004**	**0.02**
Te	2.83	0.14	2.81	0.12	2.83	0.01	2.73	0.00	2.94	0.16	0.43	0.11	0.03	0.02	0.99	0.08	0.92	0.01	2.945	0.06
Se	0.07	0.01	0.06	0.01	0.05	0.00	0.16	0.01	0.12	0.04	2.27	0.06	0.00	0.00	0.00	0.01	0.02	0.00	0.044	0.07
S	0.00	0.01	0.01	0.01	0.01	0.00	0.00	0.00	0.01	0.01	0.36	0.18	2.99	0.06	-	-	0.00	0.00	0.006	0.01
Total S,Se,Te	**2.90**	**0.15**	**2.87**	**0.13**	**2.90**	**0.01**	**2.90**	**0.00**	**3.07**	**0.13**	**3.05**	**0.08**	**3.02**	**0.08**	**0.99**	**0.08**	**0.93**	**0.01**	**2.996**	**0.02**

Unnamed phases	$(Bi,Pb)_6Te_5$		Bi_5Te_3		$Bi_4(Te,Se)_5$	Bi_5Te_4		Bi_2Te			$Bi_2(Te,S)$	$Bi_2(Te,S,Se)$		$Bi_9Te_4Se_2$	Bi_8Te_3
(wt. %)	nk10 (n=10)		nk10 (n=2)		nk4	nk2b (n=2)		nk2b	nk3 (n=3)		nk30	nk18	nk30 (n=2)		nk22	nk2d
	mean	**SD**	**mean**	**SD**		**mean**	**SD**		**mean**	**SD**			**mean**	**SD**		
Ag	0.13	0.25	0.00	0.00	0.26	0.08	0.01	<mdl	0.01	0.01	<mdl	<mdl	0.02	0.03	0.32	<mdl
Pb	3.65	0.44	0.28	0.23	<mdl	4.42	0.29	4.09	1.49	0.07	0.55	0.75	0.42	0.04	0.79	2.69
Bi	61.64	0.35	75.97	1.89	59.52	60.47	0.09	71.65	75.82	0.48	76.99	79.94	78.37	0.27	72.43	78.06
Sb	0.24	0.07	0.43	0.11	0.20	0.21	0.01	0.14	0.07	0.06	0.10	0.10	0.12	0.03	0.12	0.19
Te	33.83	0.31	20.00	5.80	33.42	34.01	0.97	23.35	23.15	0.11	16.30	15.05	16.14	0.07	18.42	18.10
Se	0.36	0.05	2.64	2.28	6.49	0.07	0.03	0.10	0.84	0.07	3.02	0.04	2.61	0.09	6.78	0.19
S	0.01	0.01	0.64	0.82	0.45	0.03	0.02	<mdl	<mdl	0	0.91	3.05	1.07	0.02	0.09	0.03
Total	**99.88**	**0.75**	**99.95**	**0.46**	**100.3309**	**99.28**	**0.77**	**99.33**	**101.36**	**0.47**	**97.88**	**98.94**	**98.75**	**0.36**	**98.96**	**99.26**
Formulae (a.p.f.u)	11		8		9	9		3	9		9	3	3		15	11
Ag	0.02	0.04	0.00	0.00	0.033	0.01	0.00	-	0.00	0.00	-	-	0.00	0.00	0.08	-
Pb	0.33	0.04	0.02	0.01	-	0.33	0.03	0.11	0.11	0.00	0.04	0.02	0.01	0.00	0.10	0.27
Bi	5.54	0.06	5.03	0.05	3.962	4.48	0.04	1.88	5.80	0.03	5.85	1.91	1.97	0.00	8.85	7.71
Sb	0.04	0.01	0.05	0.01	0.023	0.03	0.00	0.01	0.01	0.01	0.00	0.00	0.01	0.00	0.03	0.03
Total M	**5.93**	**0.04**	**5.10**	**0.02**	**4.019**	**4.85**	**0.07**	**1.99**	**5.93**	**0.02**	**5.90**	**1.93**	**1.99**	**0.00**	**9.05**	**8.01**
Te	4.98	0.03	2.18	0.71	3.644	4.13	0.07	1.00	2.90	0.01	2.03	0.59	0.66	0.00	3.69	2.93
Se	0.09	0.01	0.46	0.38	1.143	0.01	0.01	0.01	0.17	0.01	0.61	0.00	0.17	0.01	2.19	0.05
S	0.00	0.01	0.27	0.35	0.194	0.01	0.01	-	-	-	0.45	0.48	0.18	0.00	0.07	0.02
Total S,Se,Te	**5.07**	**0.04**	**2.90**	**0.02**	**4.981**	**4.15**	**0.07**	**1.01**	**3.07**	**0.02**	**3.09**	**1.07**	**1.01**	**0.00**	**5.95**	**2.99**

Table 5. Electron probe microanalyses of other tellurides and selenides

	Hessite Ag_2Te									Altaite PbTe	
(wt. %)	**NK2b**				**NK4**	**NK8**	**NK22**			**NK2b**	**NK16**
	2bnk 33	**2dnk 10**	**2bnk 27**	**2bnk 29**	**4nk 5**	**8nk 29**	**22nk 57**	**22nk 58**	**22nk 59**	**2bnk 16**	**16nk 16**
Ag	62.31	62.01	62.13	63.36	61.39	66.98	63.97	63.30	64.75	0.18	<mdl
Pb	<mdl	0.94	<mdl	<mdl	<mdl	<mdl	0.01	0.00	0.00	61.50	60.95
Bi	0.01	0.83	0.00	0.00	0.09	0.00	0.00	0.43	0.36	0.38	0.32
Sb	0.34	0.20	0.26	0.25	0.28	0.15	0.34	0.19	0.18	0.21	0.10
Te	37.22	36.87	37.60	37.41	36.84	31.91	36.64	36.36	36.88	38.18	38.48
Se	0.06	<mdl	<mdl	0.06	<mdl	0.11	0.06	0.03	0.10	0.13	<mdl
S	0.05	0.20	0.02	0.04	0.10	2.24	0.08	0.06	0.09	<mdl	<mdl
Total	**100.2**	**101.1**	**100.3**	**101.2**	**98.89**	**101.4**	**101.10**	**100.4**	**102.4**	**100.6**	**99.98**
Calculated formulae											
a.p.f.u	3	3	3	3	3	3	3	3	3	2	2
Ag	1.977	1.959	1.972	1.990	1.973	1.974	2.008	2.006	2.008	0.005	-
Pb	-	0.015	-	-	-	-	0.000	0.000	0.000	0.984	0.982
Bi	0.000	0.013	0.000	0.000	0.002	0.000	0.000	0.007	0.006	0.006	0.005
Sb	0.009	0.006	0.007	0.007	0.008	0.004	0.009	0.005	0.005	0.006	0.003
Total M	**1.987**	**1.994**	**1.979**	**1.997**	**1.982**	**1.978**	**2.017**	**2.018**	**2.019**	**1.001**	**0.990**
Te	0.999	0.985	1.009	0.993	1.001	0.795	0.972	0.974	0.967	0.992	1.006
Se	0.002	-	-	0.003	-	0.005	0.003	0.001	0.004	0.006	-
S	0.006	0.021	0.002	0.004	0.011	0.222	0.008	0.007	0.010	-	-
Total (S+Se+Te)	**1.007**	**1.006**	**1.012**	**1.000**	**1.012**	**1.022**	**0.983**	**0.982**	**0.981**	**0.998**	**1.006**

	Clausthalite PbSe							Volynskite $AgBiTe_2$	native bismuth
(wt. %)	**NK2b**		**NK2d**	**NK16**	**NK22**			**NK2b**	**NK22**
	2b13	**2b13**	**16**	**17**	**53**	**54**	**55**	**2b15**	**22nk1**
Ag	<mdl	<mdl	0.01	0.03	0.26	0.41	0.31	29.43	0.02
Pb	76.36	75.54	73.21	71.14	73.96	72.72	73.77	0.41	<mdl
Bi	0.40	0.49	<mdl	0.46	<mdl	<mdl	<mdl	28.34	97.85
Sb	<mdl	<mdl	<mdl	0.00	<mdl	<mdl	<mdl	0.22	<mdl
Te	0.90	0.78	1.01	1.07	0.29	0.33	0.23	41.80	0.03
Se	18.84	19.48	21.03	25.25	22.34	22.71	22.38	0.13	<mdl
S	3.96	3.86	2.73	0.13	2.80	2.66	2.60	0.03	<mdl
Total	**100.5**	**100.2**	**97.98**	**98.11**	**99.65**	**98.84**	**99.30**	**100.4**	**97.90**
Calculated formulae									
a.p.f.u	2	2	2	2	2	2	2	3	1
Ag	-	-	-	0.001	0.007	0.010	0.008	1.470	0.000
Pb	0.996	0.985	0.992	1.012	0.976	0.964	0.982	0.011	-
Bi	0.005	0.006	-	0.007	-	-	-	0.731	0.999
Sb	-	-	-	0.000	-	-	-	0.010	-
Total M	**1.002**	**0.991**	**0.992**	**1.020**	**0.982**	**0.975**	**0.990**	**2.221**	**0.999**
Te	0.019	0.017	0.022	0.025	0.006	0.007	0.005	1.765	0.001
Se	0.645	0.667	0.747	0.943	0.773	0.790	0.781	0.009	-
S	0.334	0.326	0.239	0.012	0.238	0.228	0.224	0.005	-
Total (S+Se+Te)	**0.998**	**1.009**	**1.008**	**0.980**	**1.018**	**1.025**	**1.010**	**1.779**	**0.001**

Table 6. Electron probe microanalyses of nickel-bearing minerals.

wt. %)	**argentopentlandite**	**Parkerite**						**unnamed ***
	$Ag(Fe,Ni)_8S_8$	**$Ni_3Bi_2S_2$**						
Sample	**NK20**	**NK16**	**NK16**	**NK16**	**NK16**	**NK16**	**NK16**	**NK16**
Spot	**(2)**	**(5)**	**(6)**	**(7)**	**(8)**	**(21)**	**(22)**	**(14)**
Cu	0.42	0.01	<mdl	0.01	<mdl	0.56	0.59	5.85
Ag	11.79	0.01	<mdl	<mdl	0.02	0.03	0.08	0.04
Au	<mdl	<mdl	0.13	0.05	<mdl	<mdl	<mdl	<mdl
Fe	35.94	0.77	0.94	0.97	0.88	1.04	1.07	11.84
Co	0.17	0.14	0.10	0.26	0.09	0.30	0.24	1.20
Ni	18.11	26.29	25.98	26.27	26.24	25.18	25.22	17.75
Pb	0.18	0.12	0.07	0.02	<mdl	0.02	0.03	1.76
As	0.06	0.06	0.01	0.05	0.07	0.04	0.03	0.14
Sb	0.07	<mdl	<mdl	0.01	<mdl	<mdl	0.03	<mdl
Bi	0.13	62.99	63.20	62.87	63.76	62.42	62.57	44.91
S	31.96	9.95	9.83	10.10	10.08	9.93	9.81	16.01
Se	0.02	0.10	0.02	0.11	0.11	0.18	0.17	0.05
Te	<mdl	0.09	<mdl	<mdl	0.03	0.14	0.18	0.02
Total	**98.85**	**100.52**	**100.27**	**100.73**	**101.27**	**99.84**	**100.02**	**99.57**
Calculated formulae								
apfu	**17**	**7**	**7**	**7**	**7**	**7**	**7**	**8**
Cu	0.054	-	-	-	-	0.057	0.061	0.544
Ag	0.897	-	-	-	0.001	0.002	0.005	0.002
Au	-	-	0.004	0.002	-	-	-	-
Fe	5.283	0.089	0.110	0.112	0.102	0.121	0.125	1.254
Co	0.024	0.015	0.011	0.029	0.010	0.033	0.026	0.121
Ni	2.533	2.905	2.892	2.880	2.880	2.795	2.804	1.789
Pb	0.007	0.004	0.002	0.001	-	-	0.001	0.050
As	0.006	0.006	0.001	0.004	0.006	0.003	0.003	0.011
Sb	0.005	-	-	-	-	-	0.002	-
Bi	0.005	1.955	1.976	1.936	1.966	1.946	1.954	1.271
Total M	**8.814**	**4.975**	**4.996**	**4.965**	**4.965**	**4.958**	**4.980**	**5.041**
S	8.184	2.013	2.002	2.026	2.025	2.019	1.997	2.953
Se	0.002	0.008	0.002	0.009	0.009	0.015	0.014	0.004
Te	-	0.004	-	-	0.002	0.007	0.009	0.001
Total (S+Se+Te)	**8.186**	**2.025**	**2.004**	**2.035**	**2.035**	**2.042**	**2.020**	**2.959**

* empirical formula aproximates to $(Ni,Fe,Co,Cu)_{3.7}Bi_{1.3}S_2$

Table 7. Electron probe microanalyses of gold/electrum

	Sample				
Wt. %	**NK2b (6)**	**NK4 (3)**	**NK18 (9)**	**NK2a (1)**	**NK2a (2)**
Cu	0.03	0.79	<mdl	0.06	0.11
Ag	47.00	2.82	10.98	22.72	45.25
Au	54.82	74.52	63.44	42.74	51.96
Bi	0.17	23.48	22.79	35.52	0.51
Hg	0.44	0.04	<mdl	<mdl	<mdl
Te	0.01	<mdl	2.91	0.59	0.13
Total	**102.46**	**101.66**	**100.12**	**101.63**	**97.95**
Calculated formulae (1 a.p.f.u.)					
Cu	0.001	0.024	-	0.001	0.002
Ag	0.607	0.049	0.183	0.349	0.609
Au	0.388	0.714	0.580	0.360	0.383
Bi	0.001	0.212	0.196	0.282	0.004
Hg	0.003	-	-	-	-
Te	-	-	0.041	0.008	0.001

Table 8. LA-ICPMS analyses of pyrite (sample NK26) in ppm

Spot	Co	Ni	As	Se	Mo	Ag	Sn	Sb	Te	Au	Pb	Tl	Bi
1	390	25.3	**10651**	12.3	<mdl	0.33	<mdl	<mdl	5.8	**3.0**	21.0	1.31	10.9
2	237	11.2	**12144**	9.7	<mdl	0.12	<mdl	<mdl	1.7	**1.7**	5.3	3.1	5.6
3	21.4	10.0	**927**	63.4	<mdl	2.9	<mdl	0.20	4.3	**0.25**	159	<mdl	89.1
4	223	35.3	**2901**	53.1	0.07	2.0	<mdl	0.24	33.5	**0.72**	35.3	1.8	144
5	22.2	0.90	**15733**	14.3	<mdl	<mdl	<mdl	<mdl	<mdl	**1.2**	<mdl	<mdl	<mdl
6	163	13.0	**16652**	13.5	<mdl	<mdl	<mdl	<mdl	<mdl	**1.4**	0.30	1.4	0.11
7	48.7	10.1	**268**	131	4.6	<mdl	<mdl	<mdl	2.4	**0.05**	11.8	1.7	2.1
8	777	24.1	**2397**	33.2	0.49	7.5	<mdl	24.4	7.8	**1.7**	784	<mdl	125
9	1.4	2.2	**1596**	21.3	0.61	5.5	<mdl	0.23	0.66	**1.1**	657	<mdl	81.8
10	30.2	38.8	**6225**	15.6	<mdl	0.94	<mdl	1.3	2.1	**1.2**	21.8	<mdl	37.7
11	7.7	59.7	**3378**	25.6	<mdl	4.2	<mdl	0.16	3.7	**0.53**	174	1.9	118
12	17.8	28.7	**1423**	91.9	2.2	4.9	<mdl	<mdl	4.5	**0.62**	253	3.2	81.3
13	29.8	17.7	**710**	134	20.8	11.3	<mdl	0.62	14.7	**0.81**	491	<mdl	531
14	0.49	2.1	**2692**	7.8	<mdl	0.12	<mdl	<mdl	<mdl	**0.30**	1.9	<mdl	7.2
15	7.0	18.0	**7962**	12.8	<mdl	0.26	<mdl	<mdl	2.4	**0.89**	8.0	1.2	7.5
16	10.3	2.0	**48**	87.9	0.51	2.4	<mdl	0.13	4.5	**0.06**	57.2	1.4	56.0
17	0.28	18.0	**1692**	19.4	<mdl	<mdl	0.20	<mdl	10.8	**<mdl**	<mdl	<mdl	<mdl
18	2.6	7.0	**600**	28.3	0.07	<mdl	<mdl	<mdl	<mdl	**0.09**	2.0	2.6	2.6
19	3.2	279	**18870**	3.3	<mdl	0.15	<mdl	0.26	0.92	**2.7**	1.5	4.1	7.2
20	16.1	57.7	**17277**	18.1	2.0	1.1	<mdl	<mdl	1.1	**0.78**	54.0	<mdl	31.9
21	55.5	41.0	**5379**	6.2	<mdl	0.44	<mdl	0.12	<mdl	**0.82**	12.7	3.2	12.1
Mean	98.3	33.4	**6168**	38.2	3.5	2.8	-	2.8	6.3	**1.0**	145	2.2	71.1
S.D.	186	58.8	**6382**	40.2	6.7	3.2	-	7.6	8.2	**0.81**	238	1.0	121
Minimum	0.28	0.90	**48.3**	3.3	<mdl	<mdl	-	0.12	<mdl	**<mdl**	<mdl	<mdl	<mdl
Maximum	777	279	**18870**	134	20.8	11.3	0.2	24.4	33.5	**3.0**	784	4.1	531

Mn was <mdl in all but 3 spots (max 2.6 ppm), Ga ranged from <0.1 to 1.2 ppm, In was <mdl in all but 3 spots (max 0.3 ppm), U ranged from <0.1 to 2.7 ppm

Table 9. LA-ICPMS analyses of arsenopyrite (sample NK24) in ppm

Spot	Co	Ni	Cu	Se	Ag	In	Sb	Te	Au	Pb	Bi
1	1333	352	<mdl	112	0.70	0.56	441	42.8	2.53	0.15	46.3
2	962	352	<mdl	61.1	<mdl	0.51	317	24.0	0.82	<mdl	3.1
3	6999	609	24.6	91.0	1.9	0.81	413	20.5	4.28	3.96	64.4
4	41576	2151	<mdl	116	<mdl	0.61	219	12.9	<mdl	0.45	5.3
5	18464	1575	<mdl	78.1	33.4	0.54	931	48.9	58.6	8.60	33435
Mean	13867	1008	-	91.7	12.0	0.60	464	29.8	16.6	3.3	6711
S.D.	17027	814	-	23.2	18.5	0.12	275	15.3	28.1	3.9	14939
Minimum	962	352	<mdl	61.1	0.70	0.51	219	12.9	<mdl	<mdl	3.1
Maximum	41576	2151	24.6	116	33	0.81	931	48.9	58.6	8.6	33435

Mn, Sn and Tl were <mdl in all spots, Mo was <mdl in all except 2 spots (0.23, 15.7 ppm), W was only >mdl in 1 spot (0.68 ppm), U was only >mdl in 1 spot (0.99 ppm)

Table 10. LA-ICPMS analysis of Molybdenite with element concentrations in ppm

North Pit

NK 25 **Abreccia**

PPM	Co	Ni	Cu	Zn	As	Se	Ag	Sn	Sb	Te	W	Re	Au	Pb	Bi	U
Mean	6.44	25.79	208.09	12.85	37.19	692.57	6.90	0.00	12.07	119.31	159.32	502.95	32.88	242.42	322.70	1.36
STDEV	6.13	46.65	252.70	12.85	79.10	97.62	21.21	0.00	12.95	85.83	114.60	312.05	72.43	233.32	263.93	2.04
Min	0.27	1.31	10.61	2.09	4.08	491.25	0.20	0.00	0.50	51.15	27.73	110.95	3.21	5.32	22.27	0.03
Max	22.11	239.41	924.27	59.17	370.95	980.18	108.06	0.00	58.19	508.96	504.14	1181	360.81	865.23	1201	4.39

NK Moly **Abreccia**

PPM	Co	Ni	Cu	Zn	As	Se	Ag	Sn	Sb	Te	W	Re	Au	Pb	Bi	U
Mean	1.49	21.55	152.98	15.70	8.98	820.32	2.31	0.39	10.37	82.30	36.48	669.39	70.46	55.49	127.84	0.50
STDEV	1.36	19.63	154.42	33.40	4.31	226.48	8.41	0.00	9.01	27.40	59.04	655.31	402.94	38.90	106.97	1.51
Min	0.08	0.54	1.83	1.32	2.64	48.06	0.07	0.39	0.15	9.92	1.79	18.48	0.07	0.34	1.00	0.01
Max	5.03	81.10	598.27	215.72	18.10	1384	56.31	0.39	36.09	171.86	310.84	2449	2712	150.71	475.75	4.79

South Pit

NK 21 **Central Diorite**

PPM	Co	Ni	Cu	Zn	As	Se	Ag	Sn	Sb	Te	W	Re	Au	Pb	Bi	U
Mean	6.71	11.21	5952	52.07	4.79	492.85	316.74	9.44	5.81	162.10	153.21	207.00	110.19	323.59	1770	0.03
STDEV	7.79	12.44	13449	58.80	3.02	191.30	511.21	10.07	5.69	214.46	69.36	162.66	161.70	391.42	1831	0.00
Min	0.18	0.65	0.94	2.54	3.07	178.44	0.24	1.10	0.48	2.68	65.05	24.87	2.71	0.84	1.15	0.02
Max	28.32	44.31	67539	206.27	11.55	846.04	2296	40.27	20.19	1088	323.99	670.54	681.77	1573	8589	0.03

NK 27 **Blackbutt**

PPM	Co	Ni	Cu	Zn	As	Se	Ag	Sn	Sb	Te	W	Re	Au	Pb	Bi	U
Mean	1.35	10.99	40.06	21.52	7.00	1561	4.10	0.00	4.38	96.24	29.33	48.41	6.87	104.28	259.22	0.77
STDEV	1.20	12.71	39.13	21.80	2.03	223.97	4.87	0.00	3.35	92.60	28.43	25.77	12.17	118.76	468.57	0.57
Min	0.18	1.19	5.76	2.27	5.56	1220	0.35	0.00	0.24	16.07	14.04	14.97	0.19	2.24	1.98	0.04
Max	3.01	40.84	113.93	52.23	8.44	1961	14.40	0.00	9.75	329.82	103.01	89.39	31.49	346.50	1527	1.32

Granite

NKGrn

PPM	Co	Ni	Cu	Zn	As	Se	Ag	Sn	Sb	Te	W	Re	Au	Pb	Bi	U
Mean	1.07	0.65	3.84	16.44	5.63	224.03	2.88	56.89	0.76	46.77	117.33	5.31	0.19	537.19	63.27	1.64
STDEV	1.27	0.44	3.83	36.87	2.80	83.82	3.54	204.19	0.51	31.81	135.55	5.66	0.15	1468	81.75	3.61
Min	0.06	0.04	0.18	1.74	0.10	56.29	0.01	0.67	0.12	5.47	21.05	0.25	0.04	0.09	0.08	0.02
Max	4.45	1.66	15.50	227.60	10.86	346.96	11.57	848.23	1.59	156.80	499.70	31.17	0.45	8208	388.06	14.52

Appendix 1a. Sample Suite descriptions

Sample	Location	Description	Main alteration	Rock type
NK 1	Central Diorite - #2	Slice from blue vein quartz. Mineralisation, chalcopyrite and pyrite	blue quartz	Quartz
NK 2a	Central Diorite - #2	Slice from vein quartz with chalcopyrite/pyrrhotite	vein quartz	Quartz
NK 2b	Central Diorite - #2	Slice from vein quartz with chalcopyrite/pyrrhotite	vein quartz	Quartz
NK 3	Central Diorite - #2	Slice from sheared rock with chalcopyrite and pyryhotite	silica rich shear zone	Diorite
NK 4	Central Diorite - #2	Slice from practice block with intergrown chalcopyrite and pyrrhotite with small cutting actinolite vein	quartz vein	Diorite
NK 5	Central Diorite - #5	Slice from quartz with actinolite veins. Mineralisation, chalcopyrite	reactivated quartz vein (actinolite)sheared	Andesite
NK 6	Central Diorite - #2	Quartz vien in un altered diorite (thin section)	reactivated quartz vein (actinolite)unaltered	Diorite
	Drill core WRD 13810-002			
NK 7	705.7m	Drill core from location WRD 13810-002. Sheared disseminated pyrrhotite/pyrite	shear zone (Si biotite alt)	Diorite
NK 8	246.3m	Reactivated quartz vien with chalcopyrite pyrrhotite core. Drill core	reactivated quartz vein (actinolite)	Dacite
NK 9	363.7m	Quartz vein with pyrrhotite. Drill core	quartz vein silica shear (silica albite vein)	Andesite
NK 10	248.5m	Vein/shear of pyrrhotite/ chalcopyrite. Drill core	shear zone silica albite + sulphide vein	Andesite
NK 11	224m	Quartz veins with alteration and brecciated vein with chalcopyrite (thin section). Drill core	silica albite and clinozoisite veins	Andesite
NK 12	223.4m	Actinolite vein in reactivated quartz vein with chalcopyrite (thin section). Drill core	reactivated quartz vein with actinolite and silica albite alteration	Andesite
NK 13	667.3m	Pyrrhotite core with overgrowth of pyrite. Drill core	sheared with quartz vein	Dacite
NK 14	261.5m	Cross cutting quartz vein with chalcopyrite silica albite alteration. Drill core	silica albite with quartz vein	Dacite
NK conc A		Cu concentrate (better)		
NK conc B		Cu concentrate (higher Bi)		
NK 15	Pipeline - #1	Actinolite vein/shear with quartz vein contact (thin section)	actinolite shear	Actinolite
NK 16	Pipeline - #6	Quartz vein with disseminated chalcopyrite and large pyrite with massive chalcopyrite vein	(silica vein)	Dacite
NK 17	Central Diorite - #8	Shear zone with chalcopyrite in sheared quartz vein sulphides in middle of polished section	silica rich shear zone	Andesite
NK 17 b	Central Diorite - #8	Shear zone with delta clast of sulphide and quartz (thin section)	silica rich shear zone	Andesite
NK 18	North Diorite - #3	Mineralised actinolite + quartz + pyrrhotite +/- pyrite	actinolite shear	Andesite
NK 19	Pipeline - #4	Actinolite shear zone with pyrite +/- pyrrhotite	actinolite shear	Andesite
NK 20	Pipeline - #1	Quartz albite alteration veining of quartz with chalcopyrite	silica albite (silica vein)	Dacite
NK 21	Central Diorite - #8	Quartz vein with chalcopyrite and molybdenite intergrowth	silica vein	Andesite
NK 22	ABreccia - #5	Sheared quartz vein with sulphide infill into shear fabric (pyrrhotite and chalcopyrite)	shear zone	?
NK 23	ABreccia - #5	Pyrrhotite disseminated in green (actinolite?)	clinozoisite vein	Quartz
NK 24	ABreccia - #5	Pyrhotite and chalcopyrite in vuggy quartz vein	silica vein	Quartz
NK 25	ABreccia - #5	Moly + chalcopyrite in quartz vein cut on angle to vein assay NK #05 a	silica vein	Diorite
NK 26	ABreccia - #5	Extremely quartz albite altered with disseminated pyrite and some chalcopyrite (assay #05 d)	silica vein	Quartz
NK 27	Blackbutt - #7	Small vienlet of pyrrhotite	silica albite	Andesite
NK 28	Blackbutt - #7	Quartz vein with actinolite plus some chalcopyrite and pyrite	silica vein	Dacite
NK 29	North Diorite - #3	Quartz vein with chalcopyrite polished block on top of vein (assay #03b)	silica sulphide vein	Diorite
NK 30	North Diorite - #3	Vein with chalcopyrite and pyrrhotite	silica albite	Dacite
NK 31	North Diorite - #3	Disseminated small blebs of chalcopyrite	clinozoisite	Diorite
NK 32	North Diorite - #3	Chacopyrite and pyrrhotite intergrowth in quartz vein (rich)	silica sulphide vein	Andesite
NK 34	Central Diorite - #2	Chalcopyrite pyrrhotite intergrowth in vuggy sulphite quartz vein (rich) assay #02a	shear zone	Diorite
NK 35	Central Diorite - #2	Quartz vein with chalcopyrite feeders + chalcopyrite on vein boundary	silica vein	Diorite
NK 36	Central Diorite - #2	Silica albite altered with faulted due to shear quartz vein with sulphides in intersection (chalcopyrite)	silica albite	Dacite
NK 37	Pipeline - #4	Quartz vein with arsenopyrite	silica vein	Quartz
NK 38	Pipeline - #4	Actinolite shear zone with chalcopyrite/ pyrite at actinolite grain boundaries vary coarse actinolite	actinolite shear zone	Quartz
NK 39	ABreccia - #5	Actinolite shear with pyrrhotite assay #05 a	actinolite shear zone	Actinolite
NK 40	Pipeline - #4	Albite altered brecciated quartz with pyrite and chalcopyrite assay #04 a	silica albite shear	Dacite
NK 41	Pipeline - #4	Albite altered brecciated quartz with pyrite and chalcopyrite (thin section not made) assay #04a		Andesite
NK Mo	ABreccia - #5	Molybdenite shear	molybdenite shear	Diorite
NK 2c	Central Diorite - #2	See 2b		
NK 2d	Central Diorite - #2	See 2b		
NK Grn/granite	472.6m	Drill core WRD-09775-002	disseminated molybdenite and chalcopyrite, pyrrhotite	Monzogranite

Appendix 1b. Assay sample rock descriptions

ASSAY	location	Description	alteration styles.	rock type
CONC A		better concentrate	-	-
CONC B		higher bismuth concentrate	-	-
ANK 08	Central diorite - #8	Central diorite quartz vein with chalcopyrite and molybdenite-polished block NK21	1 - silica sericite 2 - silica albite 3 - clinozoisite	andesite
ANK 06	Pipeline - #1	pipeline actinolite shear zone with chalcopyrite-actinolite shear	1 - actinolite	diorite
ANK 04 a	Pipeline - #4	albite altered brecciated quartz with pyrite and chalcopyrite-silica albite (brittle ductile) deformation	1-silica biotite 2-silica albite 3-later breciated vein with silica 4-shearing	andesite
ANK 04 b	Pipeline - #5	lower grade chalcopyrite and pyrrhotite-quartz vein possibly reactivated with ore fluids actinolite shear	1- silica biotite 2-actinolite	andesite
ANK 04 c	Pipeline - #6	sheared silica vein-silica shear	1-silica biotite 2-clinozoisite/actinolite 3- silica shear	andesite
ANK 05 a	Abreccia - #5	pyrrhotite stringers in shear zone some actinolite -polished block NK39	1 - actinolite	diorite
ANK 05 b	Abreccia - #5	molybdenite chalcopyrite quartz vein -polished block NK25	1 - silica albite	diorite
ANK 05 c	Abreccia - #5	quartz vein with chalcopyrite and pyrrhotite intergrowth and pyrrhotite sheared rock-quartz vein shear zone	1 - silica albite 2 - clinozoisite	andesite
ANK 05 d	Abreccia - #5	heavily silica albite altered with disseminated pyrite -polished block NK26	1 - silica albite	?
ANk 05 e	Abreccia - #5	silica sulphide vein-silica albite	1-silica sericite 2- silica albite	diorite
ANK 03 a	North diorite - #3	pyrrhotite in quartz vein with some chalcopyrite-quartz vein + sulphides	1 - silica sericite 2 - silica albite	diorite
ANK 03 b	North diorite - #3	chalcopyrite in quartz vein (polished section NK 29)	1-silica biotie 2- clinozoisite 3 silica + sulphide vein	andesite
ANK 03 c	North diorite - #3	offcuts from visible gold piece-reactivated quartz vein (actinolite)	1-silica albite 2-clinozoisite 3-reactivated actinolite	diorite
ANK 03 d	North diorite - #3	rich pyrite/pyrrhotite vein-clinozoisite and silica vein	1-silica biotite 2-clinozoisite 3-vein quartz	andesite
ANK 02 a	Central diorite - #2	very vuggy chalcopyrite pyrrhotite rich quartz -polished block NK34	1 - silica biotite 2 - silica albite 3 - clinozoisite	diorite
ANK 02 b	Central diorite - #2	vuggy chalcopyrite pyrrhotite rich quartz vein -polished block NK33	2 - silica biotite 2 - silica albite 3 - clinozoisite	diorite
ANK 02 c	Central diorite - #2	vein of chalcopyrite-clinozoisite and silica vein	1 - clinozoisite 2 - actinolite	diorite
ANK 07 b	Blackbutt - #7	quartz vein with chalcopyrite plus offcuts-sulphide veinlets (actinolite)	1-clinozoisite + sulphide 2-actinolite	?

Appendix 2. Sample descriptions

Sample descriptions

South pit

Central Diorite

Sample #NK1: sample of blue quartz vein, the blue colour of the quartz is most likely due to deformation and degree of recrystalization. Sulphides in order of abundance are chalcopyrite, pyrite with minor sphalerite, galena, native bismuth, acanthite and naumannite. Three pyrite types are present: I) veins or alteration of carbonate veins with pyrite often as euhedral grains; II) the replacement of pyrrhotite; and III) nickel-rich pyrite (observed using SEM-EDAX analysis). Sulphides are located along a clinozoisite vein within the quartz. Gangue phases present are vein quartz with orientated veins of clinozoisite.

NK 2a, 2b, 2c, 2d. These samples were quartz-albite veins. The host rock was not present in sample however it is most likely diorite. Gangue phases observed was quartz-albite with sulphides associated with shearing and later movement on a fault plane fault resulting in quartz-biotite alteration and later clinozoisite and chlorite alteration.

NK 2a: Ore minerals consist of pyrite replacing pyrrhotite, chalcopyrite, remnant pyrrhotite, native bismuth. Minor gold and tellurides are also present in this sample: native tellurium, tetradymite, stützite in pyrite, hessite, altaite, Bi+electrum and hedleyite. Native bismuth and gold are in contact with chlorite alteration. Other gangue minerals and named alteration include quartz/albite, Fe-amphibole, Fe-carbonate and Fe-oxide. Main sulphide mineralisation is coupled with the vein quartz formation. The average grain size of electrum is 10 microns.

NK 2b: Major ore minerals are chalcopyrite and pyrite. Pyrite has replaced pyrrhotite and there is remnant pyrrhotite still present. Sphalerite is a minor sulphide as is cubanite which forms exsolutions from chalcopyrite. Native bismuth as well as tellurides and electrum are minor components. The tellurides present were identified during SEM- EDAX analysis and where possible were confirmed with microprobe analysis. These are hedleyite in chalcopyrite and within tellurides in quartz, tellurobismuthite in chalcopyrite, hessite in chalcopyrite and quartz, two unnamed species with calculated formulae Bi_2Te and Bi_5Te_4, tsumoite, clausthalite in chalcopyrite, altaite in chalcopyrite and volynskite. Pyrite is present with Fe-oxides and native bismuth is present in sulphides with tellurides and in biotite. Chlorite is seen replacing K-feldspar. The sulphides appear to occur with the quartz and clinozoisite alteration with some chlorite present within the clinozoisite.

NK 2c: Major ore minerals are pyrite with chalcopyrite, where the pyrite has replaced pyrrhotite. Minor ore minerals present are cubanite (exsolved from chalcopyrite), sphalerite as inclusions in pyrite and pyrrhotite, and pyrrhotite. Trace minerals are native bismuth, S-bearing clausthalite and hedleyite. Fe-oxides occur together with pyrite mineralization and sulphides occur with chlorite and quartz alteration and veining.

NK 2d: Major ore minerals are chalcopyrite and pyrite where pyrite has replaced pyrrhotite. Minor ore minerals are cubanite (exsolved from chalcopyrite), pyrrhotite as remnant inclusions in pyrite and sphalerite. Trace minerals are native bismuth in chalcopyrite, electrum with bismuth in quartz, as well as along fractures in the chalcopyrite, tellurobismuthite in pyrite, hessite, clausthalite, hedleyite in chalcopyrite and quartz, galena in quartz, and an unnamed species with calculated formulae Bi8Te3.
Electrum grains in sample NK2 range from 2 to 20 microns in size.

NK 3: Quartz-rich shear zone consisting of altered diorite. Major ore minerals are chalcopyrite, pyrite where replacing pyrrhotite (in carbonate veins and often as euhedral grains) and pyrrhotite. Sphalerite is a minor ore mineral. Trace minerals are native bismuth, electrum within quartz (average size range from 5-10 microns), hessite clausthalite, hedleyite and pilsenite. Alteration minerals are muscovite with ore minerals occurring within quartz and bismuth oriented along biotite grain boundaries.

NK 4: Quartz vein with crosscutting actinolite vein. Major ore minerals are chalcopyrite, pyrite replacing pyrrhotite, pyrrhotite, and cubanite as exsolution from chalcopyrite. Minor ore minerals are sphalerite as inclusions in chalcopyrite.

Trace minerals are native bismuth, hessite, hedleyite, ikunolite, electrum (average grain size 10 microns) and tetradymite. Gangue minerals are predominantly quartz with overprinting actinolite.

NK 17a: Sheared and altered andesite. Major ore minerals are chalcopyrite and pyrite after pyrrhotite. There is minor sphalerite as inclusions in chalcopyrite. Sulphides occur within quartz veinlets and disseminated in the host rock. Gangue phases observed were earlier quartz sericite alteration overprinted by quartz veining with sulphides.

NK 21: Sheared and altered andesite with quartz vein, within which the sulphides occur. Major ore minerals are chalcopyrite, molybdenite and pyrite replacing pyrrhotite. Minor ore minerals are pyrrhotite, sphalerite inclusions in chalcopyrite and trace amounts of native bismuth, electrum (~10 microns). Molybdenite and chalcopyrite are intergrown within quartz and molybdenite grains are also seen within chalcopyrite. Some chalcopyrite and pyrrhotite are seen as disseminated mineralisation within host rock. Molybdenite in the quartz vein has a high abundance of inclusions of native bismuth. Gangue and alteration assemblages in order of paragenesis are 1) quartz-sericite 2) quartz-albite 3) clinozoisite.

NK 34: Vuggy quartz vein in altered diorite. Major ore minerals are chalcopyrite, pyrite replacing pyrrhotite and pyrrhotite with minor; cubanite, sphalerite and traces of native bismuth, electrum (~10 microns) in quartz and clinozoisite and hessite. Sulphide mineralisation occurs with clinozoisite alteration. Gangue associations are 1 – quartz-biotite, 2 – quartz-albite, and 3 – clinozoisite.

NK 35: Clinozoisite-sulphide feeders into quartz vein in diorite. Major ore minerals are chalcopyrite, pyrite replacing pyrrhotite as well as pyrite textures suggesting replacement of marcasites. Sphalerite is minor. Trace minerals include native bismuth and electrum (~10 microns). Gangue minerals show overprinting of quartz-albite by clinozoisite and actinolite.

NK 36: Quartz-albite vein in altered dacite. The major ore mineral is chalcopyrite, with minor pyrrhotite, sphalerite and cubanite (exsolved from chalcopyrite); trace minerals are galena and native bismuth. Galena occurs as inclusions within lamellar pyrrhotite. Sulphides occur with clinozoisite alteration and are located within the quartz vein as well as disseminated in the host rock.

<u>Blackbutt</u>
NK 27: Altered andesite with quartz vein and quartz-albite selvage. Major ore minerals are chalcopyrite, pyrite after pyrrhotite with minor molybdenite and gold. Gold occurs in inclusions up to 20 microns in size along lamellae in molybdenite. Molybdenite is disseminated within the quartz-albite but has been overprinted by clinozoisite.

NK 28: Quartz vein in quartz-albite altered dacite. Major ore minerals are chalcopyrite and pyrite after pyrrhotite, with minor covellite (occurring as rims on chalcopyrite suggesting covellite is formed via supergene enrichment). Trace minerals are native bismuth, gold, molybdenite with gold inclusions, ullmannite, Bi-telluride (too small to obtain a good analysis) and an unknown As-Fe-Ni-S phase with inclusions of bismuth, Bi-telluride and possibly also maldonite. This was, however, too small to image and may just be a finely intergrown mixture of gold and bismuth. Ore minerals occur with clinozoisite alteration that overprints the earlier quartz-albite alteration.

<u>Pipeline</u>
NK 16: Strongly-altered possible dacite precursor rock with quartz-albite/sulphide vein. Major ore minerals are cubanite and pyrite after pyrrhotite. Minor minerals are chalcopyrite, pyrrhotite, sphalerite, violarite and cobaltite. Trace minerals are native bismuth, altaite, parkerite, clausthalite, hessite, and an unnamed mineral with formulae $((NiFeCoCu)_{3.73}(Bi_{1.27}))_5S_2$. The minor and trace minerals other than chalcopyrite only occur as inclusions within the cubanite.

NK 19: Altered andesite with actinolite shear. Major ore minerals are pyrite replacing pyrrhotite with minor chalcopyrite, pyrrhotite, sphalerite, cubanite and scheelite. Trace amounts of native bismuth observed along the cleavage domains of actinolite. Late crosscutting magnetite with pyrite inclusions is also seen.

NK 20: Quartz-albite altered dacite. Major ore minerals are chalcopyrite and pyrite after pyrrhotite, with minor pyrrhotite, sphalerite and traces of galena, argentopentlandite, breithauptite and native bismuth. The sulphides are disseminated in the host rock.

NK37: Quartz vein overprinting quartz-biotite alteration with later clinozoisite clots. The major ore mineral is pyrite replacing pyrrhotite with minor pyrrhotite and chalcopyrite.

NK 38: Actinolite shear in unknown host rock with the major ore minerals chalcopyrite, pyrite after pyrrhotite with minor pyrrhotite, sphalerite and trace native bismuth, electrum and gold. Gold and electrum occur as free grains (~10 microns in size) in close proximity to and with native bismuth of similar size.

NK40: Quartz-albite altered dacite. Major ore minerals are chalcopyrite and pyrite after pyrrhotite. There is minor sphalerite and pyrrhotite inclusions and trace amounts of native bismuth in gangue.

North pit

North Diorite

NK18: Quartz-biotite altered andesite with later actinolite vein. Major ore minerals are chalcopyrite, pyrite after pyrrhotite and later pyrite veins in actinolite, sphalerite and traces of native bismuth, scheelite, galena, unnamed Bi_2TeS and gold, the latter occurring with Bi-telluride and as free, ~1-2 micron-sized grains in actinolite.

NK 29: Quartz vein in altered diorite. Major ore minerals are chalcopyrite, pyrrhotite with minor pentlandite as exsolution flames in pyrrhotite and traces of electrum (~25 microns in size) and ullmannite.

NK 30: Altered dacite (possibly andesite?) with quartz veinlets hosting ore. Major ore minerals are chalcopyrite, pyrite after pyrrhotite and in feeder veins, with minor pyrrhotite, scheelite, sphalerite and traces of native bismuth, gold, hedleyite, ikunolite, galena, and an unnamed phase $Bi_2(Te,S,Se)$. Inclusion trails and droplet-like grains of native bismuth are seen and are associated with clinozoisite in small shears and fractures within quartz-biotite alteration. The quartz veinlets also contain droplet-shaped grains of native bismuth at grain boundaries.

NK 31: Altered diorite, with clinozoisite and sulphide clots. Major ore minerals are chalcopyrite, pyrrhotite with minor pentlandite as exsolution flames from pyrrhotite, sphalerite and scheelite.

NK 32: Altered andesite. The major ore minerals are chalcopyrite and pyrite after pyrrhotite, with minor sphalerite and pyrrhotite and trace amounts of scheelite and native bismuth. Sulphides are associated with clinozoisite in a vuggy quartz vein.

ABreccia

NK 5: Sheared and altered andesite, quartz-biotite alteration overprinted by a quartz-albite vein which is sheared and overprinted by clinozoisite and actinolite. Major ore minerals are chalcopyrite, pyrrhotite with minor pyrite replacing pyrrhotite, arsenopyrite and cobaltite. Trace minerals include electrum (as free grains and in fractures within cobaltite), native bismuth and hedleyite.

NK 22: Sheared quartz-albite vein with overprinting biotite and clinozoisite. Major ore minerals are chalcopyrite, pyrite (after pyrrhotite as well as fracture infill), and pyrrhotite, with minor sphalerite. Trace minerals are native bismuth, electrum (~10-20 microns in size), molybdenite (with bismuth inclusions), clausthalite, hessite, and an unnamed species with formulae $Bi_9Te_4Se_2$. The ore minerals are associated with biotite and clinozoisite.

NK 23: Altered to clinozoisite; the precursor rock is possibly dacite. The major ore mineral is pyrrhotite with minor chalcopyrite and trace of galena. The rock is altered to clinozoisite with quartz and minor calcium carbonate

NK 24: Quartz-albite vein with overprinting clinozoisite. Major ore minerals are chalcopyrite and pyrite after pyrrhotite, with minor pyrrhotite, arsenopyrite and trace amounts of native bismuth and electrum. The ore minerals appear to be related with the quartz vein with the arsenopyrite closely associated with the clinozoisite.

NK 25: Quartz-albite altered diorite with a quartz vein hosting ore minerals. Major ore minerals are molybdenite and chalcopyrite, with trace amounts of gold in molybdenite and within the vein.

NK 26: Quartz-albite shear (possibly a mylonitic shear) with zoned euhedral arsenian pyrite with trace inclusions of arsenopyrite, pyrrhotite and galena.

NK 33/39: Actinolite shear with pyrrhotite and chalcopyrite as major ore minerals. Arsenopyrite and pyrite are minor and there are trace amounts of a Bi-telluride, possibly hedleyite.

NK Mo/moly: Molybdenite shear zone in diorite with quartz-albite alteration and clinozoisite. The major ore mineral is molybdenite with trace amounts of gold (~5-10 micron in size), chalcopyrite and pyrite.

Drill core WRD-13810-002

NK 7 – 705.7 m: dacitic texture but possibly altered diorite. Sulphides consist of lenses and disseminations of pyrite after pyrrhotite and display a minor shear fabric. Minor chalcopyrite and sphalerite are also present.

NK 8 – 246.3 m: Quartz vein with minor host rock of diorite. Major ore minerals are chalcopyrite and pyyrhotite with minor pyrite (after pyrrhotite) and sphalerite. Trace mineralogy includes native bismuth, galena and hessite (galena and hessite with native bismuth often occur as symplectite like intergrowths), with bismuth and tellurides along cleavage planes in biotite.

NK 9 – 363.7 m: Quartz vein with later cutting clinozoisite alteration. Main sulphides are pyrrhotite and chalcopyrite. With trace mineralogy of symplectite of galena and native bismuth, native bismuth is also observed as melt shaped droplets of less than a micron in size, pentlandite exsolution flames are also present within pyrrhotite, and ullmannite is a very minor phase observed but not confirmed.

NK 10 – 248.5 m: Sheared diorite with quartz veining. Major ore minerals are chalcopyrite and pyrrhotite. Minor sphalerite and costibite. With a trace mineralogy of native bismuth, pilsenite, hedleyite, tsumoite, unnamed tetradymite phase, galena and breithauptite. Pilsenite, galena and native bismuth occur as symplectite like intergrowth commonly along cleavage planes in biotite and droplet shaped within pyrrhotite.

NK 13 – 667.3: Sheared dacite with cutting quartz vein, disseminated pyrite after pyrrhotite are the main sulphide with minor relict pyrrhotite.

NK 14: 261.5 m: altered andesite with quartz sericite alteration with A1 actinolite vein with quartz albite selvage and late cutting quartz vein with chalcopyrite and pyrrhotite. trace mineralogy of native bismuth and ullmannite.

Concentrates A and B: native bismuth, various Bi-tellurides, chalcopyrite, pyrite, scheelite, galena, gold, electrum, pyrrhotite, cubanite, arsenopyrite/cobaltite, molybdenite and maldonite, as well as various gangue minerals that report to the copper concentrate currently produced.

The ‘Granite’ sample was also prepared and used for the LA-ICPMS determinations on molybdenite. This sample was supplied by Newmont after the field visit and derives from drillhole WRD-09775-002 (position 472.6 m). The sample consists of clots of molybdenite, chalcopyrite and pyrrhotite in a granite matrix.

Appendix 3. microprobe analysis of tellurides and selenides

(wt. %)	NK2a		NK2b												NK2d	
	gr 1	gr2	2b1	2b1	2b1	2b1	2b1	2b13	2b13	2b13	2b14	2b14	2b3	2b3	2dnk6	2dnk7
Ag	0.03	<mdl	0.03	<mdl	<mdl	0.1	<mdl	<mdl	0.05	0.06	<mdl	<mdl	<mdl	<mdl	0.03	0.02
Pb	3.6	2.86	2.06	2.11	1.97	2.09	1.92	2.84	2.93	3.07	2.03	3.19	3.97	3.76	2.21	2.28
Bi	75.99	78.74	78.76	77.69	79.11	77.94	78.42	77.22	77.72	78.85	77.17	76.65	75.84	74.77	76.15	76.87
Sb	0.27	0.17	0.02	0.14	0.15	0.01	<mdl	0.15	0.16	0.16	0.13	0.11	0.12	0.13	0.13	0.14
Te	20.51	18.95	19.48	19.85	19.63	19.7	19.23	18.68	18.94	19.01	20	20.32	19.78	20.8	19.18	19.26
Se	0.32	0.27	0.21	0.24	0.26	0.28	0.33	0.23	0.25	0.3	0.19	0.32	0.27	0.25	0.23	0.23
S	<mdl	0.01	0.01	0.01	0.01	0.02	<mdl	0.02	<mdl	<mdl	<mdl	0.05	<mdl	0.04	0.02	0.02
Total	**100.71**	**101**	**100.57**	**100.03**	**101.14**	**100.14**	**99.98**	**99.13**	**100.04**	**101.45**	**99.53**	**100.64**	**100**	**99.74**	**97.95**	**98.82**
Calculated formulae																
a.p.f.u	10	10	10	10	10	10	10	10	10	10	10	10	10	10	10	10
Ag	0.004	0	0.005	-	-	0.017	-	-	0.008	0.009	-	-	-	-	0.006	0.003
Pb	0.317	0.253	0.183	0.188	0.173	0.186	0.171	0.256	0.262	0.271	0.182	0.281	0.353	0.333	0.201	0.205
Bi	6.633	6.922	6.942	6.86	6.923	6.874	6.947	6.917	6.896	6.901	6.847	6.693	6.699	6.574	6.872	6.88
Sb	0.04	0.026	0.003	0.021	0.023	0.001	-	0.024	0.024	0.024	0.02	0.016	0.018	0.019	0.02	0.021
Total M	**6.994**	**7.202**	**7.134**	**7.069**	**7.12**	**7.078**	**7.119**	**7.197**	**7.19**	**7.205**	**7.049**	**6.99**	**7.07**	**6.926**	**7.098**	**7.109**
Te	2.933	2.728	2.812	2.872	2.813	2.846	2.79	2.74	2.752	2.725	2.906	2.906	2.862	2.995	2.835	2.823
Se	0.073	0.063	0.048	0.055	0.061	0.064	0.078	0.055	0.058	0.07	0.046	0.075	0.064	0.058	0.055	0.055
S	-	0.008	0.006	0.004	0.006	0.012	-	0.009	-	-	-	0.029	-	0.021	0.012	0.013
Total S,Se,Te	**3.006**	**2.798**	**2.866**	**2.931**	**2.88**	**2.922**	**2.868**	**2.803**	**2.81**	**2.795**	**2.951**	**3.01**	**2.927**	**3.074**	**2.902**	**2.891**

Appendix 3. (Cont). Electron probe microanalyses of Bi-telluride phases (Tetradymite Group): $Bi_2(Te,Se,S)$ and Bi_8Te_3 sub-groups

	Bi_2Te					$Bi_2(Te,S)$	$Bi_2(Te,S,Se)$		$Bi_9Te_4Se_2$	Bi_8Te_3
(wt. %)	**NK2b**	**NK3**			**NK30**	**NK18**	**NK30**		**NK22**	**NK2d**
	2b9	**2**	**3**	**4**	**30nk35**	**gr2**	**30nk30**	**30nk32**	**22nk62**	**2dnk8**
Ag	<mdl	0.02	<mdl	<mdl	<mdl	<mdl	0.04	<mdl	0.32	<mdl
Pb	4.09	1.41	1.51	1.54	0.55	0.75	0.39	0.45	0.79	2.69
Bi	71.65	75.66	76.36	75.43	76.99	79.94	78.56	78.17	72.43	78.06
Sb	0.14	0.00	0.10	0.10	0.10	0.10	0.10	0.14	0.12	0.19
Te	23.35	23.03	23.16	23.25	16.30	15.05	16.19	16.09	18.42	18.10
Se	0.10	0.85	0.77	0.90	3.02	0.04	2.67	2.54	6.78	0.19
S	<mdl	<mdl	<mdl	<mdl	0.91	3.05	1.06	1.09	0.09	0.03
Total	**99.33**	**100.98**	**101.89**	**101.22**	**97.88**	**98.94**	**99.00**	**98.49**	**98.96**	**99.26**
Calculated formulae										
a.p.f.u	3	9	9	9	9	3	3	3	15	11
Ag	-	0.003	-	-	-	-	0.002	-	0.075	-
Pb	0.108	0.110	0.116	0.119	0.042	0.018	0.010	0.011	0.098	0.268
Bi	1.877	5.816	5.823	5.772	5.855	1.910	1.969	1.970	8.848	7.708
Sb	0.006	0.000	0.013	0.013	0.002	0.004	0.004	0.006	0.025	0.033
Total M	**1.991**	**5.928**	**5.951**	**5.904**	**5.898**	**1.933**	**1.985**	**1.988**	**9.047**	**8.009**
Te	1.002	2.899	2.893	2.914	2.030	0.589	0.665	0.664	3.686	2.926
Se	0.007	0.172	0.154	0.182	0.608	0.002	0.177	0.170	2.193	0.049
S	-	-	-	-	0.451	0.476	0.173	0.178	0.074	0.016
Total S,Se,Te	**1.009**	**3.072**	**3.049**	**3.096**	**3.089**	**1.067**	**1.015**	**1.012**	**5.953**	**2.991**

Appendix 3. (Cont). Electron probe microanalyses of Bi-telluride phases (Tetradymite Group): $Bi_4(Te,Se,S)_3$ sub-group

	Pilsenite Bi_4Te_3										laitakarite $Bi_4(Se,S)_3$			Ikunolite Bi_4S_3	
(wt. %)	**nk3**		**NK10**								**NK4**			**NK30**	
	gr2	**gr2**	**gr1**	**gr1**	**gr2**	**gr2**	**gr3**	**gr5**	**gr9**	**21**	**gr2**	**gr2**	**gr2**		
Ag	0.02	<mdl	<mdl	<mdl	<mdl	<mdl	<mdl	0.03	0.00	0.06	0.14	<mdl	0.07	<mdl	<mdl
Pb	5.00	5.38	1.01	0.79	1.92	2.03	1.89	0.77	4.02	3.38	0.00	<mdl	<mdl	<mdl	<mdl
Bi	64.50	64.25	67.59	69.13	64.89	63.95	64.36	67.34	62.44	61.37	75.66	77.82	77.30	88.42	87.55
Sb	0.27	0.01	0.22	0.18	0.39	0.35	0.38	0.16	0.26	0.32	<mdl	<mdl	<mdl	<mdl	0.04
Te	28.44	28.35	28.84	27.97	32.16	32.32	32.23	28.94	33.04	32.42	6.18	3.59	5.45	0.13	0.58
Se	1.07	0.98	1.10	0.98	0.82	0.87	0.82	0.57	0.47	0.47	17.26	16.47	16.48	<mdl	0.01
S	0.01	0.01	0.02	0.03	0.02	0.01	0.03	0.05	0.08	0.02	0.84	1.70	0.69	9.90	10.39
Total	**99.31**	**98.99**	**98.76**	**99.09**	**100.21**	**99.53**	**99.75**	**97.88**	**100.33**	**98.02**	**100.08**	**99.59**	**99.99**	**98.45**	**98.57**
Calculated formulae															
a.p.f.u	7	7	7	7	7	7	7	7	7	7	7	7	7	7	7
Ag	0.002	-	-	-	-	-	-	0.003	0.000	0.006	0.014	-	0.007	-	-
Pb	0.295	0.457	0.060	0.047	0.111	0.118	0.109	0.046	0.231	0.199	0.000	-	-	-	-
Bi	3.778	3.785	3.968	4.072	3.709	3.673	3.688	4.004	3.558	3.584	3.860	3.937	4.024	4.042	3.921
Sb	0.027	0.001	0.022	0.018	0.039	0.034	0.037	0.016	0.025	0.032	-	-	-	-	0.003
Total M	**4.104**	**4.243**	**4.050**	**4.137**	**3.858**	**3.825**	**3.834**	**4.070**	**3.814**	**3.820**	**3.874**	**3.937**	**4.031**	**4.042**	**3.924**
Te	2.728	2.735	2.773	2.698	3.011	3.040	3.025	2.819	3.084	3.101	0.516	0.297	0.465	0.010	0.043
Se	0.165	0.154	0.171	0.153	0.124	0.132	0.125	0.090	0.070	0.072	2.330	2.205	2.271	-	0.002
S	0.003	0.005	0.006	0.012	0.007	0.003	0.013	0.021	0.028	0.007	0.280	0.560	0.233	2.948	3.032
Total S,Se,Te	**2.896**	**2.894**	**2.950**	**2.863**	**3.142**	**3.175**	**3.162**	**2.929**	**3.182**	**3.180**	**3.126**	**3.063**	**2.969**	**2.958**	**3.076**

Appendix 3. (Cont). Electron probe microanalyses of Bi-telluride phases (Tetradymite Group): Bi_6Te_5, Bi_5Te_3, Bi_5Te_4 and Bi_4Te_5 sub-groups

	$(Bi,Pb)_6Te_5$										Bi_5Te_3	Bi_5Te_4		$Bi_4(Te,Se)_5$
(wt. %)	**NK10**										**NK10**	**NK2b**		**NK4**
											gr16	**2b9**	**2b9**	**gr2 adj**
Ag	0.63	0.59	<mdl	0.03	<mdl	<mdl	0.03	<mdl	<mdl	0.05	<mdl	0.07	0.09	0.26
Pb	4.74	3.63	3.65	3.88	3.82	3.30	3.55	3.36	3.28	3.33	0.12	4.21	4.62	<mdl
Bi	61.18	61.70	61.25	61.92	61.70	62.16	61.41	61.99	61.26	61.85	74.63	60.53	60.41	59.52
Sb	0.20	0.31	0.26	0.28	0.12	0.32	0.24	0.25	0.15	0.23	0.34	0.21	0.21	0.20
Te	33.87	34.11	33.95	34.34	33.41	33.42	33.54	34.10	33.88	33.66	24.10	34.69	33.32	33.42
Se	0.37	0.40	0.43	0.30	0.38	0.27	0.35	0.33	0.38	0.37	1.03	0.09	0.04	6.49
S	<mdl	<mdl	<mdl	0.01	0.01	<mdl	<mdl	<mdl	0.04	<mdl	0.05	0.01	0.05	0.45
Total	**101.10**	**100.73**	**99.54**	**100.80**	**99.46**	**99.47**	**99.12**	**100.04**	**98.98**	**99.50**	**100.28**	**99.82**	**98.74**	**100.33**
Calculated formulae														
a.p.f.u	11	11	11	11	11	11	11	11	11	11	8	9	9	9
Ag	0.109	0.102	-	0.006	-	-	0.005	-	-	0.009	-	0.010	0.012	0.033
Pb	0.424	0.325	0.331	0.348	0.348	0.301	0.325	0.304	0.300	0.304	0.008	0.312	0.348	-
Bi	5.419	5.475	5.517	5.512	5.581	5.628	5.568	5.564	5.544	5.585	5.065	4.450	4.509	3.962
Sb	0.030	0.046	0.039	0.043	0.018	0.050	0.038	0.039	0.023	0.035	0.040	0.027	0.026	0.023
Total M	**5.982**	**5.948**	**5.888**	**5.910**	**5.948**	**5.979**	**5.936**	**5.907**	**5.867**	**5.934**	**5.113**	**4.799**	**4.896**	**4.019**
Te	4.914	4.957	5.008	5.007	4.950	4.955	4.981	5.013	5.022	4.978	2.679	4.177	4.073	3.644
Se	0.087	0.095	0.103	0.070	0.091	0.066	0.083	0.079	0.090	0.088	0.184	0.018	0.008	1.143
S	-	-	-	0.009	0.008	-	-	-	0.021	-	0.024	0.006	0.023	0.194
Total (S+Se+Te)	**5.002**	**5.052**	**5.112**	**5.086**	**5.050**	**5.021**	**5.064**	**5.093**	**5.132**	**5.066**	**2.887**	**4.201**	**4.104**	**4.981**

Appendix 3. (Cont). Electron probe microanalyses of Bi-telluride phases (Tetradymite Group): BiTe (tsumoite) and Bi_2Te_3 (tellurobismuthite) sub-groups

	Tsumoite BiTe									Tellurobismutite Bi_2Te_3		
(wt. %)	**NK2b**		**NK10**							**NK2b**		
	2b11	**2b15**	**gr7**	**gr8**	**gr10**	**gr11**	**gr7**	**gr15**	**gr14**	**2b4**	**2b4**	
Ag	1.15	1.52	<mdl	0.04	<mdl	<mdl	<mdl	0.00	0.09	0.28	0.25	0.13
Pb	1.35	0.60	3.42	3.55	3.26	3.28	3.21	3.67	3.55	<mdl	<mdl	0.10
Bi	62.22	56.22	61.63	61.94	60.94	61.06	62.40	60.60	61.10	52.74	52.09	50.79
Sb	0.15	0.11	0.22	0.30	0.26	0.17	0.23	0.23	0.22	0.35	0.32	0.30
Te	35.14	40.19	33.99	34.14	33.85	34.85	33.89	35.04	34.54	48.18	48.37	45.83
Se	0.20	<mdl	0.28	0.34	0.47	0.35	0.30	0.40	0.35	0.07	<mdl	1.24
S	<mdl	<mdl	<mdl	<mdl	0.01	0.01	0.02	0.00	0.00	0.03	<mdl	0.05
Total	**100.22**	**98.64**	**99.54**	**100.31**	**98.81**	**99.73**	**100.05**	**99.94**	**99.85**	**101.64**	**101.03**	**98.44**
Calculated formulae												
a.p.f.u	2	2	2	2	2	2	2	2	2	5	5	5
Ag	0.036	0.047	-	0.001	-	-	-	0.000	0.003	0.020	0.018	0.009
Pb	0.022	0.010	0.057	0.058	0.054	0.054	0.053	0.060	0.058	-	-	0.004
Bi	1.002	0.894	1.011	1.008	1.004	0.995	1.019	0.984	0.996	1.981	1.968	1.948
Sb	0.004	0.003	0.006	0.008	0.007	0.005	0.006	0.006	0.006	0.023	0.021	0.020
Total M	**1.064**	**0.953**	**1.074**	**1.076**	**1.065**	**1.053**	**1.079**	**1.051**	**1.063**	**2.024**	**2.007**	**1.981**
Te	0.927	1.047	0.914	0.910	0.913	0.930	0.906	0.932	0.922	2.963	2.993	2.879
Se	0.009	0.000	0.012	0.015	0.021	0.015	0.013	0.017	0.015	0.006	-	0.126
S	-	-	-	-	0.001	0.001	0.002	0.000	0.000	0.007	-	0.013
Total (S+Se+Te)	**0.936**	**1.047**	**0.926**	**0.924**	**0.934**	**0.947**	**0.921**	**0.949**	**0.937**	**2.976**	**2.993**	**3.019**

Appendix 4. Electron probe microanalyses of pyrite

	Pyrite															
(wt. %)																
spot	NK2b (2)	NK2b (20)	NK2b (21)	NK2b (43)	NK4 (8)	NK18 (1)	NK18 (2)	NK16 (28)	NK18 (3)	NK16 (4)	NK1 (1)	NK1 (2)	NK1 (3)	NK1 (4)	NK1 (5)	NK2a (5)
Cu	<mdl	0.57	0.57	<mdl	<mdl	<mdl	0.04	<mdl	0.02	<mdl	0.51	0.75	2.31	0.08	0.09	<mdl
Mn	<mdl	<mdl	<mdl	0.02	<mdl	0.01	0.01	<mdl	0.00	<mdl	0.01	<mdl	0.01	0.03	0.03	<mdl
Fe	46.72	45.59	46.57	47.09	45.78	46.03	45.70	45.02	46.08	45.73	39.64	43.34	40.56	45.85	45.67	46.72
Co	0.05	0.01	0.03	0.00	0.01	0.14	0.20	<mdl	0.14	0.14	3.77	1.26	2.83	<mdl	<mdl	<mdl
Ni	0.12	0.06	0.08	0.05	0.85	0.24	0.22	0.13	0.25	0.51	5.34	1.67	3.83	0.09	0.02	0.10
As	0.05	0.03	0.03	<mdl	0.05	0.04	0.05	0.08	0.04	0.12	0.01	<mdl	0.02	<mdl	<mdl	0.02
Sb	<mdl	0.03	0.03	0.02	0.06	0.06	<mdl	<mdl	<mdl	<mdl	0.01	0.02	0.06	<mdl	0.03	0.02
Se	<mdl	0.06	0.04	0.04	0.01	0.05	<mdl	0.02	0.01	0.02	<mdl	0.08	0.02	0.02	0.03	0.08
S	54.20	54.00	54.41	53.54	54.27	52.81	53.20	53.35	53.13	53.54	50.33	52.16	49.72	53.11	52.69	53.11
Total	**101.14**	**100.36**	**101.75**	**100.77**	**101.02**	**99.38**	**99.41**	**98.61**	**99.66**	**100.06**	**99.62**	**99.27**	**99.37**	**99.18**	**98.57**	**100.05**
Calculated formulae (a.p.f.u 3)																
Cu	-	0.011	0.011	-	-	-	0.001	-	-	-	0.010	0.014	0.045	0.001	0.002	-
Mn	-	-	-	-	-	-	-	-	-	-	-	-	-	0.001	0.001	-
Fe	0.992	0.975	0.984	1.006	0.974	0.997	0.988	0.978	0.994	0.983	0.877	0.946	0.901	0.993	0.996	1.006
Co	0.001	-	0.001	-	-	0.003	0.004	-	0.003	0.003	0.079	0.026	0.060	-	-	-
Ni	0.002	0.001	0.001	0.001	0.015	0.004	0.004	0.002	0.004	0.009	0.096	0.030	0.069	0.002	-	0.002
As	0.001	-	-	-	0.001	0.001	0.001	0.001	0.001	0.002	-	-	-	-	-	-
Sb	-	-	-	-	0.001	0.001	-	-	-	-	-	-	0.001	-	-	-
Total M	**0.996**	**0.988**	**0.997**	**1.007**	**0.990**	**1.006**	**0.997**	**0.982**	**1.003**	**0.996**	**1.062**	**1.016**	**1.076**	**0.997**	**0.999**	**1.008**
Se	-	0.001	0.001	0.001	-	0.001	-	-	-	-	-	0.001	-	-	-	0.001
S	2.004	2.011	2.002	1.992	2.010	1.993	2.003	2.018	1.997	2.003	1.938	1.983	1.924	2.003	2.001	1.991
Total (S+Se)	**2.004**	**2.012**	**2.003**	**1.993**	**2.010**	**1.994**	**2.003**	**2.018**	**1.997**	**2.004**	**1.938**	**1.984**	**1.924**	**2.003**	**2.001**	**1.992**

Appendix 5. Size and liberation characteristics of bismuth, tellurides, maldonite, gold and others observed in copper concentrate A

Concentrate A

Native bismuth

Mean diameter (µm)	Liberated (Y/N)
6	Y
5	Y
5	Y
5	Y
15	Y
5	Y
17	Y
10	N, with Chalcopyrite
10	N, with Chalcopyrite
15	Y
10	Y
2	Y
6	N, with Au
5	Y
4	Y
8	Y
4	Y
10	Y
5	N, with actinolite
5	Y
10	N, with Chalcopyrite
10	N, with clinozoisite
5	with arsenopyrite
4	Y
2	Y
6	Y
10	Y
5	Y
8	N, with Cubanite
5	Y
4	Y
4	Y
4	Y
5	Y
4	Y
5	Y
6	Y
8	Y
4	Y
4	Y
5	Y
5	Y
15	Y
8	Y
4	Y
8	Y
4	Y
5	N, with Clinozoisite
6	Y
10	Y
7	Y
15	Y

Native bismuth (cont'd)

Mean diameter (µm)	Liberated (Y/N)
5	Y
12	Y
5	Y
6	Y
4	Y
10	Y
4	Y
4	Y
4	Y
6	Y
4	Y
12	Y
8	Y
10	Y
4	Y
4	Y
6	Y
10	N, with Chalcopyrite
5	Y
10	Y
5	Y
5	Y
4	Y
4	Y

Native gold

Mean diameter (µm)	~Ag (%)*	Liberated (Y/N)
35	10	Y
3	10	N with Bi
6	3	Y
15	10	Y
10	50	N with Bi
8	10	Y
5	10	N with Bi
20	40	Y
10	70	Y
4	10	Y
5	10	Y
5	50	Y
5	50	Y
3	10	N with Bi

*EDAX data, 60 sec. count time

Maldonite

Mean diameter (µm)	Liberated (Y/N)
12	Y
4	N with Bi
4	Y
2	Y
5	N with Bi
5	Y
3	Y

Bi-tellurides

6	Y (Bi4Te)
4	Y (Bi2Te)
4	Y (Bi2Te)
12	Y (Bi2Te)
8	Y (Bi2Te)
8	Y (Bi4Te)
15	Y (Bi7Te2)
5	Y (Bi4Te)
8	Y (Bi5Te4)

Other minerals

Scheelite

20	Y
4	Y
13	Y

Galena

20	Y

Hessite

10	N, with Chalcopyrite

Appendix 5. (Cont). Size and liberation characteristics of bismuth, tellurides, maldonite, gold and others observed in copper concentrate B

Concentrate B

Native bismuth

Mean diameter (µm)	Liberated (Y/N)
4	Y
5	Y
5	Y
7	Y
12	Y
4	Y
10	Y
6	Y
5	Y
4	Y
4	Y
5	Y
6	Y
8	Y
4	Y
12	Y
10	Y
8	Y
7	N, with Bi7Te2
10	Y
6	Y
9	Y
6	Y
6	Y
4	Y
5	Y
4	Y
3	Y
9	Y
3	Y
3	Y
7	Y
8	Y
10	Y
4	Y
4	Y
5	N, with telluride
6	Y
12	N, with Au
7	Y
4	Y
4	Y
5	Y
13	Y
6	Y
7	Y
5	Y
8	Y
8	Y
7	Y
12	Y
7	N, with Bi3Te

Native bismuth (cont'd)

Mean diameter (µm)	Liberated (Y/N)
4	Y
8	Y
8	Y
10	N, with Bi7Te3
10	Y
10	Y
5	N, with chalcopyrite
15	Y
20	Y
4	Y
6	Y
5	N, with pyrite
8	Y
8	Y
6	Y
7	Y
11	Y
4	Y
4	Y
30	Y
4	Y
8	Y
4	Y
8	Y
4	Y
7	Y
4	Y
5	Y

Native gold

Mean diameter (µm)	~Ag (%)*	Liberated (Y/N)
6	5	Y
12	5	Y
3	5	N, with quartz
10	50	Y
3	20	N, with chalcopyrite
5	50	N with Bi
17	50	Y
19	5	Y
6	5	Y
10	25	Y
9	25	Y

*EDAX data, 60 sec. count time

Maldonite

Mean diameter (µm)	Liberated (Y/N)
4	Y
10	Y
5	N with Actinolite

Bi-tellurides

13	Y
4	Y
5	Y
5	Y
12	Y
5	Y
10	Y
6	Y
5	Y
4	Y
4	Y

Scheelite

10	10

Appendix 6. LA-ICPMS analysis of molybdenite, element concentrations given in ppm

Spot	Mn	Fe	Co	Ni	Cu	Zn	Ga	As	Se	Ag	Cd	In	Sn	Sb	Te	W	Re	Au	Tl	Pb	Bi	U
Sample NK21																						
1	< mdl	1999	0.97	2.0	2125	3.4	0.74	< mdl	348	3.4	2.7	0.62	4.37	0.76	14.4	153	**249**	**5.4**	0.30	32.4	88.3	< mdl
2	< mdl	66.8	0.51	0.65	13.3	6.3	< mdl	< mdl	375	0.24	2.7	< mdl	< mdl	< mdl	12.9	131	**282**	**< mdl**	0.15	0.84	1.1	0.02
3	< mdl	45.14	< mdl	< mdl	0.94	< mdl	< mdl	< mdl	442	< mdl	2.1	0.04	< mdl	< mdl	13.0	111	**351**	**< mdl**	< mdl	1.10	< mdl	< mdl
4	< mdl	< mdl	0.18	< mdl	< mdl	< mdl	< mdl	< mdl	568	5.7	2.0	< mdl	< mdl	< mdl	7.8	122	**93.7**	**3.5**	0.08	0.88	181	< mdl
6	< mdl	35.4	2.03	2.4	64.7	28.7	< mdl	11.6	758	0.78	3.1	< mdl	< mdl	< mdl	2.7	132	**27.9**	**< mdl**	0.11	7.5	27.6	< mdl
7	< mdl	9455	11.4	15.3	10846	130	0.23	3.9	840	365	4.2	4.2	16.6	1.8	283	159	**102**	**30.1**	3.3	1052	2243	< mdl
7a	1.6	219	3.03	3.0	229	41.9	< mdl	< mdl	642	738	2.8	0.07	< mdl	3.9	499	125	**53.6**	**164**	0.11	139	3469	< mdl
8	3.5	6518	6.44	43.3	6379	25.9	< mdl	3.4	683	425	3.6	1.4	7.0	13.2	290	68.7	**24.9**	**136**	3.2	791	2503	< mdl
9	2.2	926	0.33	1.4	873	2.5	0.14	< mdl	704	12.0	2.1	0.16	1.4	1.3	75.9	65.0	**38.2**	**17.4**	< mdl	315	690	< mdl
10	1.5	1209	6.01	7.9	1071	17.7	0.60	< mdl	332	282	3.6	0.33	2.4	5.1	166	183	**93.4**	**43.7**	0.74	331	2465	< mdl
11	< mdl	654	1.46	1.7	725	5.2	< mdl	< mdl	762	2296	2.7	0.16	1.1	6.6	1088	172	**66.7**	**421**	0.05	1573	3728	< mdl
12	2.2	69213	28.32	13.9	67539	206	< mdl	< mdl	365	275	4.3	16.1	40.3	20.2	235	259	**124**	**12.6**	26.4	761	1955	< mdl
13	5.1	12846	4.16	12.2	13280	31.6	0.19	3.1	484	225	3.1	2.7	9.7	5.4	112	186	**143**	**76.0**	3.0	224	679	< mdl
14	4.4	896	4.11	8.2	642	6.7	0.45	4.3	717	179	3.1	0.10	1.4	7.9	167	82.3	**50.5**	**102**	0.90	185	2398	< mdl
15	4.6	1644	3.88	8.0	158	8.0	< mdl	< mdl	597	814	3.3	0.19	< mdl	12.3	334	120	**54.8**	**248**	0.27	251	4681	< mdl
16	< mdl	150	0.75	1.3	78.9	4.8	< mdl	< mdl	704	102	2.5	< mdl	< mdl	4.1	84.8	74.6	**38.8**	**67.5**	< mdl	97.1	994	< mdl
17	< mdl	3166	3.92	3.7	2618	51.4	< mdl	< mdl	178	164	3.0	0.44	5.0	3.9	142	272	**271**	**20.6**	0.27	121	1118	< mdl
18	< mdl	< mdl	0.81	0.73	3.7	< mdl	< mdl	< mdl	419	15.3	2.9	< mdl	< mdl	1.1	36.7	99.5	**115**	**3.6**	< mdl	50.7	156	< mdl
19	3.6	560	2.25	2.1	329	2.6	< mdl	< mdl	186	160	2.8	0.08	< mdl	4.2	85.1	241	**299**	**78.6**	0.04	219	2571	< mdl
20	< mdl	296	1.92	1.9	207	< mdl	< mdl	< mdl	287	154	2.6	< mdl	< mdl	3.8	48.8	198	**219**	**153**	< mdl	1261	1442	< mdl
21	219	21502	5.64	10.4	10225	67.9	3.6	3.1	219	144	3.9	2.4	14.1	6.4	115	236	**298**	**38.9**	0.67	368	1798	< mdl
22	< mdl	39.4	1.49	1.0	6.3	< mdl	< mdl	< mdl	381	31.7	2.3	< mdl	< mdl	0.90	24.5	71.9	**301**	**19.3**	0.05	7.1	432	< mdl
23	1.4	192	10.9	23.3	464.0	71.8	< mdl	< mdl	405	32.4	2.6	0.09	1.8	2.8	52.7	105	**671**	**7.5**	0.92	159	824	< mdl
24	4.2	10855	23.2	28.1	12051	132	0.17	< mdl	413	39.8	2.9	2.8	13.9	2.1	47.8	99.2	**503**	**8.2**	1.5	108	540	< mdl
25	101	29077	14.6	18.7	29276	102	1.9	< mdl	376	535	< mdl	5.8	23.2	18.7	349	324	**306**	**424**	1.7	422	8589	< mdl
26	< mdl	6546	6.5	44.3	7027	118	< mdl	< mdl	367	143	4.4	1.9	6.3	1.7	93.9	152	**312**	**17.7**	3.9	317	990	< mdl
27	9.8	5306	6.0	9.8	4898	20.3	1.7	< mdl	463	318	3.6	1.7	6.4	16.8	159	125	**424**	**142**	1.3	318	2697	< mdl
28	5.7	190	21.1	27.5	444	176	< mdl	< mdl	417	84.1	2.6	< mdl	< mdl	2.5	46.6	275	**410**	**50.5**	0.68	112	616	< mdl
29	< mdl	518	0.94	1.0	279	14.8	< mdl	< mdl	508	6.9	2.3	0.09	< mdl	0.48	14.7	89.3	**247**	**2.7**	< mdl	46.6	113	< mdl
30	1.7	915	21.8	19.9	740	25.6	0.78	4.2	846	1634	3.3	0.40	5.7	3.2	260	163	**41.8**	**682**	1.9	436	3344	0.03
Mean (30)	23.2	6609	6.7	11.2	5952	52.1	0.95	4.8	493	317	3.0	1.9	9.4	5.8	162	153	**207**	**110**	2.1	324	1770	-
S.D.	57.6	14120	7.8	12.4	13449	58.8	1.0	3.0	191	511	0.66	3.5	10.1	5.7	214	69.4	**163**	**162**	5.3	391	1831	-
Minimum	< mdl	< mdl	< mdl	< mdl	< mdl	< mdl	< mdl	< mdl	178	0.24	< mdl	< mdl	< mdl	< mdl	2.7	65.0	**24.9**	**< mdl**	< mdl	0.8	1.1	< mdl
Maximum	219	69213	28.3	44.3	67539	206	3.6	11.6	846	2296	4.4	16.1	40.3	20.2	1088	324	**671**	**682**	26.4	1573	8589	0.03

Appendix 6. (Cont)

Sample NK25																					
Spot	**Mn**	**Fe**	**Co**	**Ni**	**Cu**	**Zn**	**Ga**	**As**	**Se**	**Ag**	**Cd**	**In**	**Sn**	**Sb**	**Te**	**W**	**Re**	**Au**	**Tl**	**Pb**	**Bi**	**U**
1	216	81147	19.7	239	213	33.1	3.9	371	575	6.5	3.1	< mdl	< mdl	58.2	117	200	**1061**	**8.6**	8.7	632	422	0.30
2	13.4	1901	6.5	19.0	823	7.7	0.31	10.3	742	3.5	1.9	< mdl	< mdl	12.2	109	88.8	**245**	**6.4**	4.6	382	454	< mdl
3	115	11935	15.3	37.2	67.4	18.7	2.6	23.4	491	7.6	2.9	< mdl	< mdl	27.4	110	504	**622**	**64.0**	4.7	697	580	< mdl
4	49.8	5158	16.1	34.2	101	8.3	1.1	19.0	734	2.5	2.7	< mdl	< mdl	23.8	131	188	**366**	**15.7**	6.3	865	561	< mdl
5	40.6	4421	9.7	26.3	283	7.6	0.95	13.0	643	2.6	2.7	< mdl	< mdl	13.7	150	140	**314**	**12.5**	8.4	297	611	< mdl
6	< mdl	189	2.3	7.3	48.4	< mdl	< mdl	4.6	783	0.70	2.0	< mdl	< mdl	6.0	91.6	60.4	**152**	**6.1**	2.9	117	162	< mdl
7	11.1	1468	7.8	19.5	420	4.9	< mdl	10.6	794	7.8	2.3	< mdl	< mdl	29.1	131	109	**318**	**40.9**	3.6	460	433	< mdl
8	< mdl	121	5.6	15.6	45.2	2.1	< mdl	4.1	710	0.53	2.8	< mdl	< mdl	7.4	84.6	56.5	**229**	**3.2**	6.7	150	191	< mdl
9	52.1	5359	22.1	47.5	83.8	7.4	0.78	19.7	667	3.2	3.9	< mdl	< mdl	30.7	131	290	**406**	**15.7**	9.3	619	613	< mdl
10	7.70	811	2.8	5.7	118	3.9	0.29	8.0	682	0.91	1.5	< mdl	< mdl	7.7	82.5	60.5	**1181**	**10.9**	2.4	107	163	< mdl
11	407	42336	7.1	48.7	36.0	59.2	8.6	14.9	575	2.4	2.4	< mdl	< mdl	7.0	74.7	344	**501**	**16.6**	1.3	150	207	0.69
12	72.7	8258	2.1	12.5	78.7	16.4	2.7	10.2	638	1.0	2.3	< mdl	< mdl	2.7	66.0	195	**340**	**6.3**	0.30	107	71.5	< mdl
13	133	13841	5.4	22.6	179	19.2	3.4	24.9	691	3.1	2.8	0.02	< mdl	9.0	148	188	**417**	**12.3**	1.3	232	489	4.4
14	36.6	3976	7.5	18.1	168	23.6	0.88	17.7	742	2.3	2.5	< mdl	< mdl	9.1	106	169	**415**	**12.0**	7.0	204	307	< mdl
15	49.1	5178	2.4	9.9	32.8	6.9	0.96	11.3	650	1.2	2.0	< mdl	< mdl	5.4	66.9	272	**400**	**7.4**	0.69	72.3	121	< mdl
16	40.5	4402	1.6	6.4	83.2	5.0	0.76	27.4	666	108	2.3	< mdl	< mdl	6.2	141	89	**718**	**361**	0.73	87.1	164	< mdl
17	162	16624	10.8	33.9	50.0	24.0	3.1	33.6	690	1.9	2.1	< mdl	< mdl	13.8	108	307	**986**	**10.6**	5.7	178	359	< mdl
18	9.1	955	0.75	1.5	13.6	2.8	0.30	41.1	656	8.5	2.6	< mdl	< mdl	0.50	131	138	**246**	**113**	< mdl	5.3	22.3	< mdl
19	10.6	1149	3.7	7.5	151	3.6	< mdl	5.4	817	0.72	2.6	< mdl	< mdl	4.4	78.8	66.4	**111**	**7.7**	2.1	137	128	< mdl
20	20.5	2829	0.67	3.4	710	19.2	0.85	< mdl	608	0.37	1.8	< mdl	< mdl	2.7	51.1	51.6	**1168**	**5.1**	< mdl	26.8	25.7	< mdl
21	30.9	3895	1.9	6.2	924	10.3	1.1	98.2	576	1.9	3.5	< mdl	< mdl	3.7	509	206	**393**	**13.2**	0.47	127	1201	0.03
22	23.8	2422	1.4	4.5	69.3	5.8	0.32	< mdl	748	2.6	2.0	< mdl	< mdl	6.2	120	105	**373**	**44.2**	0.36	82.6	311	< mdl
23	28.2	2939	6.3	12.4	319	11.5	0.40	12.7	738	2.3	2.9	< mdl	< mdl	11.1	93.2	91.6	**476**	**16.9**	1.6	182	287	< mdl
24	6.6	759	0.27	1.3	10.6	2.4	0.23	< mdl	980	0.20	2.9	< mdl	< mdl	1.0	65.5	27.7	**848**	**7.0**	< mdl	17.4	44.4	< mdl
25	4.6	358	1.2	4.0	175	5.1	< mdl	< mdl	719	0.34	2.0	< mdl	< mdl	2.7	87.7	35.8	**286**	**4.9**	0.18	125	138	< mdl
Mean (25)	67.0	8897	6.4	25.8	208	12.9	1.7	37.2	693	6.9	2.5	-	-	12.1	119	159	**503**	**32.9**	3.6	242	322.7	-
S.D.	92.3	17393	6.1	46.6	253	12.9	2.0	79.1	97.6	21.2	0.55	-	-	13.0	85.8	115	**312**	**72.4**	3.0	233	263.9	-
Minimum	5	121	0.27	1.3	10.6	< mdl	< mdl	< mdl	491	0.20	1.5	< mdl	-	0.50	51.1	28	**111**	**3.2**	< mdl	5.3	22.3	< mdl
Maximum	407	81147	22.1	239	924	59	8.6	371	980	108	3.9	0.02	-	58.2	509	504	**1181**	**361**	9.3	865	1201	4.4

Appendix 6. (Cont)

Sample NK27																					
Spot	**Mn**	**Fe**	**Co**	**Ni**	**Cu**	**Zn**	**Ga**	**As**	**Se**	**Ag**	**Cd**	**In**	**Sn**	**Sb**	**Te**	**W**	**Re**	**Au**	**Tl**	**Pb**	**Bi**	**U**
1	52.1	6102	3.0	6.7	80.8	11.0	15.6	5.6	1961	14.4	3.8	< mdl	< mdl	9.8	169	53.3	**89.4**	**4.9**	0.15	347	1527	0.61
2	1.8	206	0.175	1.2	10.6	2.3	0.38	8.4	1792	0.35	3.3	< mdl	< mdl	0.24	79.6	14.9	**45.0**	**0.19**	< mdl	4.7	8.7	0.04
3	< mdl	196.7	< mdl	9.0	114	< mdl	< mdl	< mdl	1698	1.1	4.3	< mdl	< mdl	6.7	330	15.4	**23.5**	**< mdl**	< mdl	51	467	< mdl
4	< mdl	< mdl	< mdl	2.5	< mdl	< mdl	< mdl	< mdl	1435	3.3	3.4	< mdl	< mdl	< mdl	55.0	17.2	**84.0**	**31.5**	< mdl	19.4	59.8	< mdl
5	9.9	1784	< mdl	10.3	21.3	< mdl	13.6	< mdl	1637	< mdl	3.3	< mdl	< mdl	3.7	65.5	17.4	**29.2**	**< mdl**	< mdl	182	250	< mdl
6	48.0	7146	< mdl	13.0	5.8	20.6	17.9	< mdl	1562	< mdl	2.9	< mdl	< mdl	< mdl	22.8	14.0	**44.9**	**< mdl**	< mdl	2.3	3.2	< mdl
7	140	19184	1.319	40.8	30.2	52.2	11.2	< mdl	1520	3.4	< mdl	< mdl	< mdl	3.2	101	24.3	**71.9**	**2.2**	0.78	163	151	1.1
8	< mdl	346.1	< mdl	< mdl	< mdl	< mdl	< mdl	< mdl	1503	0.88	2.9	< mdl	< mdl	< mdl	16.1	14.6	**29.8**	**0.878**	< mdl	< mdl	2.0	< mdl
9	< mdl	225	< mdl	< mdl	8.2	< mdl	< mdl	< mdl	1285	< mdl	< mdl	< mdl	< mdl	< mdl	51.0	19.1	**15.0**	**< mdl**	< mdl	2.2	25.0	< mdl
10	34.2	4306	0.894	4.3	49.7	< mdl	2.6	< mdl	1220	5.4	< mdl	< mdl	< mdl	2.7	73.1	103	**51.3**	**1.5**	< mdl	167	98.5	1.3
Mean (10)	47.6	4388	1.3	11.0	40.1	21.5	10.2	-	1561	4.1	3.4	-	-	4.4	96.2	29.3	**48.4**	**6.9**	-	104	259	0.8
S.D.	49.4	6174	1.2	12.7	39.1	21.8	7.1	-	224	4.9	0.50	-	-	3.3	92.6	28.4	**25.8**	**12.2**	-	119	469	0.6
Minimum	< mdl	< mdl	< mdl	< mdl	< mdl	< mdl	< mdl	< mdl	1220	< mdl	< mdl	< mdl	< mdl	< mdl	16.1	14.0	**15.0**	**< mdl**	< mdl	< mdl	2.0	< mdl
Maximum	140	19184	3.0	40.8	114	52	18	8.4	1961	14.4	4.3	< mdl	< mdl	9.8	329.8	103.0	**89.4**	**31.5**	0.78	347	1527	1.3

Appendix 6. (Cont)

Sample Nkmoly																						
Spot	**Mn**	**Fe**	**Co**	**Ni**	**Cu**	**Zn**	**Ga**	**As**	**Se**	**Ag**	**Cd**	**In**	**Sn**	**Sb**	**Te**	**W**	**Re**	**Au**	**Tl**	**Pb**	**Bi**	**U**
1	1.0	223	0.48	6.3	191	3.5	< mdl	4.72	713	2.2	3.3	< mdl	< mdl	5.1	64.3	3.4	**200**	**2.6**	< mdl	112	163	0.02
2	7.6	1207	1.8	21.8	91.0	4.3	0.55	7.67	748	0.80	4.0	< mdl	< mdl	15.0	87.8	14.5	**469**	**3.2**	0.05	73.9	160	< mdl
3	16.8	3245	4.5	48.1	582	17.9	1.0	10.53	667	5.7	3.4	< mdl	< mdl	29.4	101	48.5	**277**	**88.8**	0.35	151	357	< mdl
4	1.9	111	0.50	7.8	67.4	8.2	0.16	6.60	713	1.3	3.4	< mdl	< mdl	4.8	91.2	3.2	**469**	**6.9**	< mdl	100	187	< mdl
5	46.6	7296	2.5	35.8	8.9	15.1	4.3	18.10	822	0.74	4.5	< mdl	< mdl	18.8	99.3	223	**2309**	**5.7**	0.63	49.0	130	0.05
6	1.0	910	4.0	56.2	598	22.8	< mdl	10.02	1292	1.9	3.5	< mdl	< mdl	23.5	172	40.5	**686**	**21.8**	0.32	70.7	287	< mdl
7	12.7	1909	0.18	6.8	12.9	4.5	0.60	< mdl	916	< mdl	3.3	< mdl	< mdl	0.31	91.8	5.2	**563**	**0.07**	< mdl	4.1	2.5	< mdl
8	179	26593	2.6	81.1	11.7	50.3	13.6	17.4	944	1.4	4.9	< mdl	0.39	9.4	79.5	311	**2412**	**13.0**	0.07	56.9	64.3	0.04
9	3.1	741	1.9	18.1	275	6.3	0.21	9.4	852	0.84	3.6	< mdl	< mdl	12.6	116	9.4	**1055**	**5.9**	0.11	46.8	168	< mdl
10	17.1	2635	3.8	37.9	19.8	6.3	0.89	11.8	710	1.4	4.7	< mdl	< mdl	24.8	86.2	40.1	**303**	**10.1**	0.38	53.2	214	< mdl
11	6.9	1179	0.53	8.5	170	5.7	0.41	8.0	895	0.51	3.7	< mdl	< mdl	5.1	78.5	12.0	**479**	**7.1**	0.12	39.9	59.7	< mdl
12	6.5	981	0.30	7.0	123	5.8	0.40	4.1	733	0.63	3.1	< mdl	< mdl	3.8	70.3	4.6	**889**	**5.7**	< mdl	27.0	48.3	< mdl
13	< mdl	40.8	2.9	30.6	8.3	1.6	< mdl	14.1	402	1.4	2.7	< mdl	< mdl	13.7	53.3	17.4	**553**	**5.2**	0.07	22.3	173	< mdl
14	3.4	452	< mdl	1.7	< mdl	1.3	< mdl	< mdl	866	0.07	3.2	< mdl	< mdl	0.43	77.1	3.1	**27.1**	**< mdl**	< mdl	0.4	1.0	< mdl
15	6.8	1047	1.6	18.9	81.4	5.0	0.44	7.2	686	5.2	3.5	< mdl	< mdl	10.9	92.2	62.7	**303**	**9.0**	0.18	72.5	165	4.79
16	0.99	246	0.67	11.3	173	8.2	< mdl	< mdl	904	0.39	3.4	< mdl	< mdl	8.0	110	5.2	**126**	**0.8**	0.03	36.7	93.0	< mdl
17	0.95	163	1.9	22.7	45.8	2.4	< mdl	7.4	1157	1.3	3.4	< mdl	< mdl	12.7	101	25.3	**342**	**9.8**	0.19	42.7	165	< mdl
18	13.0	2032	0.40	9.4	319	19.2	0.65	< mdl	1016	0.13	3.2	< mdl	< mdl	7.3	86.1	4.1	**46.9**	**1.4**	< mdl	30.7	39.1	0.02
19	102	15309	3.3	59.3	102	29.7	5.1	15.3	869	1.4	3.4	< mdl	< mdl	36.1	90.1	147	**1527**	**13.8**	0.40	93.4	212	0.05
20	1.5	274	0.12	3.5	272	1.3	< mdl	< mdl	1016	0.12	2.9	< mdl	< mdl	2.2	90.4	3.4	**29.9**	**0.46**	0.04	9.2	11.8	< mdl
21	7.2	1275	0.53	7.8	167	9.2	0.60	< mdl	718	56.3	3.3	< mdl	< mdl	5.5	81.3	5.2	**216**	**2712**	< mdl	63.0	126	< mdl
22	10.9	1967	1.8	22.2	296	10.0	0.70	4.2	806	1.3	3.2	< mdl	< mdl	13.4	98.4	17.6	**92.4**	**12.1**	0.11	99.36	172	< mdl
23	38.8	5913	2.1	27.7	72.5	13.6	1.6	7.1	1004	1.0	2.9	< mdl	< mdl	16.8	96.0	90.4	**132**	**12.4**	0.19	80.16	138	< mdl
24	11.4	1840	5.0	46.0	125	9.5	0.77	11.9	1384	2.0	3.6	< mdl	< mdl	31.4	122	81.1	**435**	**18.8**	0.62	130	366	0.02
25	< mdl	193	0.50	8.1	174	4.8	< mdl	16.2	541	0.68	3.4	< mdl	< mdl	4.8	58.0	3.3	**2449**	**6.3**	< mdl	64.6	127	< mdl
26	5.8	1240	0.84	12.3	227	5.9	0.47	6.0	791	2.3	3.3	< mdl	< mdl	8.4	34.4	10.4	**431**	**45.4**	0.05	75.7	110	< mdl
27	5.9	1282	0.59	10.7	298	8.7	0.70	6.3	48.1	0.85	3.5	< mdl	< mdl	5.4	9.9	20.4	**478**	**21.1**	< mdl	45.7	119	< mdl
28	50.2	7687	3.7	44.7	116	18.6	3.1	15.8	784	1.7	2.9	< mdl	< mdl	23.5	62.0	86.6	**850**	**26.0**	0.34	138	266	0.03
29	< mdl	656	3.8	39.5	532	16.2	< mdl	11.0	1058	1.2	4.8	< mdl	< mdl	20.3	89.8	41.4	**675**	**15.2**	0.16	66.9	294	< mdl
30	< mdl	834	0.84	15.0	24.6	1.4	< mdl	4.1	432	0.66	3.0	< mdl	< mdl	17.3	27.7	21.0	**641**	**4.7**	0.04	89.2	171	< mdl
31	0.93	126	0.08	1.6	4.4	< mdl	< mdl	7.6	803	0.08	2.2	< mdl	< mdl	0.42	63.7	3.2	**199**	**1.4**	< mdl	2.1	1.6	< mdl
32	110	17162	2.0	64.0	406	40.8	6.2	11.0	757	1.0	2.9	< mdl	< mdl	14.5	72.6	18.6	**194**	**13.2**	0.07	69.4	104	< mdl
33	107	16301	1.4	52.3	29.1	29.2	5.8	8.9	717	0.30	2.8	< mdl	< mdl	6.4	67.2	15.6	**2386**	**2.4**	0.04	79.0	49.4	< mdl
34	18.3	2776	1.6	18.4	32.6	5.1	0.95	9.9	805	0.73	3.6	< mdl	< mdl	12.1	73.6	68.7	**425**	**16.6**	0.41	33.4	111	< mdl
35	3.9	753	0.64	13.0	245	5.9	0.25	3.6	789	1.2	3.4	< mdl	< mdl	9.6	98.8	12.3	**281**	**10.1**	< mdl	126	476	< mdl
36	3.0	395	0.27	2.5	38.2	2.7	0.13	6.9	972	0.10	3.3	< mdl	< mdl	2.9	104	34.4	**493**	**0.89**	< mdl	9.5	21.0	< mdl
37	1.4	334	1.3	13.2	103	2.7	< mdl	5.4	957	0.48	3.3	< mdl	< mdl	6.9	97.8	33.7	**524**	**6.0**	0.17	27.8	127	< mdl
38	< mdl	187	0.26	4.8	116	3.6	< mdl	< mdl	1037	0.15	2.8	< mdl	< mdl	1.2	103	8.8	**766**	**3.9**	< mdl	17.1	14.1	< mdl
39	36.2	5658	1.8	28.3	240	216	2.0	9.2	938	0.62	2.7	< mdl	< mdl	16.5	96.0	59.7	**1327**	**5.0**	0.12	76.1	123	< mdl
40	< mdl	76.8	0.15	2.7	49.7	< mdl	< mdl	16.6	796	0.31	3.0	< mdl	< mdl	1.6	83.3	3.7	**1040**	**2.1**	< mdl	53.8	67.8	0.01
41	< mdl	10.8	< mdl	0.54	1.8	< mdl	< mdl	< mdl	823	0.19	3.2	< mdl	< mdl	0.15	60.2	1.8	**1291**	**4.5**	< mdl	0.34	1.2	0.02
42	6.2	1151	0.25	10.1	211	3.37	0.31	< mdl	719	0.22	3.2	< mdl	< mdl	3.0	43.0	1.9	**126**	**1.52**	< mdl	42.0	56.2	< mdl
43	< mdl	< mdl	0.14	1.4	< mdl	< mdl	0.17	3.0	918	< mdl	3.4	< mdl	< mdl	1.3	84.0	2.4	**54.5**	**0.46**	< mdl	4.7	7.3	< mdl
44	8.9	744	0.13	4.17	36.5	5.7	0.44	2.6	918	0.10	3.0	< mdl	< mdl	0.59	88.9	2.0	**18.5**	**0.30**	0.04	10.1	17.8	< mdl
45	69.9	10549	0.62	32.4	9.4	21.3	4.0	5.7	389	0.12	2.3	< mdl	< mdl	1.2	30.8	3.8	**1100**	**0.32**	< mdl	14.2	18.3	< mdl
46	16.6	2411	1.3	15.1	22.6	5.9	0.80	6.8	912	0.93	2.7	< mdl	< mdl	8.2	100	46.1	**1104**	**16.8**	0.06	42.3	94.1	< mdl
Mean (46)	24.8	3291	1.5	21.6	153	15.7	1.9	9.0	820	2.3	3.3	-	-	10.4	82.3	36.5	669	70.5	0.19	55.5	128	0.50
S.D.	39.4	5573	1.4	19.6	154	33.4	2.8	4.3	226	8.4	0.56	-	-	9.0	27.4	59.0	655	402.9	0.17	38.9	107	1.5
Minimum	< mdl	< mdl	< mdl	0.54	< mdl	< mdl	< mdl	< mdl	48.1	< mdl	2.2	< mdl	< mdl	0.15	9.9	1.8	18.5	0.07	< mdl	0.34	1.00	< mdl
Maximum	179	26593	5.0	81.1	598	216	13.6	18.1	1384	56.3	4.9	< mdl	0.39	36	172	311	2449	2712	0.63	151	476	4.8

Appendix 6. (Cont)

Sample NKgrn																						
Spot	**Mn**	**Fe**	**Co**	**Ni**	**Cu**	**Zn**	**Ga**	**As**	**Se**	**Ag**	**Cd**	**In**	**Sn**	**Sb**	**Te**	**W**	**Re**	**Au**	**Tl**	**Pb**	**Bi**	**U**
1	< mdl	< mdl	0.06	< mdl	< mdl	1.7	< mdl	8.5	288	< mdl	2.8	< mdl	< mdl	< mdl	40.9	61.7	**2.1**	**< mdl**	< mdl	2.7	8.1	< mdl
2	< mdl	< mdl	< mdl	< mdl	< mdl	5.9	< mdl	8.4	282	< mdl	3.4	< mdl	< mdl	< mdl	38.1	56.2	**2.1**	**< mdl**	0.12	24.8	5.6	0.05
3	< mdl	< mdl	< mdl	0.39	< mdl	5.5	< mdl	7.3	261	< mdl	2.8	< mdl	< mdl	< mdl	28.8	83.9	**1.2**	**< mdl**	< mdl	0.21	0.08	0.02
4	< mdl	< mdl	< mdl	0.43	< mdl	9.0	< mdl	4.6	257	< mdl	2.9	< mdl	< mdl	< mdl	120	47.7	**0.6**	**< mdl**	0.03	45.3	151	< mdl
5	< mdl	< mdl	< mdl	0.42	1.2	9.7	< mdl	< mdl	60.7	< mdl	3.1	< mdl	< mdl	< mdl	6.5	394	**4.6**	**< mdl**	< mdl	0.09	< mdl	< mdl
6	< mdl	< mdl	< mdl	< mdl	< mdl	6.3	< mdl	< mdl	216	0.26	2.4	< mdl	0.67	< mdl	17.5	109	**0.88**	**0.10**	< mdl	1.1	3.35	0.03
7	7.9	745	0.85	0.58	2.8	34.4	0.58	< mdl	303	1.2	2.9	< mdl	2.0	1.1	31.2	36.6	**31.2**	**0.10**	3.6	316	55.7	0.68
8	< mdl	< mdl	< mdl	1.14	< mdl	23.9	< mdl	< mdl	56.3	< mdl	2.9	< mdl	< mdl	< mdl	57.5	500	**4.9**	**< mdl**	< mdl	1.7	81.6	0.04
9	87.2	9430	4.4	1.7	15.5	228	7.8	9.3	195	11.6	3.3	0.31	39.1	1.5	157	210	**14.0**	**0.45**	26.2	8208	388	14.5
10	< mdl	< mdl	< mdl	< mdl	< mdl	10.6	< mdl	8.9	280	0.09	3.5	< mdl	< mdl	< mdl	34.4	63.3	**2.7**	**< mdl**	< mdl	< mdl	< mdl	< mdl
11	< mdl	< mdl	< mdl	0.36	< mdl	9.2	< mdl	7.4	276	< mdl	2.6	< mdl	< mdl	< mdl	29.9	32.3	**0.64**	**< mdl**	< mdl	< mdl	< mdl	< mdl
12	< mdl	< mdl	< mdl	< mdl	< mdl	3.4	< mdl	5.5	277	< mdl	3.0	< mdl	< mdl	< mdl	36.9	66.1	**2.0**	**< mdl**	< mdl	< mdl	< mdl	< mdl
13	< mdl	< mdl	< mdl	< mdl	< mdl	6.1	< mdl	8.8	263	0.01	2.9	< mdl	< mdl	< mdl	33.8	49.2	**2.3**	**< mdl**	< mdl	0.13	< mdl	< mdl
14	< mdl	35.9	0.78	< mdl	< mdl	13.4	< mdl	< mdl	261	1.1	2.7	< mdl	3.0	1.0	65.7	21.9	**6.5**	**< mdl**	2.7	638	54.2	0.43
15	< mdl	< mdl	< mdl	< mdl	< mdl	6.8	< mdl	< mdl	255	< mdl	2.9	< mdl	< mdl	< mdl	49.3	21.5	**6.6**	**< mdl**	< mdl	11.69	1.7	< mdl
16	< mdl	19.8	0.16	1.1	< mdl	7.1	< mdl	< mdl	262	1.05	2.9	< mdl	0.99	< mdl	67.9	23.8	**6.3**	**< mdl**	2.1	273	35.5	0.11
17	< mdl	< mdl	< mdl	< mdl	0.18	< mdl	< mdl	5.1	245	< mdl	2.5	< mdl	< mdl	< mdl	76.3	71.1	**1.6**	**< mdl**	< mdl	8.9	60.0	< mdl
18	1.5	435	0.29	< mdl	0.85	16.2	1.5	1.4	263	8.1	2.2	0.06	8.7	0.12	118	33.5	**4.5**	**0.04**	2.9	26.3	118	1.85
19	< mdl	< mdl	< mdl	< mdl	< mdl	4.2	< mdl	< mdl	247	0.08	3.4	< mdl	< mdl	< mdl	48.3	30.5	**5.1**	**0.14**	< mdl	6.3	4.0	< mdl
20	< mdl	< mdl	< mdl	< mdl	< mdl	5.5	< mdl	< mdl	256	< mdl	2.2	< mdl	< mdl	< mdl	46.8	25.2	**4.8**	**< mdl**	< mdl	1.5	0.21	< mdl
21	< mdl	< mdl	0.07	0.57	< mdl	14.3	< mdl	< mdl	236	0.23	2.4	< mdl	< mdl	< mdl	52.1	24.9	**5.1**	**< mdl**	< mdl	67.1	6.6	< mdl
22	< mdl	< mdl	< mdl	< mdl	< mdl	11.8	< mdl	< mdl	252	< mdl	2.3	< mdl	< mdl	< mdl	44.6	32.3	**4.5**	**< mdl**	< mdl	0.16	0.17	0.03
23	79.2	6396	3.73	< mdl	4.42	15.6	3.87	2.69	256	8.2	2.4	< mdl	6.5	0.29	84.9	25.4	**5.4**	**0.07**	3.0	413	90.9	1.6
24	< mdl	< mdl	0.20	< mdl	< mdl	< mdl	< mdl	< mdl	267	0.31	2.8	< mdl	< mdl	0.33	39.4	27.2	**13.2**	**< mdl**	0.20	123	25.4	0.03
25	< mdl	95.2	1.8	0.33	2.8	16.9	0.26	4.4	291	2.5	3.2	0.04	3.7	1.6	62.5	25.5	**8.4**	**0.06**	5.5	853	110	3.4
26	< mdl	4.1	< mdl	< mdl	< mdl	2.6	< mdl	< mdl	261	< mdl	3.1	< mdl	< mdl	< mdl	24.3	21.0	**5.4**	**< mdl**	< mdl	12.4	1.8	< mdl
27	< mdl	37.0	0.69	< mdl	1.93	9.5	0.22	< mdl	71.9	1.2	3.0	< mdl	3.40	0.35	28.9	332	**< mdl**	**< mdl**	1.8	813	79.2	0.61
28	< mdl	< mdl	< mdl	< mdl	< mdl	6.1	< mdl	3.3	276	< mdl	3.2	< mdl	< mdl	< mdl	24.1	41.3	**1.4**	**< mdl**	< mdl	17.7	5.3	< mdl
29	55.9	5506	2.48	< mdl	4.95	45.0	5.3	10.9	260	7.6	2.6	0.22	26.2	1.5	64.8	46.7	**1.6**	**0.14**	6.0	860	164	1.9
30	< mdl	< mdl	0.58	< mdl	< mdl	3.0	< mdl	4.4	296	1.3	2.9	< mdl	< mdl	0.44	43.2	28.8	**0.25**	**< mdl**	2.8	599	77.3	0.28
31	< mdl	< mdl	< mdl	0.04	< mdl	3.1	< mdl	4.4	268	< mdl	3.0	< mdl	< mdl	< mdl	30.9	57.9	**2.0**	**< mdl**	< mdl	1.0	0.39	0.03
32	< mdl	< mdl	0.16	0.41	2.25	2.3	< mdl	< mdl	64.7	3.0	2.9	< mdl	1.4	0.24	14.2	319	**6.3**	**0.35**	0.03	135	51.8	< mdl
33	27.5	3423	1.6	< mdl	1.4	5.5	2.00	4.2	108	9.4	3.5	0.05	3.4	1.3	79.9	193	**8.6**	**0.41**	7.7	3608	245	0.71
34	< mdl	< mdl	0.18	0.95	6.6	24.9	< mdl	2.5	89.6	0.11	2.6	3.5	848	0.49	6.2	208	**5.6**	**< mdl**	0.07	6.91	12.9	0.13
35	< mdl	22.8	0.53	< mdl	5.1	6.1	< mdl	0.10	73.6	3.8	3.0	< mdl	1.5	0.53	13.1	200	**3.0**	**0.39**	0.61	208	128	0.31
36	1.5	269	1.5	< mdl	3.9	20.2	0.69	5.0	347	4.2	2.4	0.12	15.9	0.69	53.5	39.8	**12.3**	**0.11**	5.5	1333	92.2	10.7
37	< mdl	< mdl	< mdl	< mdl	< mdl	2.3	< mdl	< mdl	74.3	< mdl	1.8	< mdl	< mdl	< mdl	5.5	389	**1.5**	**< mdl**	< mdl	< mdl	< mdl	< mdl
38	< mdl	< mdl	< mdl	< mdl	< mdl	2.4	< mdl	< mdl	95.4	< mdl	2.3	< mdl	< mdl	< mdl	39.0	486	**14.2**	**0.07**	0.14	232	43.5	0.19
39	< mdl	< mdl	< mdl	< mdl	< mdl	10.2	< mdl	6.9	282	0.17	3.0	< mdl	1.1	< mdl	35.6	108	**2.4**	**< mdl**	< mdl	3.2	11.7	< mdl
40	< mdl	< mdl	0.19	< mdl	< mdl	< mdl	< mdl	< mdl	284	0.93	3.0	< mdl	1.3	< mdl	20.1	152	**1.2**	**< mdl**	0.79	487	37.4	0.06
Mean (40)	37.2	2032	1.1	0.65	3.8	16.4	2.5	5.6	224	2.9	2.8	0.62	56.9	0.8	46.8	117	**5.3**	**0.19**	3.6	537	63.3	1.6
S.D.	36.8	3149	1.3	0.44	3.8	36.9	2.7	2.8	83.8	3.5	0.39	1.3	204	0.5	31.8	136	**5.7**	**0.15**	5.8	1468	81.8	3.6
Minimum	< mdl	< mdl	< mdl	< mdl	< mdl	< mdl	< mdl	< mdl	56.3	< mdl	1.8	< mdl	< mdl	< mdl	5.5	21.0	**< mdl**	**< mdl**	< mdl	< mdl	< mdl	< mdl
Maximum	87.2	9430	4.4	1.7	15.5	228	7.8	10.9	347	11.6	3.5	3.5	848	1.6	157	500	**31.2**	**0.45**	26.2	8208	388	14.5